博士論文

論文題目　Mobile microplate technology
for multi-angle observation of adherent cells
(微小プレートによる接着性細胞の多角度観察)

氏名　手島 哲彦

A dissertation submitted in partial fulfillment of
the requirements for the degree of
Doctor of Philosophy

In the subject of

Information Science and Technology

The University of Tokyo
Tokyo, Japan

December, 2013

Doctoral Committee:

Professor Hiroyuki Fujita
Professor Isao Shimoyama
Professor Ryohei Kanzaki
Professor Yasuhiko Jimbo
Associate Professor Shoji Takeuchi, Chair

TABLE OF CONTENTS

LIST OF FIGURES

LIST OF TABLES

ACKNOWLEDGEMENTS

Through this dissertation, I have felt that Ph.D. life is like a journey with a lot of ups and downs. This journey made me excited to find good companion and see the hidden treasures along the roads, due to many people that I was fortunate to interact and inspired. I'd like to use this opportunity to show my deep gratitude to them.

First and foremost, I would like to thank and express my sincerest gratitude towards my advisor, Prof. Shoji Takeuchi, for giving me the precious opportunity to learn from him throughout my 5-year graduate career. Thinking back to five years ago when I was still poorly experienced, unsure, and hesitant about my future, it was accidental meeting with him in Komaba campus that connected me to "bioMEMS". His enthusiasm and passion of pursuing new sciences conducted and ultimately inspired me to explore the unfamiliar territories. He gave me freedom and environment that I could explore my original topics at the interface among MEMS and parasitology, and opportunities to work with great people and develop myself as an independent researcher. Even if I caused so much trouble to him due to my careless and narrow-viewed behaviors, he never abandoned me, but has always strengthened me with his patience when I was struggling, with his guidance when I was lost, and with his encouragements when I was down. I am very thankful and proud to have been one of his apprentices who enjoyed his advices in research. Many lessons I learned from him will always be treasured in my heart and serve as basis for all of my future endeavors.

Next, I would like to thank my committee members for all their support, help, teaching, advice, and guidance throughout my graduate studies. Prof. Hiroyuki Fujita, Prof. Isao Shimoyama, Prof. Ryohei Kanzaki, and Prof. Yasuhiko Jimbo were kind enough to take time off their busy schedule to give helpful advice on how to improve the thesis. More specifically, when I started to learn MEMS five years ago, I pored through the textbook written by Prof. Fujita, which fascinated me and motivated me to study MEMS. Had it not been for the experiences to read his book, I should not have decided to leap into new academic field. I would also like to gratefully acknowledge Prof. Kazuhiko Ishihara for providing the MPC polymer, and Prof. Takeomi Mizutani for his helpful discussions and novel insights into imaging technology. Prof. Satoshi Sawai, Dr. Akihiko Nakajima, Prof. Junichiro Yajima, and Prof. Takashi Tsuboi kindly suggested further biological applications of mobile microplates.

The work presented in this thesis is an outcome of multiple collaborations with Kanuka lab of Jikei University. I am deeply grateful to Prof. Hirotaka Kanuka for his expertise, assistance, and teaching in all of the microbiological sides of my projects. His sustained interest in applying innovative micro-technologies to study parasite infection opened up the opportunities for the wonderful collaboration from the start of my doctor course. His tremendous support and

encouragements have motivated me, made me introduced to my original thesis topic to start my research, and always provided significant contributions to this research. Dr. Hiroka Aonuma pleasantly trained me all the parasite-related experimental skills without any reservation. She always not only prepared to give me directions and profound insights in the research, but also suggested me the scientific significance ranged in widely-ranged infectious disease. I also like to thank Prof. Kenji Ishiwata, Prof. Masahiro Kumagai, Prof. Takeshi Annoura, Dr. Kiyoshi Okado, Dr. Erisha Saiki, and Takuya Yokoyama. Thanks to their kindness, I fully enjoyed the time in Kanuka lab.

I would also like to express my special thanks to Dr. Hiroaki Onoe, for all the constructive advice and profound insights he has provided. A lot of great ideas were generated during our discussions and drinking with him; I was always impressed by the plentiful and creative solutions he proposed for the problems that I encountered. His continued teachings on microfabrication and material science, constructive criticisms, and encouragements have not only helped me reach a meaningful high-quality research that none had found, but also shaped me into an independent and confident researcher to conduct the research step by step. They will always serve as my role models for the rest of my career, and I really appreciate his deep insight and excellent mentorship which made this work possible.

In addition to the professors, I would also like to gratefully recognize the friendship, collaboration, and help from all former and current Tlab members. Especially, I appreciate the helpful discussion and collaborations about cell biology and microfluidics with Dr. Shigenori Miura, and the helpful discussion about magnetic actuation with Soichiro Tottori. I am also grateful to Prof. Teru Okitsu, Dr. Koji Sato, Dr. YunJung Heo, Dr. Midori Negishi, Akiko Sato, Dr. Shintaroh Iwanaga, Dr. Amy Y. Hsiao, Dr. Won Chul Lee, Dr. Satoshi Hiyama, Dr. Michinao Hashimoto, Dr. Fumiaki Tomoike, and Prof. Ryan Sochol for the fruitful discussion. I also thank Tlab technical manager, Maiko Onuki, who have worked closely with me and offered me much help and lectures throughout the microfabrication process; secretaries, Maiko Ito and Kazuko Katagiri for their administrative supports; technical assistants, Fumiyoshi Ishidate, Akane Itou, Hirofumi Yoshida, and Saori Mori. Thanks to all of KAST members, I had wonderful opportunities to find new approaches of research. I appreciate Dr. Toshihisa Osaki to take care of me since I was a M1 student in Tlab. I’d like to draw on his steady and considerate attitudes to the research and any lab members. Dr. Ryuji Kawano showed me his breath and depth of knowledge on biochemistry as well as his insights capturing underlying principles of membrane dynamics. He opened my eyes on the topics on “parasite-infected artificial cells”. I will never forget the first year in Tlab when he kindly talked about many things including research and studying in U.S.A. in the Italian restaurant. It has been fun to work with Dr. Koki Kamiya who lectured me how to produce artificial membrane and protein analysis. The time he spent for me enriched their technical help and insightful feedbacks to my biochemical works.

Prof. Nobuo Misawa, Dr. Daisuke Kiriya, Dr. Kaori Kuribayashi-Shigetomi, and Prof. Masahiro Takinoue offered me a lot of helps and advices in the past years. Especially, I learned from Prof. Misawa many principles such as trust to coworkers, desire of exploration, importance to drink, and insistency to meaningful work, which are very precious and will surely significantly benefit my future career. Dr. Kiriya has taught me many things, including not only attractive and logical presentation skills but also how to behave as one of the student member in the laboratory and organize all of Tlab members. Without any hesitation, he has spent for me countless time and sometimes stayed up all night in order to complete my presentation documents. I never forget that precious and fruitful time from now on.

I like to thank my lab mates with whom I have enjoyed my Ph.D. study. I have been extremely fortunate to have the privilege to work with friends who joined Tlab in the same year, Taishi Tonooka, Tomoaki Kurakazu, Yuto Shimoyama. Especially, I spent the longest time with Tonooka to discuss about our philosophy and future. We shared all the fun, stressful moment to complete assignments or meet the deadlines, and achievements coming from the success, throughout the pursuit of my Ph.D. It was his contributions and helps that made this dissertation possible. I would like to express my deepest gratitude towards all of the wonderful memory with him. I would also like to thank senior students, Hirotaka Ishihara, Kosuke Iwai, and Yuya Morimoto. Without Ishihara's continued guidance and support for me, this work would not have been possible. His hard-working and courteous lecture of the ABCs of fabrication process had a tremendous influence on my professional development. Besides, I have truly learned from his intuition, and obtained a lot of inspiration for my research. Notably, I am also grateful to three students, Shotaro Yoshida, Yoshinobu Iimura, and Hiromasa Hasegawa, who worked with me. Their insights and dedication reminded me what it is like to be an ambitious and optimistic student. I also enjoyed time with Shinsuke Sugimoto, Daniela Serien, Shohei Habasaki, Hiroshige Hamano, Renai Tei, Yongseung Lee, and Yumi Mukoyama, and I want to send my best wishes for their future. I will miss all the laughter and tears I shared with all of them.

Finally, I would like to express my deepest gratitude to my family for their endless encouragements and support throughout my long journey. My parents always unconditionally support me and I thank them for everything they have given me. Their belief and confidence in my abilities through times of my successes and failures are main reasons for all achievements. Their delicate care and tenderness also sustained me in every step of progress I achieved in my research. I also show many thanks to my grandparents, who have always been proud of all of my accomplishments, and my brothers, who have always been a source of encouragement of my decisions all years long. Without their helps, I could not continue my Ph.D. study. I would also like to thank my wife-to-be, Kaho Tominaga, who accompanied me for 9 years. During the whole graduate study, she has been always standing beside me, giving me support, sharing my pleasure and encouraging me. This thesis is dedicated to such a great family.

Dissertation Advisor
Shoji Takeuchi

Author
Tetsuhiko Teshima

Mobile microplate technology for multi-angle observation of adherent cells

ABSTRACT

The objective of this dissertation is to manipulate adherent cells for multi-angle observation of cell membrane boundaries by using the mobile microplate technologies. A real-time investigation of membrane deformation not only provides fundamental information about cell behaviors such as endocytosis and exocytosis, but also extends the applications of research field, including microbial infection. Although, conventionally, membrane deformation of two-dimensionally cultured cells has been observed in the experimental systems to optimize the viewing angle toward multi-angle observation, there are still technical limitations on inclination of the optical pathway and difficulty in adjusting the microscopic focus on the targeted samples after light path optimization, which interferes with the high-resolution observation of the plasma membrane surface. In this dissertation, we proposed mobile microplate technology to achieve angle-tunability in cell-culturing substrates for multi-angle observation. Mobile microplates have two types of structures: hinged microplates, termed microflaps, for the long-term cell culture and observation; microplates without hinges to increase the degree of freedom in location and motility, termed microdisks, for the short-term observation with high magnification. In the applied magnetic field, both of two types of cell-laden microplates can be inclined in the desired orientation and equipped on the conventional microscopies including bright-field and confocal microscopes, enabling us to observe the cells loaded onto the microplates from desired angles. Magnetically inclined

microplates enable observation of the cells from multiple angles without physical microscopic obstruction or limited resolution. By using the microplates in the bright-field microscopes, we revealed that *T. gondii* exhibited a distinctive pattern of behaviors during invasion into host cells. By applying the microplates to confocal observation, we obtained the single scanned image that indicates the dynamic deformation of host cell cytoskeleton during parasite invasion under the confocal microscopes. The new and detailed knowledge of parasite motion during infection cannot be accomplished without high angle-tunability and experimental versatility of the mobile microplate. This system does not require an experimental setup in which the light path is inclined, and it is suitable for multi-angle observation of plasma membranes under the conventional microscope. Furthermore, the micro-sized inclination of the cell-laden microflaps facilitates easy adjustment of the microscopic focus, which enables cellular observation with high-magnification lens. Since infectious microbes, including parasites and bacteria, generally behave with motions in *x*-*y*, *y*-*z* and *x*-*z* plane, multi-angle observation on the microplates will be a promising method for real-time detailed analysis of the microbial motility under the conventional optical and confocal microscopes.

CHAPTER 1

INTRODUCTION

Cells are the building blocks of living organisms, as the smallest unit with their own structures and functions. Cells contain many biomolecules such as proteins and nucleic acids inside their tiny body with approximately 10–30 μm in diameter enclosed within cell plasma membrane. Since they are not only tiny but also colorless and translucent, cells are visible only under the microscope. Since Matthias J. Schleiden and Theodor Schwann used a primitive light microscope to describe cells in 1838, the development of various types of microscopes has greatly extended the ability to reveal subcellular structural features and has yielded much real-time information on molecular composition element, biochemical alteration, and biophysical motility of living cells. Recently, the ability to observe or inspect cells from multiple angles is an important requirement for many biological issues, since it allows us to obtain the detailed information about three dimensional (3D) cellular morphology and motility. Nevertheless, optical microscopes have great difficulty in performing the experiments involving multi-angle observation, as they are primarily used for top-down observation. Therefore, researchers must develop experimental systems to manipulate the cell-culture dishes and place it in the required position or at the appropriate angle toward multi-angle observation, which hampers the standardization of experimental methods and the reproducibility of results. Here, this study is about the development of a mobile substrate for manipulating and inclining adherent cell toward the multi-angle observation of cell membrane, and the biomedical

applications such as observation of microbial infection. This substrate enables us to incline the adherent cells in the desired orientation, and equipped to any types of conventional microscopy, which facilitates to the observation of cells with high magnification while maintaining the adhesive property of cells. In this chapter, we will start with the background, where we will cover some basics regarding the analysis of cell component, behavior and morphology, and multi-angle observation of adherent cells at both multi-cell level and single cell level. This background leads to the discussion in the next section about previous works and their challenges that remain to be solved. We then state the objectives and significance of this work, and the strategies we are adopting. Lastly, we will present the overview of the organization and structure of this dissertation.

1.1 Background

1.1.1 Dynamics in cell component and morphology

Cell plasma membrane is a crucial and specialized barrier for a cell to carry out vital functions. Cell membrane encloses the cell to define the cell boundary, shape and volume as shown in Figure 1-1(a), thereby serving to separate a cell from the extracellular environment throughout the cell cycle, e.g., during cell migration (Kay et al., 2008; Rappoport et al., 2003), division (Hesse et al., 2012; van Meer et al., 2008), or physiological volume changes (Ikonen, 2008; Wymann et al., 2008). Hence, cells always take in or detect the molecules located outside the cells such as hormones “across” their plasma membranes (An et al., 2010; Llobet et al., 2003). Infectious microbes also access the host cell plasma membrane to invade the cells (Brandenburg et al., 2007; Handa et al., 2007; Riglar et al., 2011). These extracellular stimuli trigger the bending and stretching dynamics of the membrane, induce local variations in the membrane tension and intracellular signaling molecules (Boothroyd et al., 2008; Gundelfinger et al., 2003). Consequently, the membrane surface is a critical interface for cell function and

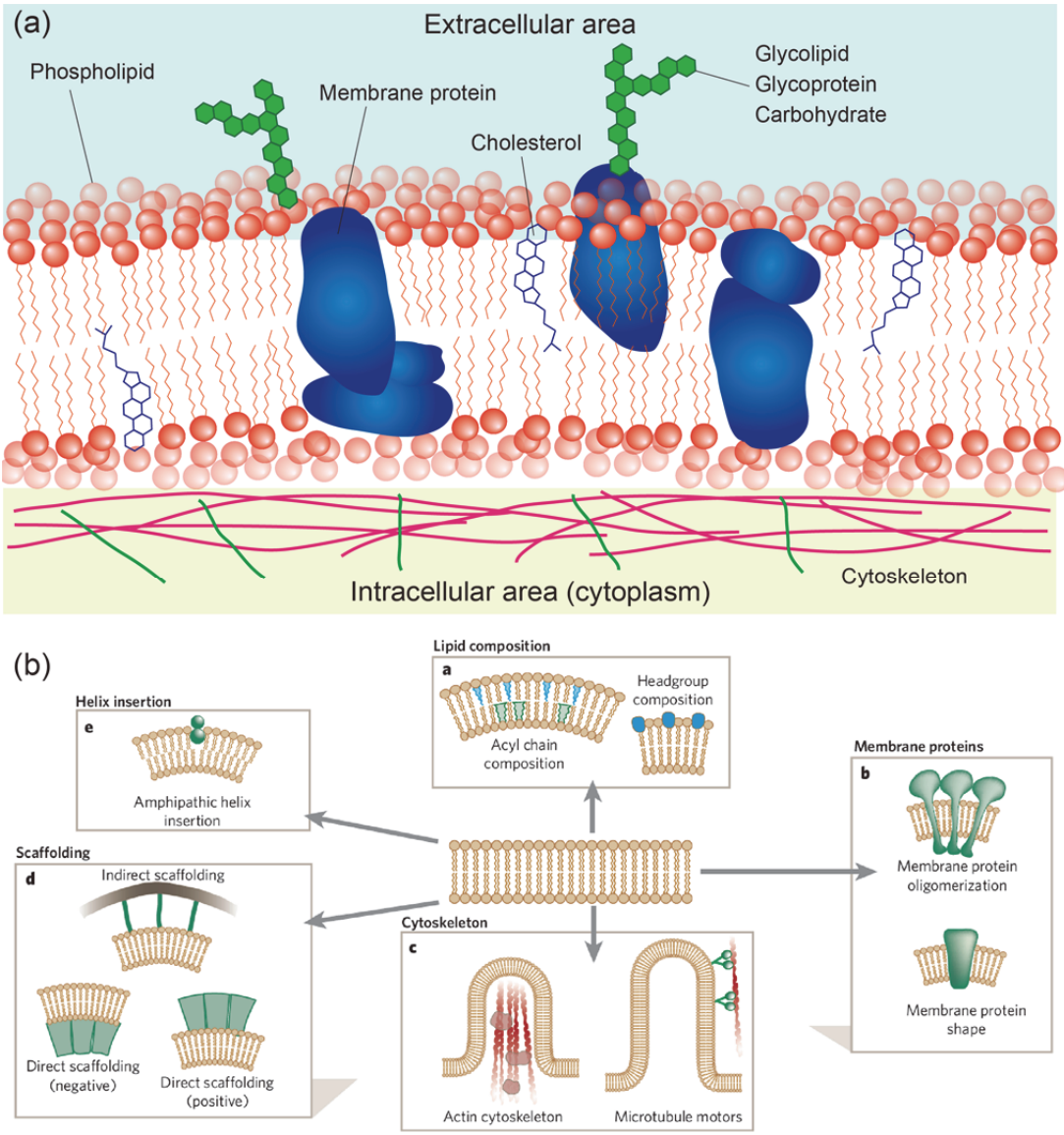

Figure 1-1. Component and deformation of cell plasma membrane. (a) A schematic illustration of cell plasma membrane. The structure of phospholipids defines the boundary of cells to separate from the environment surrounding it. Cell plasma membrane has cholesterol molecules and proteins that allow the membrane to function properly. (b) Molecules of cytoskeleton and modification in lipid or protein composition are primarily responsible for giving the membrane the rigidity it needs to hold the cell's shape and flexible deformations. Proteins embedded in the membrane also play important roles in changing the curvature of membrane and shape. The image of 1-1(b) was transferred from the following reference, (McMahon et al., 2005).

behaviors.

The cytoskeleton has a critical role in many intracellular processes: cell mobility (Felsenfeld et al., 1999), cell morphology (Wodarz, 2002), the uptake of external materials (Purich et al., 1999), organization of the cell shape to anchor of organelles (Soldati et al., 2006). Because the cell membrane is inelastic, the membrane is internally pinned to the cytoskeleton to preserve their membrane integrity (Sheetz, 2001). Above all, it is involved with various dynamic membrane activities by being associated with proteins embedded in membrane. The membrane protein molecules mediate dynamic functions of the membrane and serve as structural links that help the cytoskeleton to interact through the lipid bilayer with extracellular environment, extracellular matrix and an adjacent cell (Knodler et al., 2001). Consequently, cell plasma membrane supported by cytoskeleton critically acts as sensors of external environments, allowing the cell to change its behavior in response to environmental cues to transfer information across the membrane.

Deformation of cell plasma membrane mediated by cytoskeleton, such as membrane budding and fusion, plays an important role in the cellular response to external stimuli and in the spontaneous secretion of proteins. This deformation is attributed to the dynamic modification in structure and organization of the two main constituents of cells: membrane and cytoskeleton (McMahon et al., 2005) (Figure 1-1(b)). For example, cells that are prone to changes in their area maintain an intrinsic membrane reservoir in the form of lipid vesicles. Where there is a demand for area expansion, vesicles are added to the cell membrane (exocytosis) (Tam et al., 2010) and are retrieved upon compression (endocytosis) (Doherty et al., 2009; Liu et al., 2009; Sudhof et al., 2009). The complex morphological transformations of the cell membrane during exo- and endocytosis inevitably require specific protein machinery in the cytoskeleton and reconstitution of membrane lipid components. The technologies to harness the cell membrane penetration are able to be applied to the drug delivery system such as cancer

nanotheranostics by engineered nano-particles (Kievit et al., 2011) (Figure 1-2(a)). In addition, deformation of cell plasma membrane is involved in a multistep process of microbial infection into host cell, including bacteria, virus, and parasites including malaria (Cowman et al., 2006) (Figure 1-2(b)). The infection mechanism of parasites consists of parasite contact to host cells, intimate attachment, parasite motility, and then penetration. When one type of infectious microbes, *Toxoplasma gondii* (*T. gondii*), prepare the invasion into the host cells, they attached to the host cell membrane and showed gliding motilities to secrete various proteins from apical organelles (micronemes and rhoptries) through the cell plasma membrane while interacting with lipid and membrane proteins (Boothroyd et al., 2008; Carruthers et al., 2007) (Figure 1-2(c, d)). When penetrating into the host cell, the host cell plasma membrane is dynamically invaginated, envelopes the invading parasite and is eventually pinched off while being mediated by polymerized actin fibers and microtubules. Dynamic membrane protrusions driven by actin polymerization are interestingly hijacked by *Cryptosporidium parvum* to enter host cells. The membrane protrusion depends on the polymerization of actin fibers and the change of cell volume (Chen et al., 2005) (Figure 1-2(e)). Taken together, it is quite crucial to comprehend how the dynamics in morphological modification inside the cells occur, and where or when this dynamics are linked with transition of cellular components such as proteins and lipids. Therefore, a real-time investigation of membrane and cytoskeleton deformation not only provides fundamental information about cell behaviors such as endocytosis and exocytosis, but also extends the applications of research field, including microbial infection through host cell membrane and cell penetration in drug delivery.

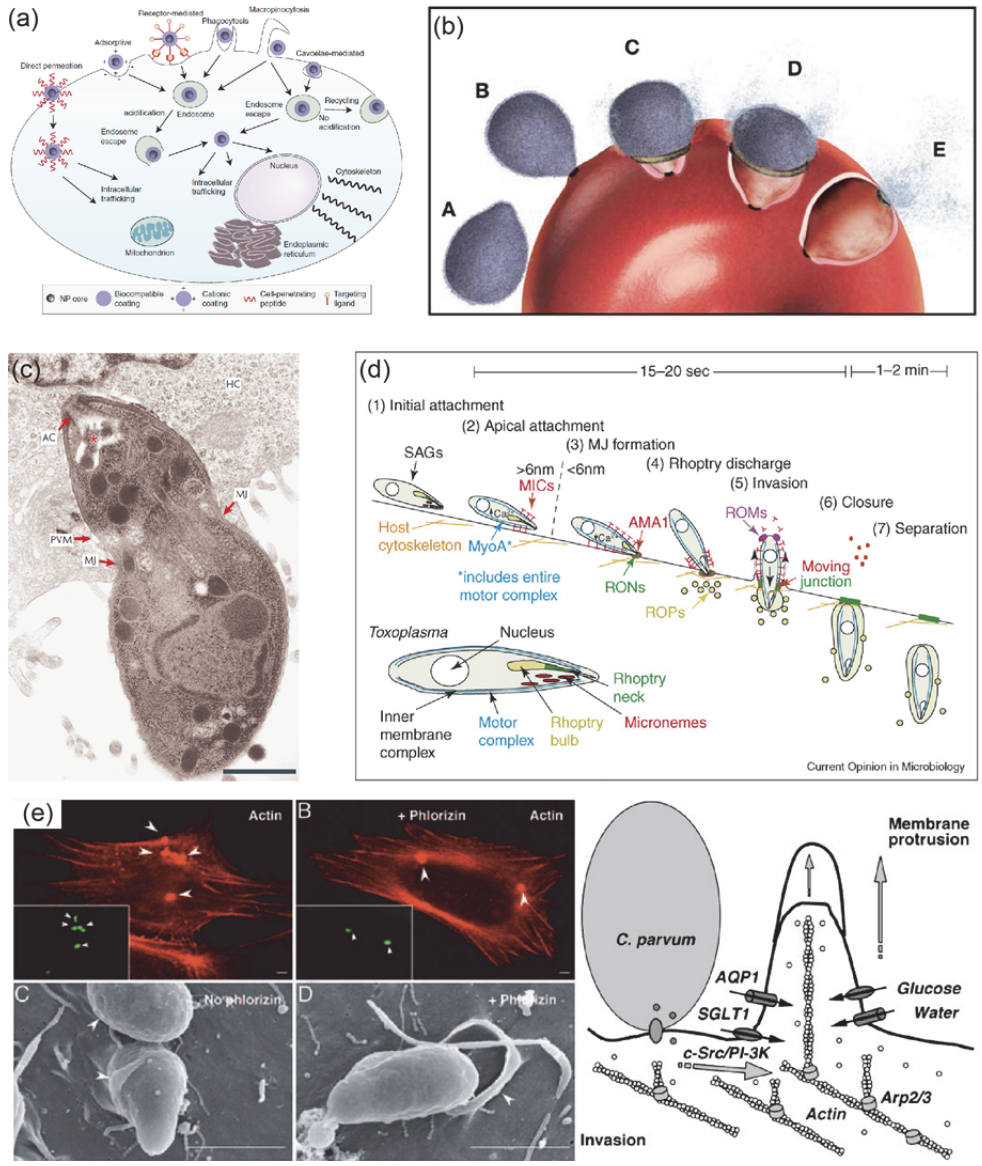

Figure 1-2. Deformation of cell plasma membrane. (a) Entry of NPs into the cell across the cell membrane can occur by direct permeation, or by various types of endocytosis mechanisms (Kievit et al., 2011). (b) Malaria invasion. The host cell surface coat is shed at the moving junction by a serine protease, resulting in penetrating the membrane (Cowman et al., 2006). (c) *T. gondii* invading HeLa cell membrane (Boothroyd et al., 2008). (d) A model of *Toxoplasma* invasion. The parasite actively penetrates by 'pulling' (lateral arrows) transmembrane, thereby invaginating the host plasma membrane (Carruthers et al., 2007). (e) *Cryptosporidium parvum* attachment to host-cell membrane induce actin remodeling at the parasite-attachment site (Chen et al., 2005). All images were transferred from each reference.

1.1.2 Multi-angle observation of adherent cells

The study of how cell plasma membrane is deformed in response to extracellular signals is a burgeoning field of biology. The invaginations in membranes can be driven by their spontaneous curvature, membrane fission arises from lipid phase separation, and increased lipid tension facilitates membrane fusion. These deformations occur in the micro- or nano-sized space, and have parameters of the trajectory and displacement in three-dimension. Therefore, it is not until the microscopes with high resolution and magnification become available that I would discover the mechanism of these tiny phenomena in the deformation of cell plasma membrane and cytoskeleton.

Conventionally, deformation of the plasma membrane surface of two-dimensionally (2D) cultured cells has been observed under an optical inverted microscope. In optical microscopic setup, the cells cultured in the Petri-dishes are put on the stages that are located between light source and objective lenses as shown in Figure 1-3(a). In this case, unidirectional optical observation from the top or bottom of the cultured cells provides the information about the cells in two-dimension (x-y layer); thus, the observers cannot capture the cross-sectional view of membrane deformation. Here, if we were able to rotate or incline the view angle in the desired orientation, it is possible to observe the components of adherent cells while maintaining cellular adhesive property (Figure 1-3(b, c)). Here, multi-angle observation of the deformed membrane would enable us to obtain the cross-sectional image of cell, reveals its precise shape, and provides information on membrane transportation, i.e. the trajectory of endocytosis and invasion angle of infectious microbes at the interface of the plasma membrane. Accordingly, the obtained cross-sectional image of cell not only would enlighten us about detailed analysis of fundamental cellular morphology and behavior, but also it could also provide a method to pursue the biomedical researches.

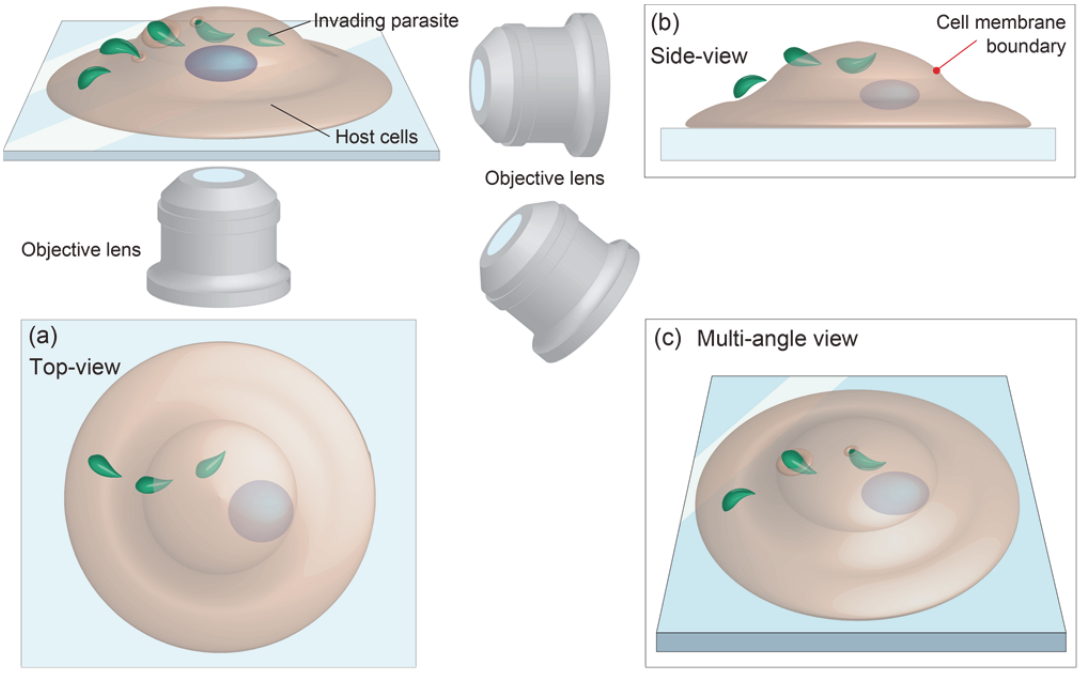

Figure 1-3. Observation of boundaries of cell plasma membrane from multiple angles. (a) Conventionally, the cells cultured in the Petri-dishes are put on the stages that are located between light source and objective lenses. (b, c) Multi-angle observation of the deformed membrane would enable us to obtain the cross-sectional image of cell, reveals its precise shape, and provides information on membrane transportation.

1.1.3 Single-cell analysis

To investigate cellular responses to external signals, most biologists have mostly performed the bulk-scale methods to measure average outcomes for a population of cells. In the ordinary cell-based assay, multi-cells are cultured and treated in the single petri-dishes. In addition, the methods commonly used for cell-based assays rely on a well-established microwell-plate format. Another experimental method, such as polymerase chain reaction (PCR), enzyme-linked immune-sorbent assay (ELISA) and western blotting has been extensively performed to monitor gene and protein expression inside the multiple cells. They enable us to detect or quantify the

average amount of bio-molecules, including DNA and protein, in the mixture of a number of cells. Despite the success of these assays cellular responses and cell behaviors depend on the character of individual cells, cell-type, dose of chemical stimuli, and number of neighboring cells. The population-wide studies thus mask the behavior of individual cells, which resulting in insufficient experimental results for characterizing biological processes with the standard error of the mean (Di Carlo et al., 2006b; Rao et al., 2002; Spiller et al., 2010) (Figure 1-4(a)). It is critically due to the variable initial population states and the difficulties in dealing with poorly controlled cell distributions, and accordingly the assay of individual cells among the collection of unsorted cells cannot be easily accomplished (El-Ali et al., 2006; Lindstrom et al., 2010).

When we establish the experimental setup for multi-angle observation of adherent cells, we also should consider the gap between cell behavior at single-cell level and multi-cell level. For instance, gap junctions are present in cell membrane to communicate with neighboring cells (Ali et al., 2004). Cells cling to one another or to the ECM through direct cell-cell junctions, including tight junction, adherens junctions, and desmosomes (Cavey et al., 2008; Etienne-Manneville et al., 2002). The analysis of this cell-cell communication provides them with a variety of biological findings, such as the exchange of soluble signaling factors, the temporal and spatial aspects of the signals, the localization of membrane or intracellular proteins and the extracellular factors to enhance the communication. Especially in pharmaceutical fields and regenerative medicine, the knowledge about will certainly bring the breakthroughs that will improve drug discovery and the rearrangement of cells and ECMs at single cell, multilayered cell, or tissue level. For example, Ingber's group proposed an array-like formats to position and pattern the cells, allow them to attach to particular spots and then keep track of that area during cell growth for analysis (Chen et al., 1997) (Figure 1-4(b)). Surface coatings and patterning with particular size can be modified to optimize conditions for each cell type. This core technologies have been widely applied to microfabricated square-shaped patterns that allow for the analysis

of cell polarity of cytoskeleton (Thery, 2010; Thery et al., 2006a; Thery et al., 2006b), high throughput cell stretching for mechano-transduction single cell studies (Tseng et al., 2012), and the estimation of cell traction forces at the surface of arrayed pillars (Fu et al., 2010) (Figure 1-4(c-e)). Here, the selection, separation, and collection of single adherent cells with specific characteristics from a heterogeneous cell population are fundamental needs in many areas of cell biology, tissue engineering, and cell therapy.

Single-cell isolation methods have been developed to address various aspects of micro-environmental control measurements on fast timescales, and isolation of secreted bio-molecules. For the measurement of cellular responses at single-cell level, flow-cytometry integrated with automated microscopy has been widely used for the massive throughput combined with fluorescent labeling, which allows the quantitative determination of various protein levels in a population of cells. For instance, the microfluidic devices have also been developed as one of the most powerful tools to manipulate (Di Carlo et al., 2006a; Di Carlo et al., 2006c; Di Carlo et al., 2006d) (Figure 1-4(f)), relocate (Deutsch et al., 2006), rotate, and pair single cells (Skelley et al., 2009) (Figure 1-4(g)). Non-adherent cells such as lymphocyte, erythrocyte, and monocytes naturally behave in a floating manner, and they are functionalized even while suspended in the flow (Figure 1-4(h)). While there are numerous strategies for practical identification and separation of non-adherent cells from a mixed population, the application of these techniques to manipulate single adherent cells is limited and still poorly established.

Traditionally, adherent cells have been detached from their growth surface mechanically or enzymatically for manipulation in the microfluidic devices. Since adherent cells cannot survive without adhering on a substrate, the process to detach cells them from a substrate results in cellular perturbations such as loss of morphology, removal of cell surface markers, and alterations in cell physiology. To avoid these perturbations, a platform for manipulating adherent

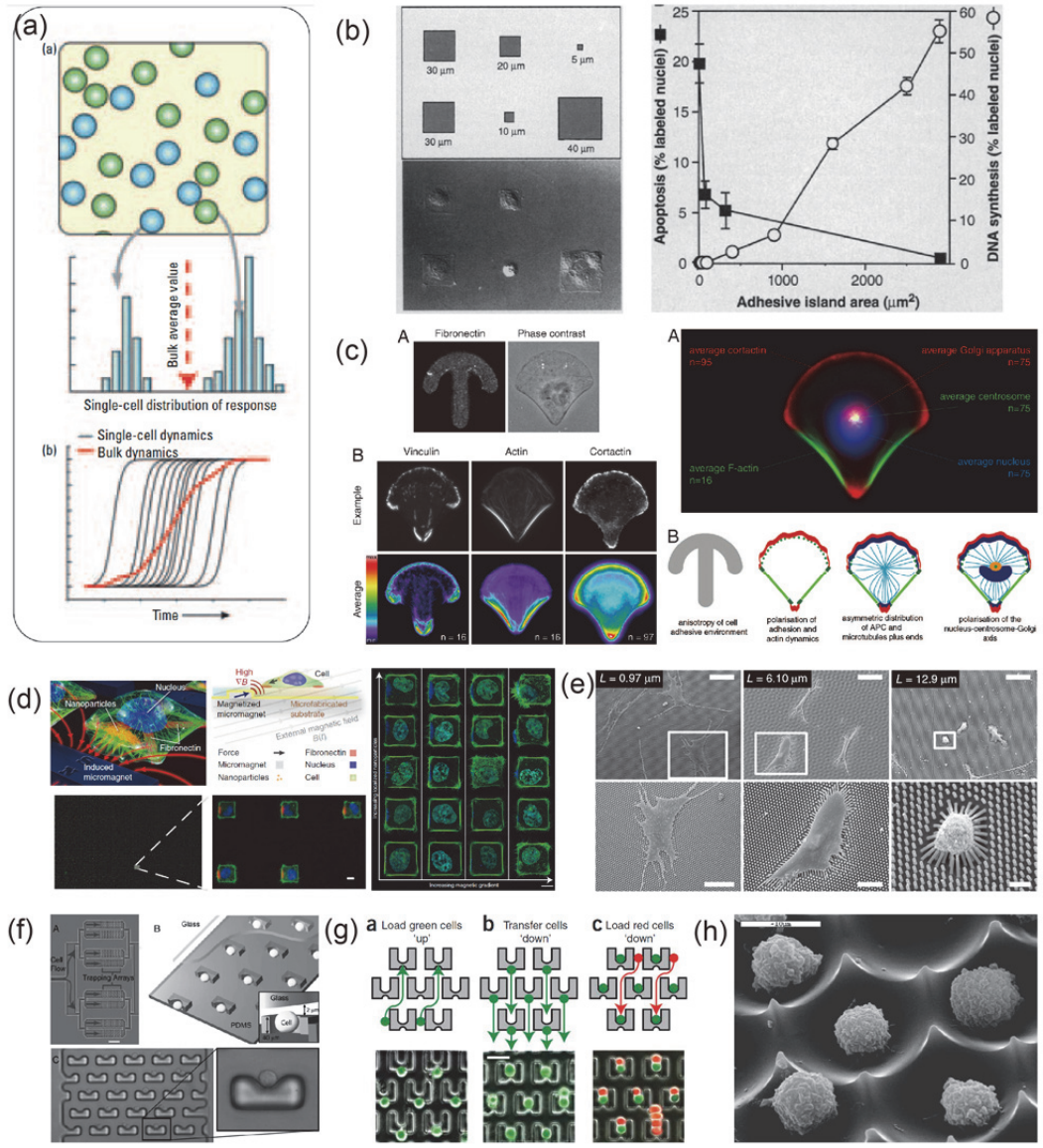

Figure 1-4. Single cell analysis of cell behaviors and morphology. (a) Population heterogeneity in distributions causes misleading of single cell behavior (Di Carlo et al., 2006b). (b) ECM micro-printing method to isolate adherent cells (Chen et al., 1997). (c) Micropatterns to control the morphology of single adherent cells (Thery et al., 2006a; Thery et al., 2006b). (d) Magnetic manipulation of single square-shaped adherent cells (Tseng et al., 2012). (e) Micropillars to measure a traction force of single adherent cells (Fu et al., 2010). (f) A microfluidic channel for trapping and making an array of single cells (Di Carlo et al., 2006d). (g) A microfluidic device for pairing and fusion single cells (Skelley et al., 2009). (h) Microwell-base single cell array (Deutsch et al., 2006). All images were transferred from each reference.

cells without stripping the cells from their growth surfaces would be of great value in the investigation of live adherent cells with their adhesive state preserved. Accordingly, Integration of the technique to track biological responses in individual cells with the mobile substrate to preserve their adhesive properties of adherent cells would facilitate to bridge the gap between isolated single adherent cells and cells with cell-cell communications during the process of repositioning cells.

1.2 Previous works

Toward the multi-angle observation of adherent cells, we will discuss the previous approaches to observe adherent cells for and point out the disadvantages of the previous methods. In this section, we review the microscopic experimental setup toward multi-angle observation, including the inclination of stages and culture dishes, and the stacks of optically sectioned in-focus images, followed by the technology for manipulating and inclining multiple and single adherent cells themselves.

1.2.1 Inclination of microscopic components

The modern, detailed understanding of cell architecture including cytoskeleton and plasma membrane is based on optical and electron microscopy (Dormann et al., 2006b). All optical microscopes designed for viewing cells share the same basic components of the light path: ocular lens, objective lenses, focus knobs for adjustment, stage to hold the cell-culture dishes, light source, diaphragm and condensers. Many researchers have developed their own experimental setups to optimize the viewing angle toward multi-angle observation by rearranging the position of two following components: the stages and objective lenses. In the previous reports, reconstruction of 3D models of zebrafish embryo, Medaka embryo, and single tumor cells have been reconstructed by inclining the stages loading cell-culture dishes or

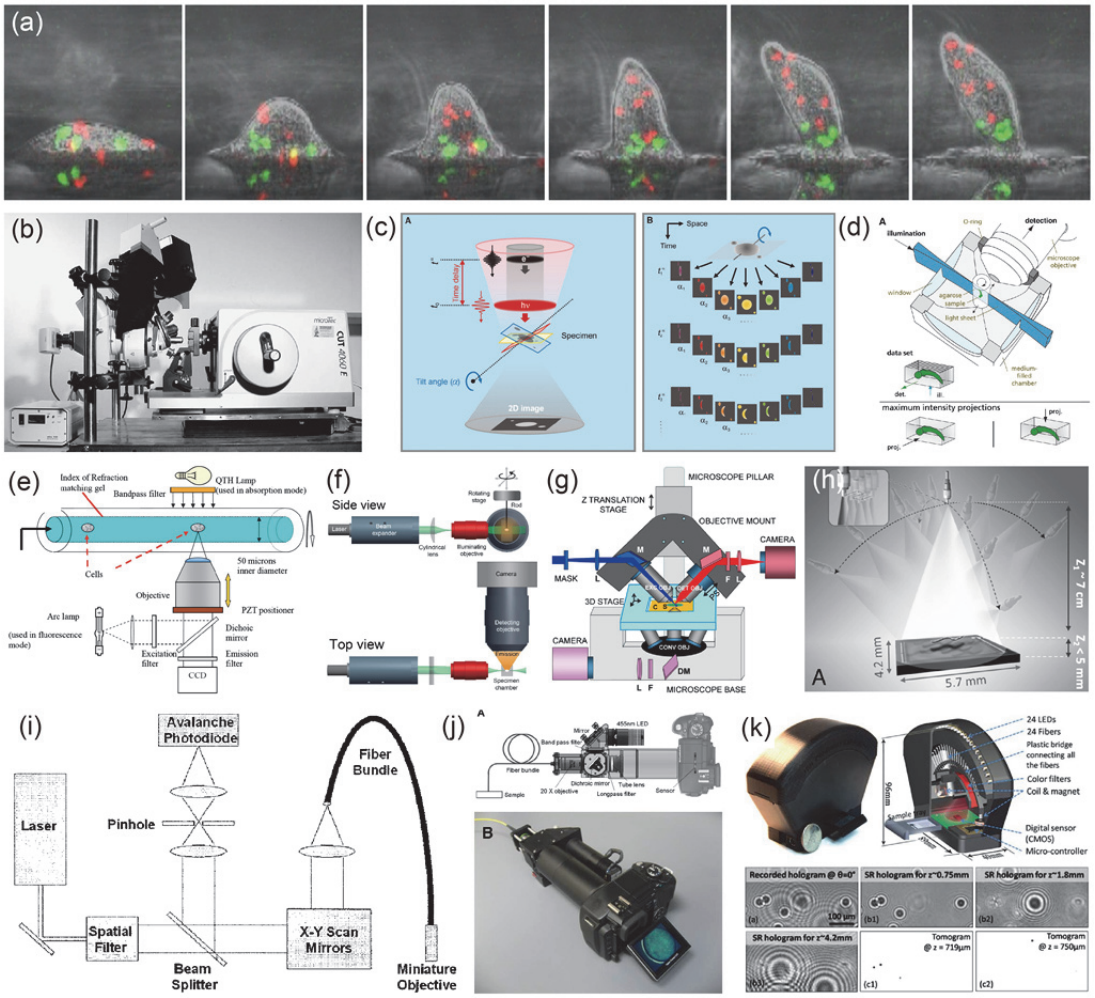

Figure 1-5. Multi-angle observation of biological samples. (a) Multi-angle observation including side view of a mound of wild-type cells containing a small number of fluorescently labelled protein (Dormann et al., 2006a). (b-d) Experimental setup to incline the stages that are loading cell-culture dishes. Microscope equipped with fluorescence filter sets and a digital video camera was modified to align the optical axis by changing (b) the block holder (Weninger et al., 2006), (c) stage direction (Kwon et al., 2010), and (d) rotating the cell-encapsulated sample (Huisken et al., 2004). (e-g) Microscopic optical pathway was inclined by changing the position of objective lenses (e) (Santi, 2011), (f) (Wu et al., 2011), (g) (Isikman et al., 2011a), and (h). (h-j) Fiber microscopes are utilized for the multi-angle observation. (i) (Carlson et al., 2005), (j) (Shin et al., 2010), (k) (Isikman et al., 2011b). All images were transferred from each reference.

rotating the cylindrical hydrogel tube that embeds cells as shown in Figure 1-5(b-e) (Huisken et al., 2004; Kwon et al., 2010; Weninger et al., 2006). Some researchers observed the living samples such as rat brain, zebrafish head, neuronal cells, and whole body of *C. elegans* by inclining objective lenses as shown in Figure 1-5(e-h) (Isikman et al., 2011a; Santi, 2011; Wu et al., 2011). Fiber-based optical microscopes have been highly developed, which mainly aim at *in vivo* 3D imaging with high resolution or clinical use (Figure 1-5(i-k)) (Carlson et al., 2005; Isikman et al., 2011b; Kumar et al., 2008; Shin et al., 2010). Fiber-optic elements are used in various ways to miniaturize or bring flexibility to the implementation of bright-field and fluorescent microscopes, which leads to multi-angle observation from the desired orientations. All of these previous studies mentioned above monitored cellular events through the cell membrane by using inclined microscopic components, and revealed the structure and motility of cells, and protein involved in membrane deformation. Nevertheless, there are still technical limitations on inclination of the optical pathway because cell culture dishes and microscope components, such as lenses and stages, physically obstruct each other. In addition, the difficulty in the phase contrast observation arises from the large scale alterations in the experimental microscope setups and optical pathway, which cause to hinder the observation of colorless and transparent micro-sized samples such as living cells. Furthermore, it is difficult to adjust the microscopic focus on the targeted samples after light path optimization, which interferes with the high-resolution observation of the plasma membrane surface.

The fundamental principles of electron microscopy are similar to those of optical microscopy; the major difference is that electromagnetic lenses, focus a high velocity electron beam instead of visible light. In typical electron microscopes, electrons have the properties of a wave with a wavelength of only 0.004 nm (Joy, 2002); thus, a resolution of 0.10 nm can be obtained under optimal conditions, which is 2000 times better than the resolution of the optical microscopy. Because electrons are absorbed by atoms in air, the microscopic system with

targeted samples must be maintained under an ultrahigh vacuum. Although this approach reveals much information, a critical question about such results is how true to life the image of a biological specimen that has been fixed, stained, and dehydrated. Because we cannot obtain "real" view of a living cell in electron microscopes, it is essential to establish the techniques for multi-angle observation of living adherent cells with high magnification.

1.2.2 Assembly of focal stack of 2D images into 3D images

A fast and sensitive acquisition of the cross-sectional images from reconstructed 3D data is one of the main challenges in observation of living adherent cells. Multidimensional imaging of a spatiotemporal pattern of protein expression offers critical information of various cellular vital functions and dynamics of living cells. Since the last decade, much attention has been paid to the techniques to obtain the three-dimensional (3D) image of cellular structures by means of a focused laser beam. Among these technologies, confocal laser scanning microscopy (CLSM) has been used to resolve the structure of numerous topologically complex cells and tissues, including the deformation in cell plasma membrane and the networks of cytoskeletal fibers in the cytoplasm. CLSM avoids the problem in the inclined microscopic system by visualizing fluorescent molecules in a single plane of focus, thereby acquiring optically sectioned in-focus images from selected depths. At any instant during confocal imaging, only a single small part of a sample is illuminated with exciting light from the focused laser beam, which rapidly moves to different spots in the sample focal plane. This system enables us to assemble of a focal stack of 2D images acquired using sequential refocusing from 3D images for the cross-sectional images by using a reconstruction algorithm to understand interior structures of adherent cells. Deconvolution algorithms are also commonly applied to 3D data in applications where photo-damages and acquisition times are limiting factors and confocal imaging is not reached.

Although CLSM allows us to observe the cells from multiple angles, this method suffers

from the limitation in a marked difference between the lateral and axial resolution. Spatial resolution in axial direction is generally more than three times inferior to that of lateral plane; the details of intracellular structures are obscured by this effect (the detailed explanation of the principle behind this difference is provided in the experimental section). To overcome the limitations, alternatively, high axial resolution has been enriched in ultra-resolution microscopes with imaging modalities, such as wide-field, laser-scanning confocal, spinning-disk confocal and light-sheet microscopy. However, such specific microscopes are too tedious and expensive to be accessible and do the efficient experiments with multiple trails. Besides, this microscopic observation process is time consuming and can yield ambiguous spatiotemporal information because the focal planes are recorded not simultaneously but only single layer. Thus, the system that we propose in this study is designed with the following two considerations: (i) long term scanning leads to photobleaching and phototoxicity; (ii) multiple focal planes lead to dominating depth-induced spherical aberration. Here, if we make the targeted samples physically turned perpendicular to the optical detection axis, we could acquire a cross-sectional image by only single scanning layer at the desired orientation and direction. Furthermore, photo-damages derived from multi-layer scanning and artifacts arising from absorption and scattering within the sample in conventional 3D reconstructed images would be suppressed.

1.2.3 Cell-laden micro-carriers

As the platform to manipulate and incline the cells, we focused on the engineered mobile substrates to culture adherent cells and maintain their adhesive property while the manipulation. Conventionally, various microfabrication technologies have contributed to the isolation and manipulation of single adherent cells, as discussed in 1.3.3. Genetic transfection method to visualize specific protein inside living cells integrated with cell-micropatterning method can also yield the single cell investigation, such as the estimation of the distribution of protein

content in specific single cells. To further apply this method to multi-angle observation, the means to manipulate, incline, and immobilize cells at desired angle and timing is highly required to advance the understanding of cellular behavior, however still poorly established.

Microfabricated mobile platforms enable adherent cells to retain their adhesive properties during manipulation. Hui et al. has reported the mobile cell co-culture platform for the dynamic regulation of cell-cell interactions via direct manipulation of adherent cells with micrometer-scale precision (Hui et al., 2007) (Figure 1-6(a)). The micro-machined silicon comb chips to separately culture two different types of mass-cultured adherent cells successfully control the distance between them, more than 80 μm. Their findings indicate that the maintenance of the hepatocellular phenotype triggered by fibroblast cells requires direct contact for a few hours, which amplifies the secretion of proteins. Allbritton's group proposed the use of micro-sized blocks mounted on a glass substrate as a means to separate live adherent cells individually (Gunn et al., 2010; Salazar et al., 2007; Wang et al., 2010; Wang et al., 2007; Wang et al., 2008) (Figure 1-6(b, c)). Onoe, et al., have also presented a method for easy handling of single adherent cells by using mobile and disk-shaped glass (SiO_2) microplates (Onoe et al., 2008) (Figure 1-6(d)). These cell-laden microcarriers have proven beneficial for the separation and collection of various types of specific adherent cells from a mixed population at both multiple- and single-cell level. Nonetheless, these methods suffer from inherently low throughput because adherent cells are released from substrates one-by-one via time-consuming and highly laborious techniques based on focused laser pulses or mechanical flow. The block-shaped microcarriers also hamper precise control of the cell-adhesion area and cell morphology because cells migrate randomly around the surface of the blocks. Beside the application to the angle-tunable manipulation is still poorly accomplished (Gunn et al., 2010) (Figure 1-6(e, f)). It is limited by the inability to precisely control the inclination of cell-laden substrates and angle tunability for the stable observation under the microscopes. These

disadvantages lead to low efficiency and difficulty in analysis of controlled number of adherent cells, and handling or manipulation in the desired orientation. Additional properties to incline adherent cells would broad the efficiency of multi-angle observation while preserving adherent property of cells.

1.3 Challenges

When we overview the previous works for multi-angle observation, we can notice each challenge that all of previous works have. In the system to incline the stages of microscope setup, the viewing angle can be controlled and optimized toward multi-angle observation, but

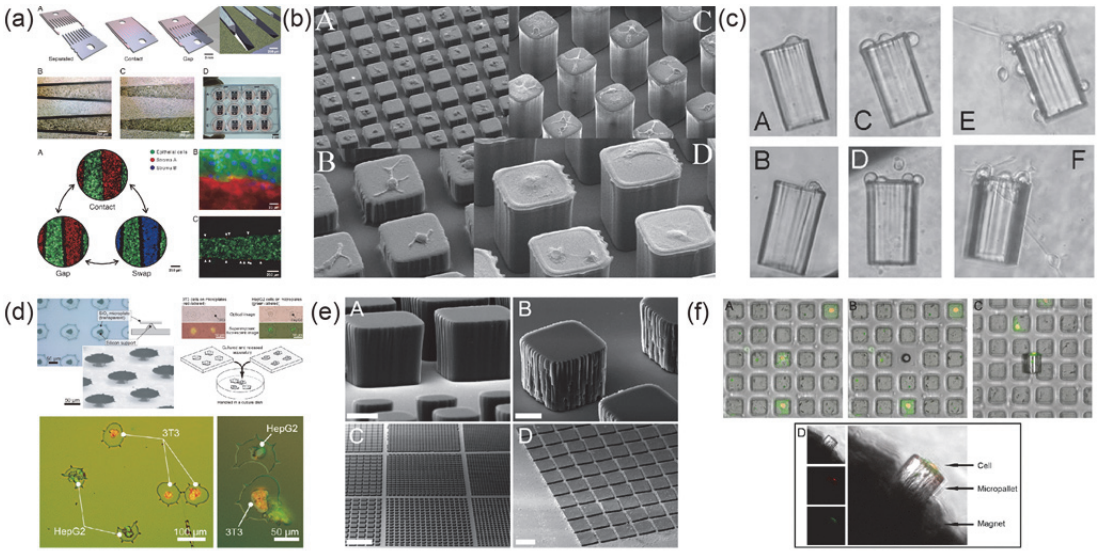

Figure 1-6. Mobile substrates to manipulate adherent cells. (a) Mobile cell co-culture platform for the dynamic regulation of cell-cell interactions (Hui et al., 2007). (b, c) Micropallet technologies to manipulate, sort and pick up adherent cells: (b) (Wang et al., 2007;), (c) (Salazar et al., 2007). (d) Mobile and disk-shaped glass (SiO_2) microplates (Onoe et al., 2008). (e, f) Magnet-active micropallets to handle adherent cells in the applied magnetic field (Gunn et al., 2010). These micropallets were fabricated by SU-8 photoresists embedding magnetic particles. All images were transferred from each reference.

there are still technical limitations in inclination of the optical pathway because cell culture dishes and microscope components physically obstruct each other. When focusing on assembly of focal stack of 2D images into 3D images in the microscopes such as CLSM, they suffer from inherently low axial resolution, resulting in obscure obtained images of multi-dimensional intracellular structures. Here, if the cells were on the mobile micro-carriers physically turned perpendicular to the optical detection (lateral) axis, we could acquire high-resolution cross-sectional images of cells. There have been previous reports about cell-laden micro-carriers such as the block-shaped microcarriers. However, the additional function to control the inclination angle is poorly established. Besides, the block-shaped microcarriers hamper precise control of the cell-adhesion area and cell morphology because cells migrate randomly around the surface of the blocks. These disadvantages lead to low efficiency and difficulty in cell handling, observation, and analysis. Taken together, three requirements must be fulfilled as follows:

i). High angle tunability

ii). Ability to maintain cellular adhesive property

iii). Low cytotoxicity

Here, our approach is fabricating the mobile platform with flat surface to culture the controlled number of adherent cells, incline with high angle tunability, and acquire cross-sectional image of loaded cells with a resolution exceeding that of conventional CLSM.

1.4 Objectives and significance

Main objective of this dissertation is to establish an angle-tunable mobile microplate for culturing and inclining adherent cells that can be “added-on” to conventional microscopes. We propose two types of mobile microplate structure: hinged microplates, termed microflaps to manipulate multiple adherent cells; microplates without hinges, termed microdisks to culture

single adherent cells and increase the degree of freedom in location and motility. Both of these platforms can load the adherent cells onto its surface of device and facilitate multi-angle observation of cell morphology, which will have enormous potential for fundamental cell biological studies, biomedical applications, and drug testing. To this end, we first aim to design and fabricate a reliable and multifunctional platform to realize the high angle-tunability, maintain adhesive properties and morphology of cells during the manipulation, control of the number of cells, and reduce the cytotoxicity. We carefully select the material for this platform from three perspectives: biocompatibility, transparency, and magnetic permeability. This platform should be facile to operate, be capable of handling large number of adherent cells simultaneously, and possess enough dexterity to allow for single cell manipulation. Subsequently, this technology for multi-angle observation will be extended to trace the invasion of parasite into host adherent cells.

The significance of this study contains three points as follows: high angle-tunability, experimental versatility of the devices, and availability for researchers in any research field. Although multi-angle observation can be achieved by conventional microscopic setups, they possess the limitations in angle tunability, easy adjustment of focal plane, and low resolution in axial direction. They are also too sophisticated, personalized or expensive to be accessed and used for multiple trials. Here, the platforms we develop in this dissertation are simple and inexpensive enough to allow for accurate and efficient analysis, which will eventually lead to user-friendly and accurate experimental setups. In this platform, it is possible to achieve high angle tunability ranged from 0 degree to 90 degrees, and be equipped to any types of conventional microscopies, which enables us to observe the biological phenomena or morphology with high magnification that has never been reported. Since this device is fabricated using only inexpensive materials through the microfabrication technologies, which leads to a promising method that can be mass-produced, with low piece-to-piece variations, and

available at low cost. This observation technique is thus user-friendly and broadly applicable for the researchers in any field.

1.5 Strategy and originality

Our strategy involves using microfabricated magnetically responsive microplates integrated with biocompatible and transparent materials. We aim at two points of strategies: the microfabricated structure and biocompatible materials. First, all of the devices are fabricated by utilizing a transparent biocompatible polymer, parylene and alginate hydrogel as the sacrificial

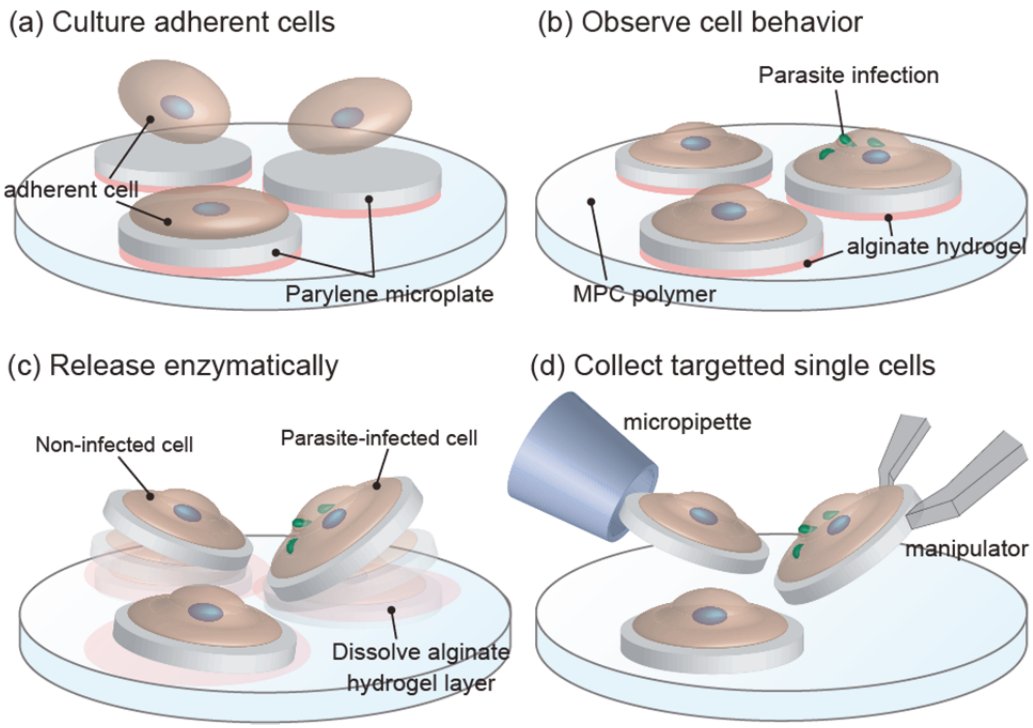

Figure 1-7. A schematic illustration of the procedure for handling adherent cells on mobile microplates. All of the devices are fabricated by biocompatible materials, parylene and alginate hydrogel. After the dissolution of alginate hydrogel sacrificial layer, the specific cells can be selected to manipulate and observe them. Reprinted with permission from (Teshima, et al, Small, 2014). Copyright 2014, Wiley.

layer as shown in Figure 1-7(a-d). The biocompatibility of parylene and alginate hydrogel ensures long-term culture of seeded adherent cells without cytotoxicity. Since high transparency of parylene does not disturb the light path of microscopes, it is possible to equip the microflap system to both upright and inverted microscopes. This system does not require an experimental setup in which the light path is inclined; these approaches thus overcome conventional problems of physical obstruction of microscope components that resulted in technical limitations on inclination of the optical pathway. An ability of microflaps to "add-on" to any types of conventional microscopy, which allows multi-angle real-time observation of inclined cells with high magnification. In this study, conventional lithography and soft lithography techniques will

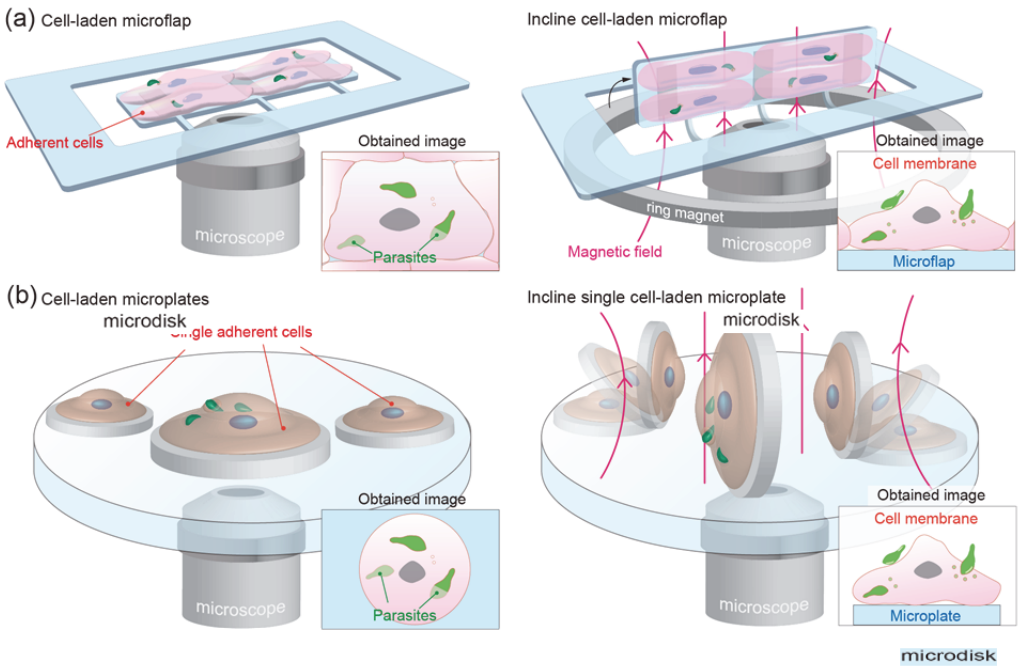

Figure 1-8. A schematic illustration of the procedure for magnetic inclination of cell-laden microplates. (a) Microflaps can be loaded with multiple adherent cells and incline them in the desired orientation. (b) Microdisks can isolate, rotate, and incline single adherent cells in the magnetic field. (a) Reprinted with permission from (Teshima, et al, Advanced Materials, 2014). Copyright

be utilized to fabricate all our devices.

Second, we design mobile micro-sized structure to achieve angle-tunability in cell-culturing substrates for multi-angle observation. High magnetic permeability of permalloy embedded in this platform facilitates easy control of inclination angle of cell-laden microflaps by controlling the strength of the applied magnetic field, enabling observation of the cells from multiple angles without physical microscopic obstruction or limited resolution. Figure 1-8(a, b) describes the schematic image of magnetic inclination of released cell-laden microplates in the desired orientation. Unlike electrically or thermo-kinetically actuated microflaps, magnetically responsive microplate does not require electric wiring, and large magnetic forces can be readily generated by putting magnets close to the cell-culture dishes. Remote actuation of cell-laden microflaps from the outside of culture dishes enables us to avoid the risk of contamination and exposure to infectious microbes. Since the behavior and governing equations of magnetic inclination in micro-scale are well understood, it is possible to design robust, rough, and well-behaved manipulation of cell-laden substrates for precise control of inclination angles.

Collectively, this dissertation highlights sophisticated utilization of microfabrication technology to develop user-friendly platforms and engineered accurate models that magnetically manipulate both multiple and single adherent cells and reveal the shape of their cell plasma membrane and cytoskeleton. In addition, the developed platforms allow for accurate, efficient, and effective analysis of interaction between infectious microbes and their host cells, which will eventually lead to advancements in fundamental medical biology and anti-microbe drug development. Our approach is unique in offering multidisciplinary perspectives. While the problem that needs to be solved in this study originates from cell biology, the means to solve it is based on the microfabrication technologies including soft lithography, mechanics of materials, and optics. Furthermore, the feasibilities of fabricated devices are demonstrated by not only the observation of cell, but also the microbiology including microbial infection. Therefore, this

research can be achieved only by integrating cross-sectional perspectives in the multiple fields mentioned above. The eventual translational goal is to introduce our easy observation system to a wide range of researchers, especially biologists or medical investigators, to enable efficient and reliable experimental setup to obtain high resolution cross-sectional images of targeted samples.

1.6 Thesis Outline

In this dissertation, we will develop a mobile substrate for inclining adherent cells and biomedical applications based on the analysis of microbe-host cell interactions. Chapters 1 introduced background to analytical measurements of cell components and multi-angle observation based on optical microscopes. This chapter establishes a background for the theoretical simulation and experimental results shown in Chapters 2, 3 and 4.

In Chapter 2, we will cover the theoretical aspects and introduce the concepts behind our inclination system integrated enzymatic releasing. This chapter provides a better understanding of what physically occurs in the magnetic inclination of both microflaps and microdisks. We will also discuss how to control the number of cultured cells. Finally, a brief introduction for the materials used and the fabrication methods for all the devices, which includes various experiment setups, reagents and procedures for conventional soft lithography techniques will be outlined. Extensive details regarding fabrication are provided in the appendices.

Chapter 3 will describe and their respective experimental results and discussions for the (i) verification of the design criterion for our microflaps, (ii) preliminary testing of loading, culture and patterning of adherent cells, (iii) feasibility study of the multi-angle observation of cells inclined on the microflaps, and (iv) observation of parasite infection into adherent host cells as a model for observation of the plasma membrane.

In Chapter 4, a series of experiments were conducted to demonstrate that the microdisks can

be used as a tool in isolation and multi-angle inclination of single adherent cells, and applications to the microscope observation, namely, as the ability to “add-on” to the conventional microscopy. We also demonstrate the significant benefits available to biomedical single-cell investigations by the selection and manipulation of single parasite-infected cells to. For the latter demonstration, we will discuss the preliminary data on confocal observations of the dynamics and cell-cell interactions between parasites and adherent host cells.

Finally, we will present the conclusions derived from this study in Chapter 5.

CHAPTER 2

DESIGN & FABRICATION

Under this chapter, we will discuss the design methodologies for magnetic actuation, strategies for raising the resolution of obtained microscopic images, and fabrication process that are required to realize a mobile substrate to manipulate adherent cells. First, we derive the design criterion for magnetic actuation for inclination based on the estimation of values of torques. We will also show that this criterion is sufficient to incline the devices at desired orientation with high angle-tunability, which allows the multi-angle observation. Second, the concept for resolution of obtained images in the microscopy will be introduced. Third, we will discuss the method to pattern adherent cells at multi-cell level and single-cell level using extracellular matrix and polymers for cell adhesion inhibition. Finally, fabrication methods for all the devices including preparation of adherent cells and infectious parasites, conventional soft-lithography and photo-lithography techniques will be covered.

2.1 Design criteria of magnetic actuation

2.1.1 Design of microflaps and microdisks

When we consider the design of angle-tunable cell-laden substrate, there are three following requirements for the fabrication process: (i) the surface of cell-laden substrates is flat to maintain the morphology and shape of adherent cells; (ii) the driving force to actuate mechanically is based on room temperature to escape thermal cytotoxicity and electrolysis of

media; (iii) the out-of-plane structure composed of flat substrate and anchoring flexible mobile areas that enables physically stable and long-term observation. There are a lot of conventional devices with the driving force to actuate flat substrates magnetically (Chung et al., 2011; Drotlef et al., 2013; Kim et al., 2011b), thermokinetically (Kaajakari et al., 2003), or electorically (De Volder et al., 2012; Kim et al., 2013; Suzuki et al., 1994; Takeuchi et al., 2003) to realize micro-engineered opto-electro-mechanical components such as free-space beam-steering reflectors (Daneman et al., 1996), tunable Fabry–Perot etlons (Wu, 1997), and corner cube reflectors (Reid et al., 1997). Both thermokinetical and electrical actuations require electric wiring, causing to the temperature change and electrolysis that influence on cellular behavior. On the other hand, magnetically responsive microstructure allows remote not only room temperature experiments, but also actuation of cell-laden microflaps from the outside of culture dishes, which enables us to avoid not only the temperature change but also the risk of contamination and exposure to infectious microbes. Beside, from the perspective of material mechanics, the actuation mechanism is mainly categorized into three deformations: tension or compression (Jager et al., 2000a; Jager et al., 2000b; Kaajakari et al., 2003), torsion bar (Akiyama et al., 1997; Chang et al., 2009; Judy et al., 1997; Tsai et al., 2011), and bending of beam (Pister et al., 1992; Yi et al., 1999; Zou et al., 2001). Among these deformations, two types of anchoring mobile structure, including torsional beams and hinges, have been commonly utilized for magnetic actuation; the low stiffness of the torsional/hinge beams allowed for large angular. Compared with the torsional beams, hinge beams have less degree of freedom in mobility or vibration, which leads to physically stable and long-term observation of loaded cells. In addition, since the proposed devices contain the biocompatible sacrificial hydrogel layer (the details are explained in the section 2.2.3), it is difficult to obtain thick sacrificial layer due to the low viscosity of hydrogel. Since the fabrication process of hinged structures permits the thin sacrificial hydrogel layer (< 1 μm), we employed the magnetic actuation of hinged

microstructure in this study.

In this dissertation, we propose a microfabricated magneto-active flap and disk-shaped mobile substrate integrated with an enzymatic batch release, termed a microflap and microdisk, respectively. Both of these devices achieve angle-tunability in cell-culturing substrates for multi-angle observation. To make the microflaps and microdisks, we used a combination of three materials: a transparent biocompatible polymer, parylene; an alloy with high magnetic permeability, permalloy; alginate hydrogel for the sacrificial layers. By using a microfabrication technology with these three materials, we produced an array of microstructures for manipulating

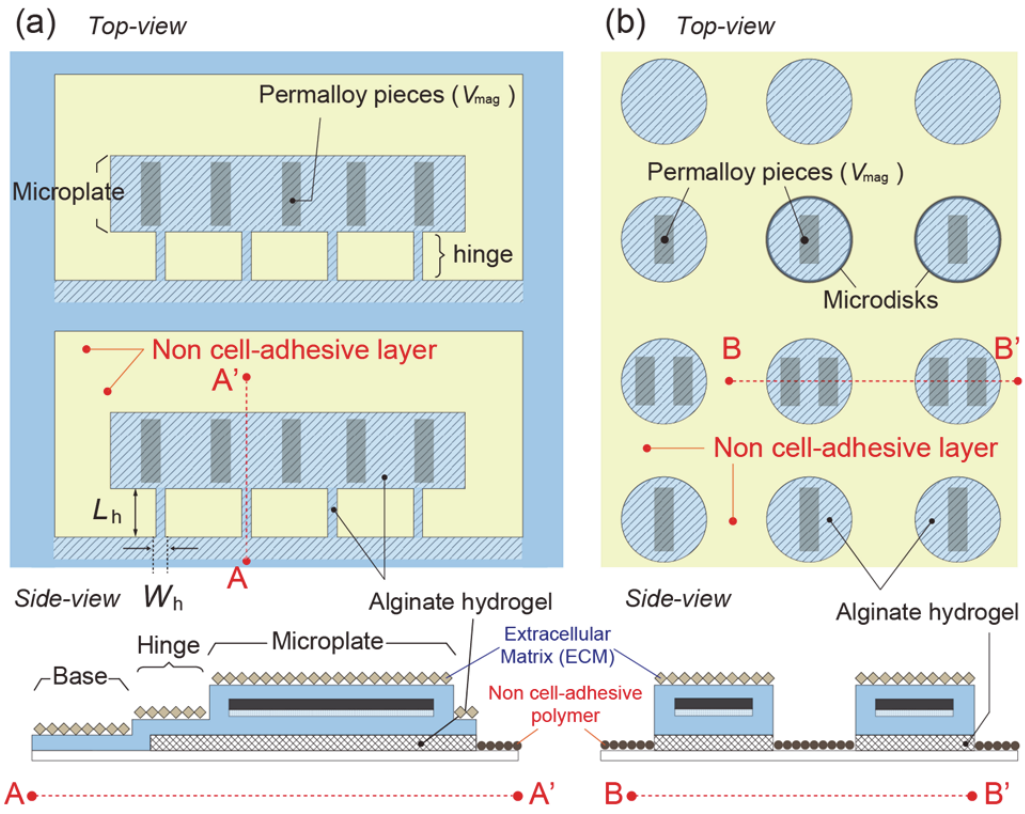

Figure 2-1. Geometry of mobile substrate for culturing adherent cells. Both of microflaps (a) and microdisks (b) are composed of three parts: parylene structure with embedded permalloy pieces, and sacrificial layer made from alginate hydrogel underneath a glass substrate. (a) Reprinted with permission from (Teshima, et al, Advanced Materials, 2014). Copyright 2014, Wiley.

living adherent cells without cytotoxicity.

The geometry of the microflap and microdisk is illustrated in Figure 2-1(a) and 2-1(b) (the details of the fabrication process are provided in the fabrication section). A parylene microflap was composed of three parts: square parylene microdisks with embedded permalloy pieces, a base layer that directly attaches to a glass substrate, and hinges that anchor the microdisks and base layer. The hinges of microflaps were composed of multiple 8 μm hinges in width. The fabricated microflaps were immersed in the phosphate-buffered saline or cell culture media throughout the magnetic manipulation and cell culture process. To release the microflaps from the glass substrate, we enzymatically dissolved the alginate sacrificial layer underneath the microdisks. A set of multiple rectangular permalloy pieces were embedded in the microdisks; this magneto-active material was used for the magnetostatic actuation of the microflaps under an external magnetic field.

We also demonstrate a disk-shaped mobile microdisk system for manipulating single adherent cells as illustrated in Figure 2-1(b). We fabricate microdisks to culture single cells by parylene and permalloy. As the sacrificial layer of the microdisks, we also use alginate hydrogel that can be dissolved by adding an enzyme; the enzymatic dissolution of the hydrogel achieves a batch-release process of arrayed cell-laden microdisks without cytotoxicity. Furthermore, the disk-shaped structure of the microdisks allows the cells to settle only on the microdisk surface. These microdisks allow us to culture various types of mammalian adherent cells on the microdisks to investigate the single-cell loading efficiency, cell behavior, and cell morphology.

In the case of both microflap and microdisk, the array of parylene structure with embedded permalloy pieces facilitates the batch manipulation of cell-laden mobile substrates under the control of a magnetic field, enabling observation of the cells from multiple angles without physical microscopic obstruction or limited resolution. The parylene surface and the glass substrate are coated with cell-adhesion protein and non-cell-adhesive polymer, respectively;

thus cells are patterned only onto parylene surface. This system does not require an experimental setup in which the light path is inclined, and it is suitable for multi-angle observation of plasma membranes under the conventional microscope. Furthermore, the micro-sized inclination of the cell-laden microflaps facilitates easy adjustment of the microscopic focus, which enables cellular observation with high-magnification lens.

2.1.2 Concept and design criterion of microflap

The motion of inclination of cell-laden microdisks was caused by the bending hinges that functions as the cantilever beams. Due to rigid connection between the out-of-plane microflaps and the hinges, a magnetic force was transferred to the microflaps, inducing hinges. The permalloy pattern is rectangular shaped, so that a long axis of patterns is aligned to the same direction of magnetic fields. When the hinges were bent, the surface of microflaps remained flat and was not deformed. The movement of the microflap under the magnetic force induced by the magnetic easy axis can be analyzed in terms of a simple analytical model. Under the magnetic field, the microflap experiences both a magnetic torque owing to the induced magnetic moments of the rectangular permalloy pattern and a mechanical restoring force owing to the deflection of the hinges. Consequently, the microflaps with permalloy pieces of squared shapes can be rotated off the glass substrate in a predetermined sequence, so that the inclination with optimized angles becomes possible. This actuation method is space-efficient and capable of addressing a batch-scale inclination in parallel. The behavior of a ferromagnetic material in a magnetic field can be explained as follows. The permalloy pattern is rectangular, so the long axis of the pattern was aligned in the direction of the applied magnetic field. With an external static magnetic field, H_{ext}, applied perpendicularly to the substrate as shown in Figure 2-2(a), a permalloy film interacts with H_{ext} to induce a magnetic torque τ_{mag} acting on a sputtered film.

During the testing, the magnitude of the magnetic field is increased slowly by manually

outing magnets closer to the microflaps, so that the loading is applied in a quasistatic state. The magnitude of the torque, therefore, can be expressed as (Judy et al., 1996; Judy et al., 1997; Yi et al., 1999; Zou et al., 2001):

$$\tau_{\text{mag}} = V_{\text{mag}} M H_{\text{ext}} \cos\theta \tag{2-1}$$

where V_{mag} is the volume of the sputtered permalloy film and θ is the angle between inclined

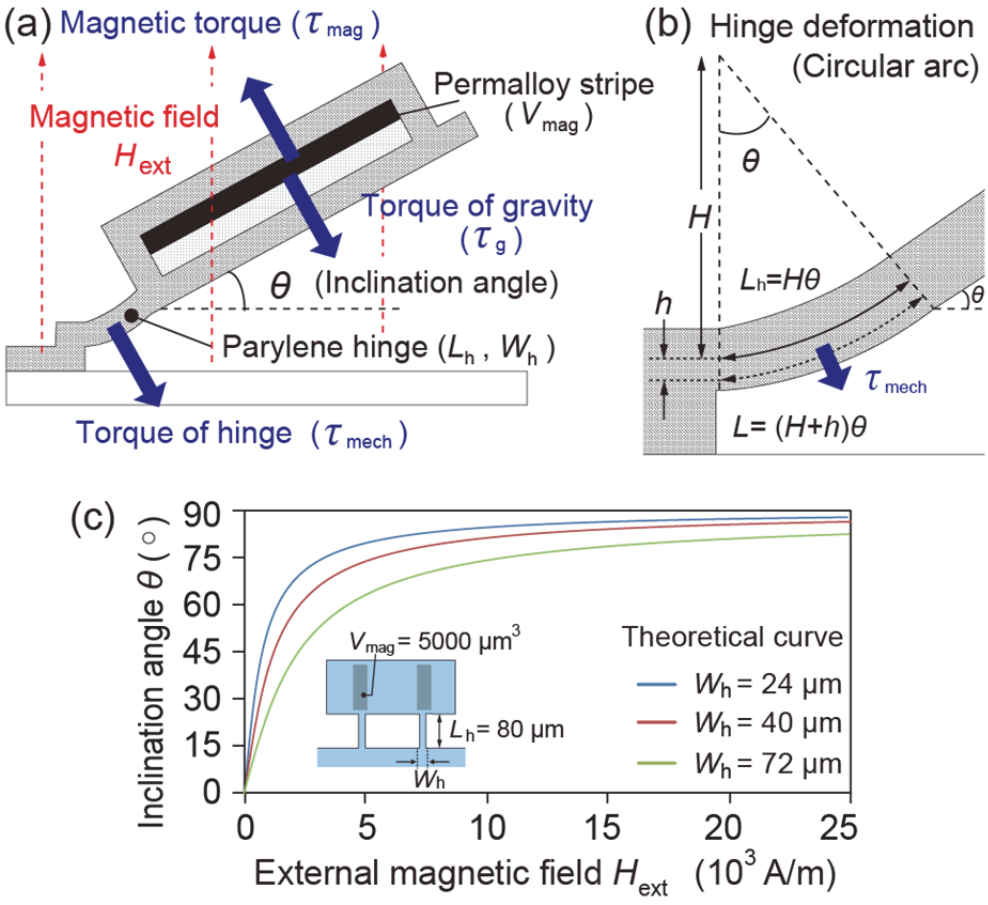

Figure 2-2. Hinge deformation of microflaps. (a) A schematic illustration of deformed microflaps. We can define three torques: the magnetic one, the one of gravity, and torque of hinges. (b) A schematic image of deformed hinges. (c) A graph of simulated inclination angle of microflaps. Reprinted with permission from (Teshima, et al, Advanced Materials, 2014). Copyright 2014, Wiley.

microflaps and the glass substrate. M is the spontaneous magnetization of permalloy. Because the hinge area is made of the elastic polymer, it functions as a beam to make microflaps inclined. The microflap can be regarded as a rigid plane because it is much larger than the hinges with 8 μm in width. Because of the elastic deformation, the distortion of hinges, ε is calculated as:

$$\varepsilon = \frac{(H+h)\theta - H\theta}{H\theta} = \frac{h}{H} \tag{2-2}$$

where H and θ are curvature radius of hinges (Figure 2-2(b)). The bending moments, τ_{mech}, generated by the elastic deformation of the hinge is given by

$$\tau_{mech} = \int_A \varepsilon E_h \, h \, dA = \int_A \frac{h^2 E_h}{H} dA = \frac{E_h}{H} I \tag{2-3}$$

where E_h, A, and I indicate the Young's elastic modulus, cross-sectional area, and geometrical moment of inertia of the parylene hinge, respectively. Since the cross section of the microflap is rectangular, torque of mechanical deformation τ_{mech} can be calculated by using the geometrical moment of inertia of microflaps as follows (Iwase et al., 2005):

$$\tau_{mech} = E_h \frac{W_h \cdot T_h^3}{12 L_h} \theta \tag{2-4}$$

where L_h, W_h, and T_h indicate the length, width, and thickness of the hinge, respectively. In this case, we must consider the effect from the torque produced by gravity, τ_g.

$$\tau_g = \{V_{pa}(\rho_{pa} - \rho_w) + V_{mag}(\rho_{pe} - \rho_w)\} \cdot \frac{d}{2} \cdot g \cdot \cos\theta \tag{2-5}$$

where V_{pa}, ρ_{pa}, ρ_{pe}, and ρ_w indicate the volume of parylene structure, the density of parylene and permalloy, and the density of water respectively; d is the diameter of microdisks. T_{field}, and τ_{mech} with τ_g become equal at the equilibrium state, and we can calculate the angular mechanical deflection with τ_{field}, and τ_{mech} because τ_g is much smaller than τ_{mech}. From these values, Iwase, et. al., showed the relation between the inclination angle of the hinged microstructure and an

external magnetic field can be calculated as follows:

$$\tau_{\text{mech}} + \tau_{\text{g}} = \tau_{\text{mag}} \tag{2-6}$$

The inclination motion of the microflaps was tuned by a magnetic field applied perpendicularly to the glass substrate. The gravitational force is negligible when compared with the magnetic force. By calculating the magnetic torque on sputtered permalloy and the torque generated by the elastic hinge deformation, the angle of inclined microflaps (θ) was analyzed as a function of an external magnetic magnitude (H_{ext}) as previously reported (Iwase et al., 2005; Iwase et al., 2006);

$$\frac{\theta}{\cos\theta} = \frac{12M}{E_{\text{h}}} \cdot \frac{V_{\text{mag}} \cdot L_{\text{h}}}{W_{\text{h}} \cdot T_{\text{h}}^{\,3}} \cdot H_{\text{ext}} \tag{2-7}$$

Since $\theta/\cos\theta$ is a monotonically increasing function of θ, the inclination angle increases as the right side of Equation (2-7) increases. With the fixed design of microflaps, the ratio of $\theta/\cos\theta$ tends to be linear in external magnetic magnitude. By changing the external magnetic magnitude, it is possible to rotate parylene microflap at different angles. With this model, we can easily and precisely control the actuator characteristics by varying the microstructure geometry during fabrication. In this study, the Young's elastic modulus of parylene polymers is about 3 GPa (Fang et al., 2005; Hassler et al., 2010). Permalloy has high magnetic susceptibility and large magnetic saturation values, 1.0 T (Donolato et al., 2013; Donolato et al., 2010), which makes a large torque produced even in a weak magnetic field. Therefore, the estimation of the bending angle θ as a function of H_{ext} with four independent parameters, V_{mag} = 5000 μm^3, L_{h} = 80 μm, W_{h} = 24, 40, and 72 μm (= 8.0 μm × 3, 5, and 9 hinges), and T_{h} = 350 nm, given by Equation (2-7) is simulated as shown in Figure 2-2(c).

2.1.3 Concept and design criterion of microdisk

To increase the degree of freedom regarding the mobility and inclination angle of microdisks, we removed the hinges from the microflap structure. The microdisk can be regarded as a rigid plane and rotated at the contact point of the glass substrates and microdisks as shown in Figure 2-3(a). In the case of microdisks without hinges, we take account of not the effect from the torque generated by the elastic deformation of the hinge, but only the effect from the torque by gravity; thus, the relation between the inclination angle of the microdisks and an external magnetic field can be calculated as follows:

$$\tau_{\mathrm{g}} = \tau_{\mathrm{mag}} \tag{2-8}$$

By substituting Equation (2-1) and (2-5) for (2-8), we obtain the following equation (2-9) about the external magnetic field strength:

$$H_{\mathrm{ext}} = \frac{V_{\mathrm{pa}}(\rho_{\mathrm{pa}} - \rho_{\mathrm{w}}) + V_{\mathrm{mag}}(\rho_{\mathrm{pe}} - \rho_{\mathrm{w}})}{V_{\mathrm{mag}} M_{\mathrm{s}}} \cdot \frac{d}{2} \cdot g \tag{2-9}$$

With the fixed design of microdisks, only one value of external magnetic magnitude, $H_{\mathrm{ext}} = H_0$, can be obtained where the equation (2-9) holds. Since this equation does not include the value of bending angle θ, this value of H_{ext} does not depend on the inclination angle of microdisks, and we can introduce one value of H_{ext} which leads to the equation (2-9). Compared with the inclination angle of microflaps, thus, the one of microdisks is unstable, resulting in the low angle tunability from 0 degree to 90 degree, when H_{ext} is changed. With this model, a permalloy has magnetic saturation values, 1.0 T, which makes a large torque produced. The estimation of the bending angle θ as a function of H_{ext} is described as Heaviside step function:

$$\theta[H_{\mathrm{ext}}] = \begin{cases} 0^\circ, & \tau_{\mathrm{g}} > \tau_{\mathrm{field}} \\ 90^\circ, & \tau_{\mathrm{g}} < \tau_{\mathrm{field}} \end{cases} \tag{2-10}$$

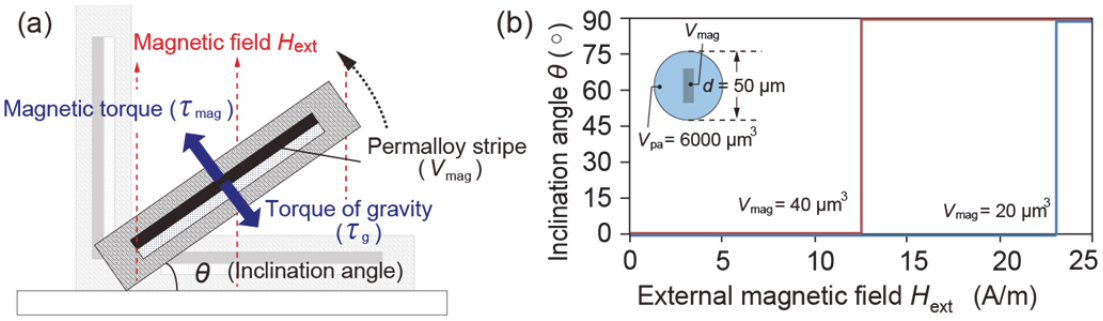

Figure 2-3. Magnetic inclination of microdisks. (a) Schematic image of magnetic inclination of microdisks. (b) A graph of simulated inclination angle of microplates with V_{mag} = 20 and 40 μm^3.

For example, when we fix five independent parameters as follows; V_{pa} = 4000 μm^3, V_{mag} = 20 μm^3, ρ_{pa} = 1.29 g/cm^3, ρ_{pe} = 8.75 g/cm^3, and ρ_w = 1.00 g/cm^3, d = 50 μm, the relation between inclination angle and external magnetic magnitude is simulated (H_0 =23.1) as shown in Figure 2-3(b). Because the inclination of microdisk has low angle tunability, the experimental setup to incline the direction of magnetic fields is required for multi-angle observation.

2.2 Lateral and axial resolution in confocal microscopy

Confocal laser scanning microscopy (CLSM) acquires optically sectioned in-focus images from selected depths within topologically complex cells and tissues by means of a focused laser beam, which allows the reconstruction of acquired images into three-dimensional artificial images of interior structures. The image formed by a point light at the focal plane is not a single point, instead the point distributed in a peripheral area from illuminated point-source, called point spread function (PSF). The PSF describes a disc with a central high intensity spot (Airy disk) surrounded by series of concentric bright and dark rings in the lateral plane (Airy pattern). According to Rayleigh criterion, the optical resolution of a lens is determined by the full width of half maximum (FWHM) of the airy disk which is a diameter of the inner ring where the

intensity drop to its half maximum. The radius of the inner ring is related to the numerical aperture (NA) of the objective lens; thus, the smaller the NA becomes, the larger the PSF and the bigger the inner ring, as a result, the lower the optical resolution becomes. Because the light diffraction depends on the wavelength of the light in use, the lateral resolution of CLSM is dependent on the NA of the objective lenses. When pinhole is infinite close to zero, (in practical, < 0.25 AU), the lateral resolution is calculated as follows:

$$R_{\text{lateral}}=0.37\frac{\lambda_{\text{exc}}}{\text{NA}_{\text{obj}}} \tag{2-11}$$

where R_{lateral}, λ_{exc}, and NA_{obj} indicates resolution of airy, wave length of excitation light, and the

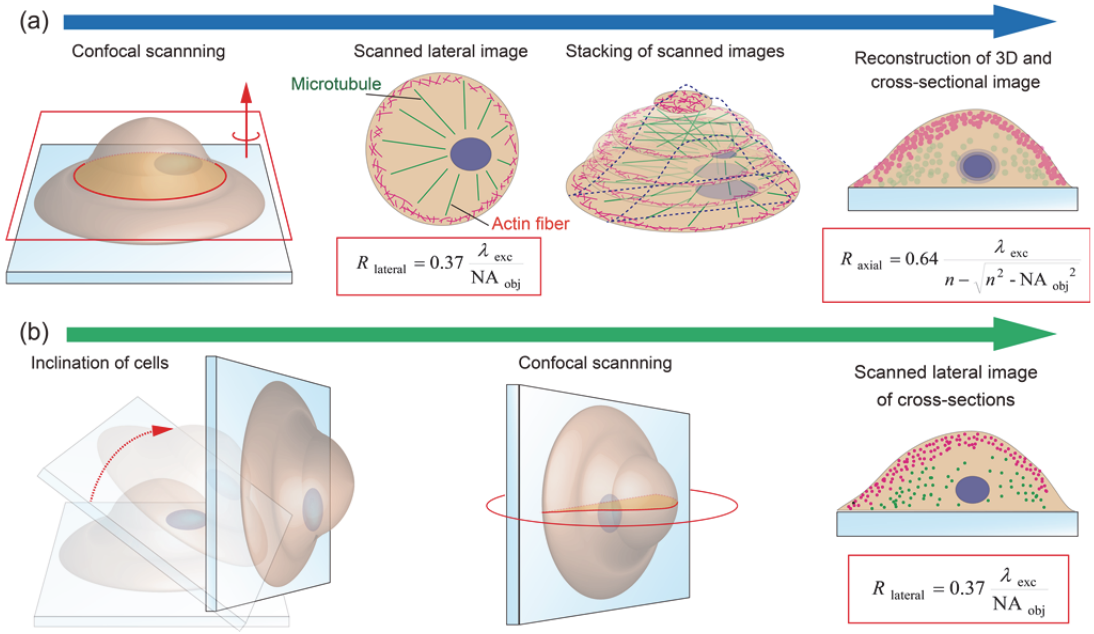

Figure 2-4. Resolution of CLSM scanning images. (a) To reconstruct the 3D or cross-sectional images, x-y scanned images are stacked layer by layer. Confocal system provides twice higher lateral resolution than axial one. (b) By using the system to incline adherent cells, the cross-sectional images are obtained by single scanning without reconstructing the 3D or cross-sectional images.

numerical aperture of the objective lens, respectively. Instrument parameters such as scan rate and pin-hole diameter can be set to achieve maximum resolution described in equation (2-11). However, since the pinhole size cannot be infinite to zero in reality, a value of coefficient in equation (2-11) is changed to ranging from 0.37 to 0.5, corresponding to the value of pinhole from 0.25 to 1 AU (Figure 2-4(a)).

Point spread function is applied not only to the focal plane horizontally, but also to the plane vertically. A perpendicular cut of the Airy disc shows elongated cones in the axial, which results in the difference of resolution between in lateral and axial plane. When pinhole is infinite close to zero (0.25 AU), the axial resolution is estimated as follows (Wilson, et. al., 1987; De Grauw, et. al., 1997):

$$R_{\text{axial}} = 0.64 \frac{\lambda_{\text{exc}}}{n - \sqrt{n^2 - \text{NA}_{\text{obj}}^2}} \tag{2-12}$$

where n is a refractive index of media and samples. For example, when we observe GFP-labeled samples with an oil-immersion objective with 1.4 NA and the 488 nm laser, the axial resolution is estimated to be about 400 nm. By comparing these two equations, (2-11) and (2-12), it is clearly seen that, in theory, confocal system provides more than twice higher lateral resolution than axial one. In this study, we propose a microfabricated platform to incline adherent cells at the desired orientation as shown in Figure 2-4(b). This platform makes it possible to obtain the cross-sectional images of cells by only confocal lateral scanning, which achieves a fast and sensitive acquisition of the cross-sectional images without reconstructing 3D data.

2.3 Patterning of adherent cells

2.3.1 Patterning of cell-adhesive and non-adhesive area

Selective surface modification by using a material to prevent non-specific binding is

generally required for the micro-patterning. Much attention have been paid to biomimetic phosphorylcholine (PC)-based polymers have, because they exhibit an excellent ability to inhibit protein adsorption and cell adhesion due to a large hydration layer; they have been widely applied to coating medical devices including artificial hearts, artificial joints, stents and biosensors. The duration of inhibition in the PC polymers lasts longer than in other materials, such as poly(ethylene glycol) (PEG), oligo(ethylene glycol) (OED), and bovine serum albumin (BSA), that were previously used to inhibit protein and cell adhesion. In general, to make micro-patterns of the polymers, researchers have developed a method using photo-reactive PC polymers with a photo mask, inkjet printing and micro-contact printing. However, these techniques require special photo-reactive polymers or technical skill for printing, resulting in the limitation in achievable resolution of the pattern. In this study, we utilized the coating of 2-methacryloyloxyethyl phosphorylcholine (MPC) polymer to repel cell and protein adhesion by the lift-off process of a deposited Al mask by chemical etching. MPC polymer enables the surface to inhibit protein adsorption and cell adhesion (Ishihara et al., 1996; Ishihara et al., 1998; Kuribayashi-Shigetomi et al., 2012). The advantages of this patterning method over conventional methods is uniformity and high resolution patterning over a large area due to the resolution of Al micro-sized pattern in standard lithography. We confirmed that a commonly available MPC polymer grafted onto a glass substrate was not ablated in the presence of Al etchant.

As a material of mobile substrates, we used poly (dichloro-di-para-xylylene) (parylene-C) that is one of a potential candidate for fabricating biomedical devices. Parylene-C is a thermoplastic, crystalline, pinhole-free, chemically inert as well as great barrier against diffusion of moistures and gases, and non-biodegradable polymer that is extensively used as a coating for insulating implantable biomedical devices. The parylene is biocompatible and easy to culture adherent cells, by forming a thin, flexible and transparent film when deposited by

chemical vapor deposition. Due to its high processability, it is widely applied for the substrate to culture adherent cells such as glial and neuronal cells (Delivopoulos et al., 2011; Delivopoulos et al., 2009), fibroblast cells (Wright et al., 2007), astrocytes (Unsworth et al., 2011), and hepatocytes (Chang et al., 2007), and embryonic stem cells, (Jinno et al., 2008). By taking advantage of the merits of our technique, the array of parylene microflap and microdisk was treated to form a non-cell-adhesive layer by using MPC polymer. This step enables the surface to repel proteins and prevent cell adhesion. The fabricated device comprises two areas: an array of fibronectin-coated parylene microdisks and non-cell-adhesive glass surface coated with MPC polymer. The hydrophobic parylene surface permitted the conjugation of functionalized extracellular matrix (ECM) proteins by using hydrophobic bonds (Chang et al., 2007); the surface was selectively converted to one type of ECM, fibronectin, by a 30-min immersion in fibronectin solution. To promote the cell adhesion of non-fibroblast cells, an appropriate ECM for each cell type might be selected, such as Matrigel for hepatocytes and HeLa cells or laminin for neuronal cells.

2.3.2 Loading of single adherent cell

To pattern single cells on single microdisks, the number of cells per microdisk must be controlled. We found that three parameters strongly regulate single-cell patterning: the size of the microdisks, the gap distance between adjacent microdisks and the cell density. First, we varied the diameter of the microdisks from 10 to 90 μm and counted the number of cells on each microdisk after suspending HFF cells at the optimized density. As the microdisks become larger, the average number of cells will increase because the yield of cell adhesion to the microdisk is regulated by the probability of cellular contact on the microdisk surface. However, if the diameter of the microdisks became smaller, the alteration to cellular geometry in the micropatterned substrates leads to cellular perturbations such as nuclear deformation, apoptosis

and cell division. Second, to investigate the effects of the gap distance between adjacent microdisks, we culture cells on the microdisks in variation of gap distance. Cells on the microdisks tend to bridge between pairs of microdisks, resulting in lower yield of single cell patterning on single microdisks. Third, the number of cells on microdisks is controlled by changing the density of suspended cells to realize single-cell cultures on single microdisks.

2.3.3 Biocompatible sacrificial layer

Release and mobilization of micro-structures can be achieved by dissolving sacrificial-layer, whereby a sacrificial layer is deposited underneath the free-standing structure that will be released. Subsequently, this sacrificial layer is dissolved or removed by selective etching. For example, silica (SiO_2), titanium, and aluminum etched by aqueous hydrofluoric acid (HF) and porous silicon etched by alkaline environment (KOH) are commonly employed as sacrificial layer in microfabrication process. The poor selectivity of these etching processes, however, limits its compatibility with fragile materials, and its toxicity makes it inconvenient or hazardous for inexperienced users. Accordingly, organic polymers, such as poly(imide), and photoresist, have been highly required for the sacrificial layers for surface micromachining. In the presence of cultured cells, the removal of poly(imide) films by reactive ion etching (RIE) and dissolution of photoresist by acetone are incompatible with maintaining the viability of cells. Sacrificial layers of photoresist are, therefore, restricted to under-etching inorganic materials, and to processes having a minimal exposure to high temperatures. In the application to the biomedical tools, especially for handling cells or tissues, the correct selection of the material for sacrificial layer requires great care, since ideally the release step should not affect the viability and cytotoxicity of cells.

This dissertation describes the application of water-soluble polymers as sacrificial layers in surface micromachining. Although the water-soluble poly(vinyl alcohol) and PAA with dextran

has already been previously reported for biomedical applications, this process have been excluded to the application for the device to culture cells due to the exposure to high temperatures. The most important properties of the biocompatible sacrificial layers, thus, were the homogeneity of the films after spin-coating, the processibility at room temperature, and their solubility in water. Here, we employed the alginate hydrogel layer as the sacrificial layer of the microflaps and microdisks (Figure 2-5). Sodium alginate is a copolymer of β-D-mannuronic acid (MA) and α-L-guluronic acid (GA) that are covalently bound in a linear fashion, form aqueous solutions. Metal (II) cations such as Ca^{2+} convert sodium alginate solution into cross-linked hydrogels owing to chelation of carboxylate groups of MA and GA as shown in Figure 2-5. Due to the biocompatibility and non-immunogenic property, this hydrogel is widely used in a variety of biomedical applications such as a scaffold for cell culture (Tan et al., 2007a), tissue engineering (Ashton et al., 2007; Khetan et al., 2011), and non-invasive substrates for anchoring and detaching cells (Nagai et al., 2013). We harnessed this gel-sol transition of alginate hydrogel by ion exchange of Na^{+} with Ca^{2+} for the materials of sacrificial layer. Since alginate hydrogel can be dissolved by its enzyme, the enzymatic dissolution of the hydrogel achieves a batch release process of arrayed cell-laden microstructures without cytotoxicity. In general, sodium alginate solution becomes gel after combining with calcium (Ca^{2+}) ions, and calcium alginate hydrogel can be immediately removed by introducing phosphate buffered saline (PBS) without Ca^{2+} ions or a chelating agent such as ethylene diamine tetra-acetic acid (EDTA). In the absence of Ca^{2+} ions, adherent cells were detached from the microdisks as reported previously. We thus employed enzymatic reaction by alginate lyase for dissolving hydrogel to escape the cell damage in this study (Ashton et al., 2007; Breguet et al., 2007; Kim et al., 2011a; Wong et al., 2000). This technology will expand multilevel fabrication to a range of biocompatible materials that previously were excluded.

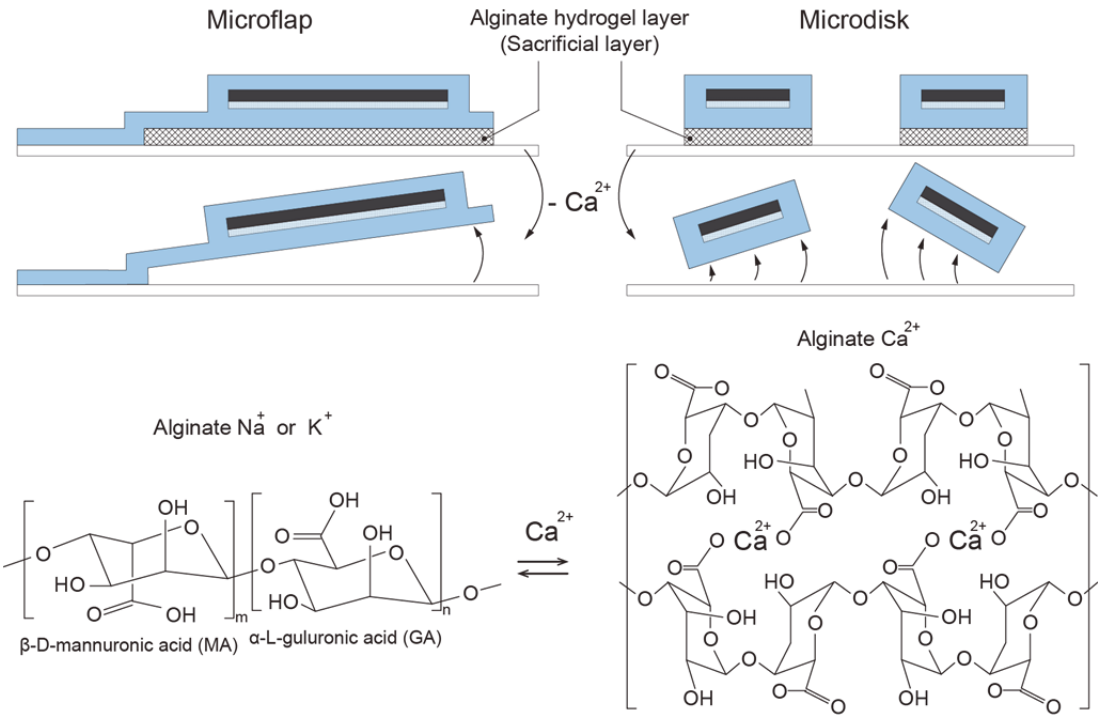

Figure 2-5. Enzymatic release of sacrificial alginate hydrogel layer. Throughout the fabrication process, the microplates and microflaps are attached and immobilized on the surface of glass substrates. We harnessed this gel-sol transition of alginate hydrogel by ion exchange of Na^+ with Ca^{2+} for the materials of sacrificial layer. Since alginate hydrogel can be dissolved by its enzyme, the enzymatic dissolution of the hydrogel achieves a batch release process of arrayed cell-laden microstructures without cytotoxicity.

2.4 Fabrication of microflaps and microdisks

2.4.1 Fabrication process of microflaps

Figure 2-6 illustrates the process flow of microflap fabrication and cell patterning. First, we spin-coated 1% sodium alginate (alginate Na^+, Sigma-Aldrich, USA) on a glass substrate (Matsunami, 0.12–0.17 mm thick) with appropriate dimensions and immersed it in 100 mM calcium chloride ($CaCl_2$, Wako Pure Chemical Industries Ltd, Japan) to gelate and obtain an alginate hydrogel layer with Ca^{2+} ions. We deposited an initial 190-nm layer of parylene-C using a chemical deposition system (LABCOTER PDS2010, Specialty Coating Systems). The

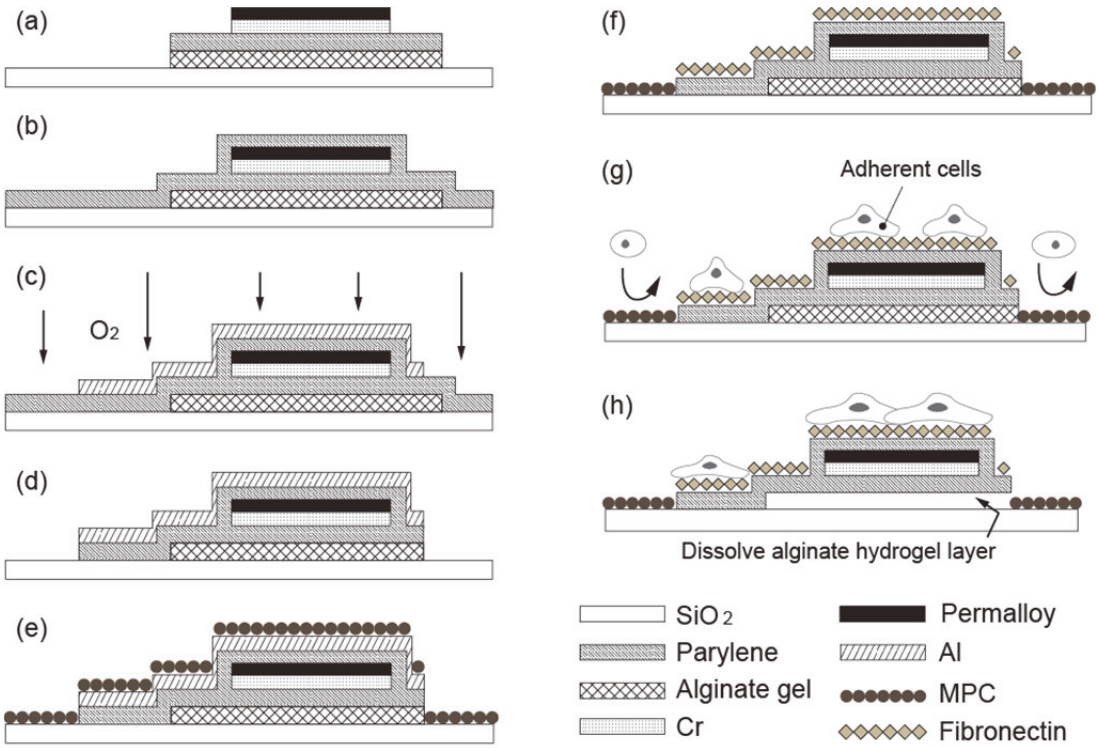

Figure 2-6. Fabrication process of microflaps for culturing adherent cells. Microflap is made of parylene and a magneto-active material, permalloy. Alginate hydrogel are coated underneath the parylene layer. Reprinted with permission from (Teshima, et al, Advanced Materials, 2014). Copyright 2014, Wiley.

deposition process consists of three steps: dimer (di-p-xylene) vaporization at approximately 175 °C, monomerization at 690 °C, and finally polymerization at room temperature. The thickness of the parylene film is dependent on the initial amount of the dimer (di-p-xylene). We deposited chromium (Cr, New Metals and Chemicals, UK) / permalloy (78 Permalloy, Nilaco Corp., Japan) at 120/20 nm via sputtering onto the surface of the first parylene layer. Permalloy is an alloy of nickel (80%) and iron (20%), and has a high magnetic permeability; therefore, it is widely used for soft magnetic manipulation in MEMS application. The Cr layer provides a proper adhesion between the permalloy and parylene surfaces. After patterning with S1818 photoresist (Shipley, MicroChem, USA), we etched the permalloy with aqua regia, and then the

Cr layer was stripped in HY solution (Cr etchant, Wako Pure Chemical Industries Ltd, Japan). We patterned the aluminium (Nilaco Corp., Japan) and etched parylene with oxygen (O_2) plasma (RIE-10NR, SAMCO, Japan) to form microdisk geometry as shown in Figure 2-6(a) (Kuribayashi-Shigetomi et al., 2012; Meng et al., 2008). To prevent cytotoxicity from the dissolved permalloy, we coated the permalloy layer with another deposited 160-nm parylene layer after removing Al layer by Al etchant (Kanto Chemical Co., Inc, Japan) (Figure 2-6(b)). Then, we patterned Al onto the second layer of parylene and etched the parylene with O_2 plasma (Figure 2-6(c, d)). MPC polymer was spin-coated onto the whole area and then dried in a stream of ethanol at room temperature (Figure 2-6(e)). The substrate was baked at 70°C for 4 h to covalently graft the MPC polymer to the substrate by a dehydration reaction. MPC polymer enables the surface to inhibit protein adsorption and cell adhesion (Ishihara et al., 1996; Ishihara et al., 1998; Kuribayashi-Shigetomi et al., 2012). Finally, the Al layer was removed by dipping the substrate into a tetramethylammonium hydroxide solution (2.38%, NMD-3, Tokyo Ohka Kogyo, Japan) mixed with Dulbecco's phosphate-buffered saline with calcium chloride and magnesium chloride (DPBS Ca^{2+} 10×, Sigma-Aldrich, USA) at a 2:1 ratio (Figure 2-6(f)).

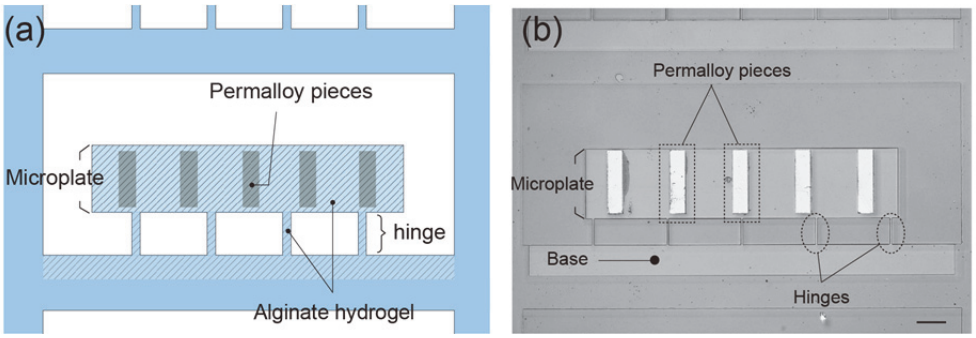

Figure 2-7. Fabricated parylene microflap with embedded permalloy layer. (a) Schematic illustration of microflaps with hinges. (b) Phase-contrast images of fabricated microflaps. The scale bar is 100 µm. Reprinted with permission from (Teshima, et al, Advanced Materials, 2014). Copyright 2014, Wiley.

Figure 2-7 shows the schematic illustration of microflap geometry (a) and the phase-contrast image of the fabricated microflap (b), respectively.

2.4.2 Fabrication process of microdisks

Figure 2-8 shows the fabrication process of the microdisks for culturing adherent cells. As well as microflap fabrication, we used parylene-C as a material of the microdisks. At first, we spin-coated 1% sodium alginate on a glass substrate with appropriate dimensions and immersed it in 100 mM calcium chloride to gelate and obtain an alginate hydrogel layer with Ca^{2+} ions as a sacrificial layer for detaching the microdisks from the substrate easily. We deposited a first 1-μm layer of parylene-C using a chemical deposition system. To add magnetic function to parylene microdisks, we evaporated Chromium and sputter permalloy onto the surface of the first parylene layer (Figure 2-8(a)). The thickness of Permalloy and Chromium layer was about 100 nm and 20 nm, respectively. We patterned the photoresist S1818, etched Permalloy by putting into aqua regia in a few seconds, from 5 to 8 seconds at room temperature and etched Chromium by HY solution for 10 seconds (Figure 2-8(b)). To prevent the toxic damage to cells due to dissolution of permalloy, we coated the layer of Permalloy and Chromium with parylene films, in order not to make adherent cells contact to their layer directly (Figure 2-8(c)). The thickness of the second parylene layer was about 1 μm. Therefore, the sum of parylene thickness is about 2 μm. We patterned Al mask onto the second layer of parylene and etch parylene by O_2 plasma (Figure 2-8(d-f)). We spun the MPC solution in the way shown previously (Figure 2-8(g)). We remove Al mask layer by Al etchant and coat the substrate with MPC polymer (Figure 2-8(h)). We spun the MPC solution at 2000 rpm for 30 seconds and then dried the substrate in a chamber with an ethanol atmosphere at room temperature for 20 min to form the polymer layer uniformly. We used MPC solution for use on the glass substrate. Then, we baked the substrate coated with MPC at 70°C for 4 hours to covalently graft the MPC

polymer to the substrate by a dehydration reaction. We removed Al mask layer removed by dipping the substrate in NMD-3 mixed with DPBS Ca^{2+}, and washing it in distilled water and drying it with a nitrogen stream. The array was exposed to UV light for 5 min for sterilization

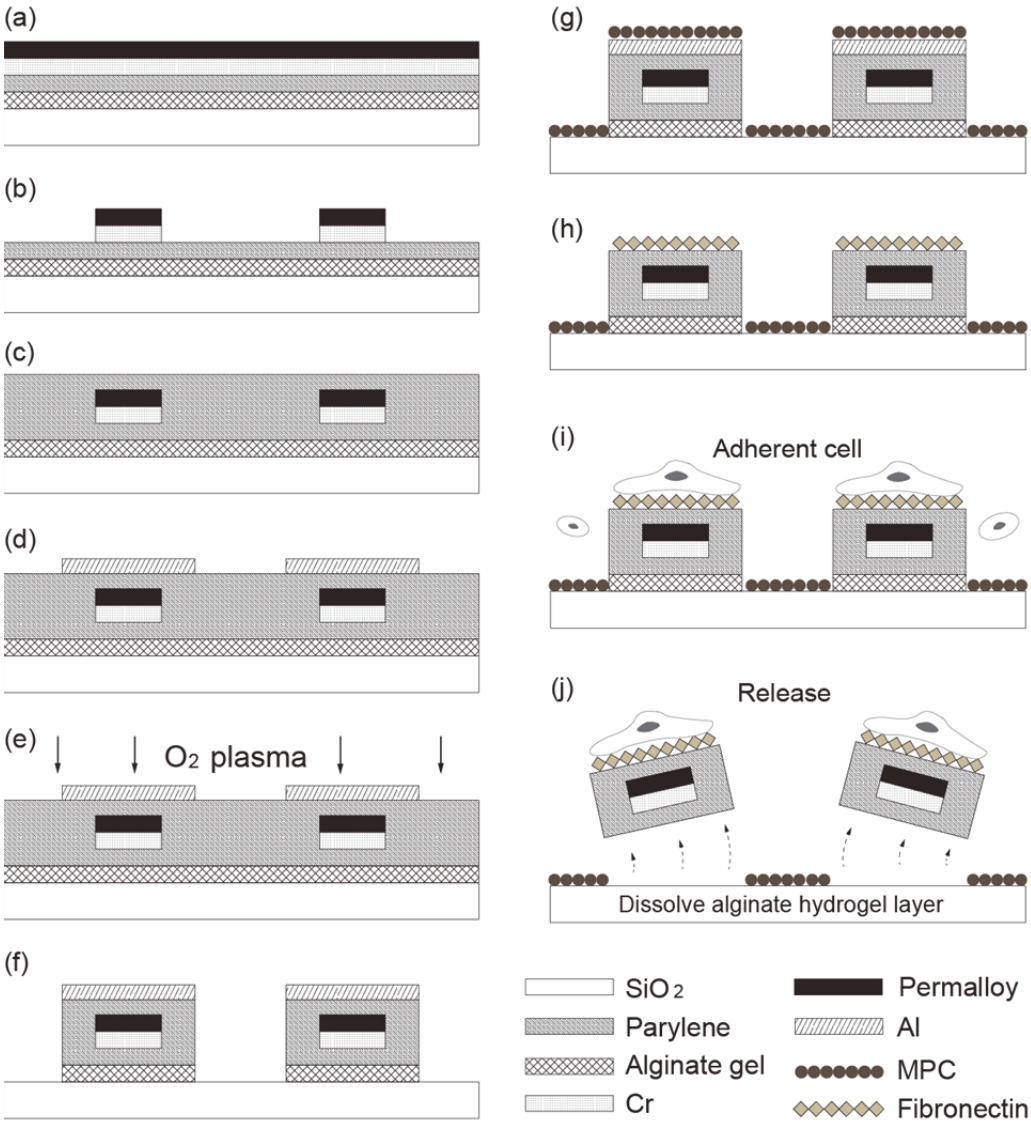

Figure 2-8. Fabrication process of microdisks for culturing single adherent cells. Microdisk is made of parylene and a magneto-active material, permalloy as well as microflap. Alginate hydrogel are coated underneath the parylene layer.

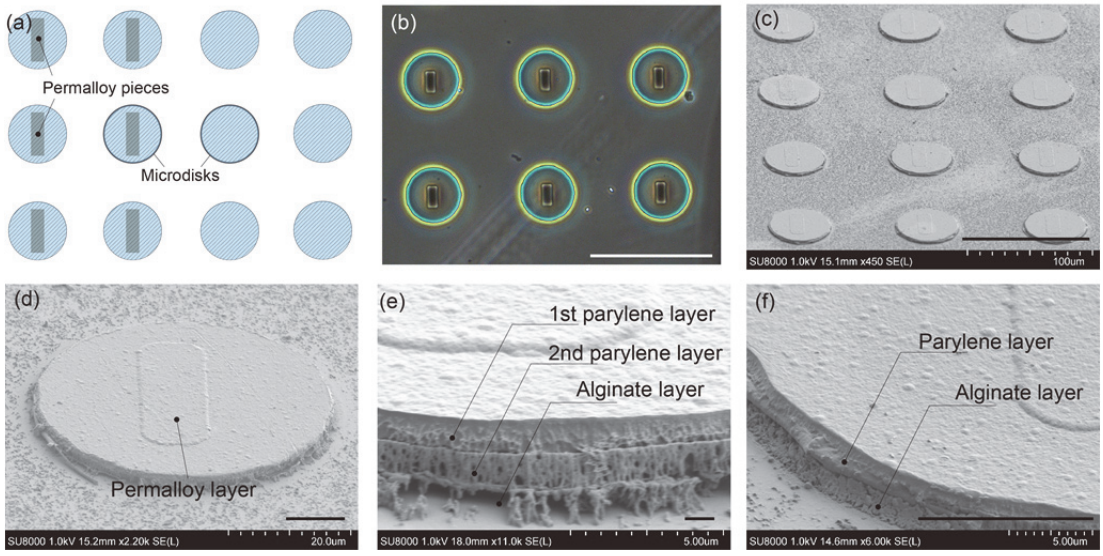

Figure 2-9. Fabricated parylene microdisks with embedded permalloy layer. (a) A schematic illustration of microdisk. (b) Phase-contrast images of fabricated microdisks. (c-f) SEM images of microdisks with embedded permalloy layer and alginate hydrogel layer. The scale bars are (b, c) 100 μm, (d, f) 10 μm, and (e) 1 μm.

and stored in a vacuum desiccator until use.

Figure 2-9 shows schematic, optical, and SEM images of fabricated microdisks. A schematic illustration in Figure 2-9(a) indicates the top-view image of disk-shaped microdisks with rectangular permalloy pieces taken after all of the fabrication procedures were completed. It is designed to load and isolate single adherent cells only onto the microdisk area. Figure 2-9(b) shows the phase-contrast images of fabricated microdisks. They encapsulate black and non-transparent permalloy within them. The SEM images in Figure 2-9(c-d) indicated thatmicrogrooves with about 100 nm depth are formed along the magnetic bar. The numbered circular microdisks were photo-lithographically defined as an array of 100,000 microdisks with dimensions of 5-100 μm × 2 μm (diameter (φ) × thickness (H)) with a 10- to 100-μm gap between the microdisks on the glass substrate. Tiny particles around the microdisks seem to be

the fragments of MPC polymer. It is designed that along the formed lines of magnetic force, microdisks would be rotated and oriented in the direction of longer sides of magnetic bar. The SEM images in Figure 2-9(e-f) shows the edge of parylene microdisks and alginate hydrogel layer. We observed that alginate hydrogel formed solid underneath the parylene microdisk layer. While optimal O_2 plasma etching process produced the perpendicular edge to the glass substrates, over-etching of O_2 plasma made the edge of microdisks slope-shaped and alginate hydrogel layer exposed.

2.4.3 Fabrication of microfluidic channels

Figure 2-10 describes the procedure to produce PDMS microfluidic channels. Microfluidic channels to create an array of collected cell-laden microdisks were fabricated in poly(dimethylsiloxane) (PDMS, SILPOT 184 w/c silicone elastomer, Dow Corning TORAY, Japan) using conventional soft lithography techniques in a manner similar to that described previously (Tan et al., 2007b; Tan et al., 2008; Teshima et al., 2010). Briefly, the microchannel design was patterned onto a glass photo-mask using a mask exposure machine (NanoSystem solution, inc., Japan). First, a thick negative photoresist (SU-8 100, MicroChem Corp., USA) was spin-coated onto a silicon wafer to achieve a resist thickness of 40 μm (Figure 2-10(a)). The photoresist was then exposed to UV light through a glass mask to crosslink the exposed microchannel pattern by a mask aligner (Union Optical co., ltd., Japan), and the un-exposed photoresist was removed using SU-8 developer (Figure 2-10(b, c)). The microchannel pattern was then used as a mold, and a PDMS elastomer with a 10 : 1 (w/w) ratio of crosslinking agent was poured into the SU-8 mold (Figure 2-10(d)). After curing the PDMS, holes were formed as inlets and outlets in the PDMS to connect the microchannels by disposal biopsy punches (KAI industries co., ltd., Japan) (Figure 2-10(e)). The PDMS and precleaned glass slides were then treated with O_2 plasma (Model FA-1, SAMCO. Inc., Japan) and bonded to each other (Figure

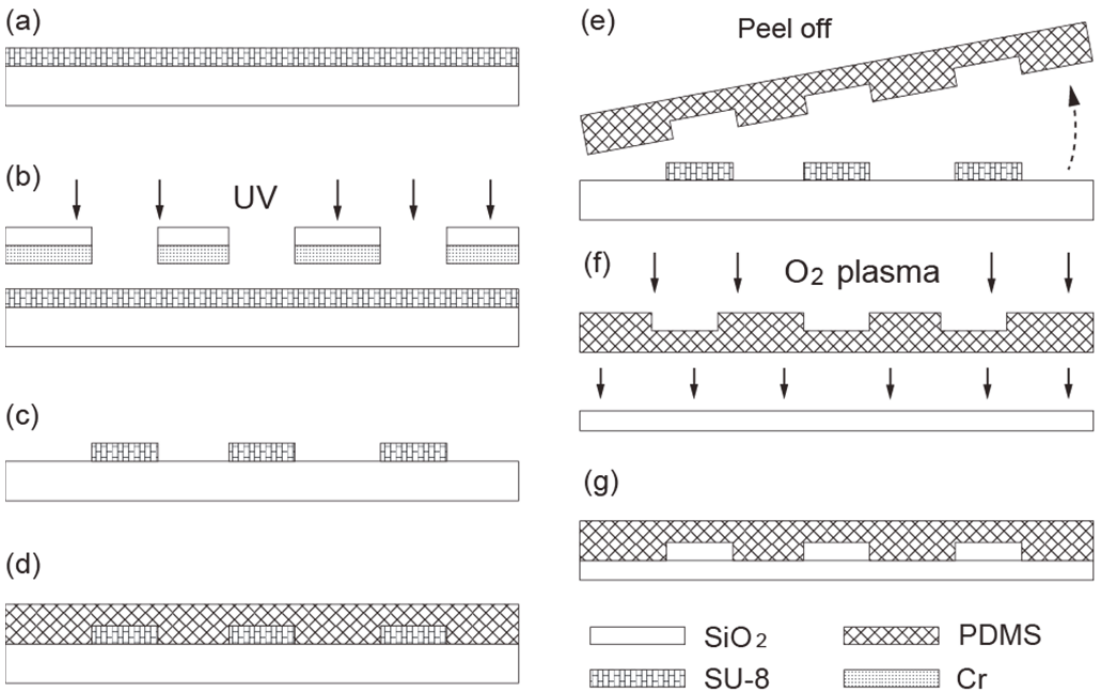

Figure 2-10. Fabrication process of PDMS microchannels. (a-c) The mold is made from the photoresist, SU-8 by the photolithography technology. (d-g) By pouring PDMS into the fabricated mold and bonding with the glass substrate, PDMS microchannels were fabricated.

2-10(f)). We then baked the device on a hotplate for 1 hr at 76°C to strengthen the bonding. The image of PDMS microchannels bonded with the glass substrates is shown in Figure 2-10(g).

2.5 Loading of cells and enzymatic release

2.5.1 Preparation of adherent cells

The cell lines HFF (human foreskin cell, Figure 2-11(a, b)), NIH/3T3 (mouse fibroblast-like cell line), HepG2 (human hepatoma cell line), HeLa (human cervical cancer cells, normal/Fucci-gene transfected cells) and PC12 (pheochromocytoma cell line derived from a rat adrenal medulla) were employed to compare cell behavior on the microdisk surfaces as models of adherent cells. The NIH/3T3, HepG2 and PC12 cells were cultured in Dulbecco's modified

Eagle's medium (DMEM, D5796, Sigma-Aldrich, USA) containing 10% fetal bovine serum (FBS, Nichirei Bioscience Corp., Japan) supplemented with 1% L-glutamine and 10 μg/ml gentamicin (Invitrogen, USA). The HeLa cells were cultured in DMEM with a low glucose density, 10% FBS and 10 μg/ml of gentamicin. The HFF cells were cultured in D10 medium supplemented with DMEM, 10 mM HEPES (Invitrogen, USA), 10% FBS, 2 mM L-glutamine and 10 μg/ml gentamicin. All of the cells were maintained at 37°C in a humidified incubator containing 5% CO_2. Once the cells were confluent, they were trypsinized with 0.025% trypsin in a 0.01% ethylene diamine tetra-acetic acid (EDTA, Sigma-Aldrich Co., USA) solution and passaged at a 1:3 subculture ratio.

2.5.2 Parasite separation

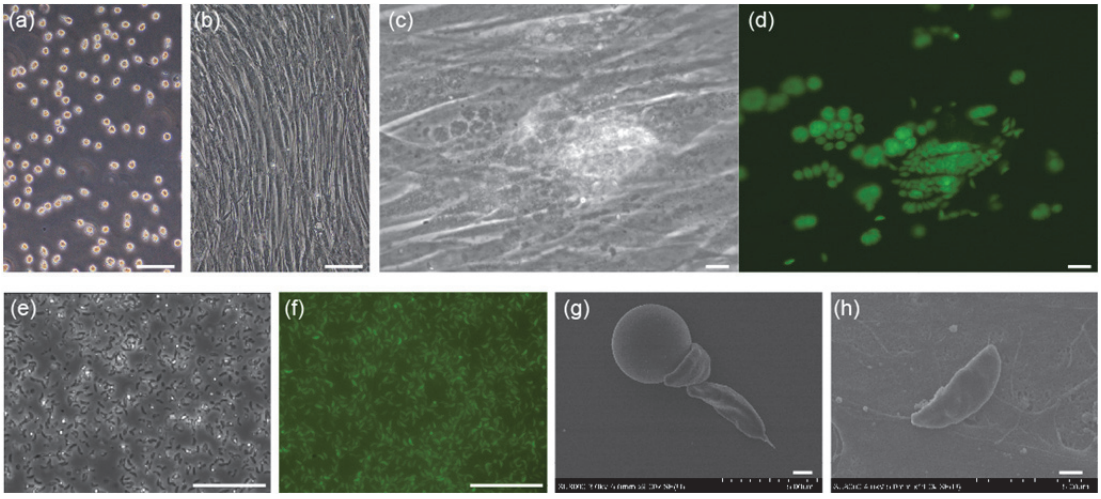

Figure 2-11. HFF host cells and *Toxoplasma gondii*. (a) The phase-contrast image of HFF cells after trypsinization. (b) The phase-contrast image of confluent HFF cells. (c, d) The phase-contrast and fluorescent images of HFF cells infected by *Toxoplasma gondii* (*T. gondii*). (e, f) The phase-contrast and fluorescent images of isolated *T. gondii* expressing GFP protein. (g) An SEM image of *T. gondii* beside 4 μm microparticles. (h) An SEM image of *T. gondii* invading host HFF cells. The scale bars represent 100 μm (a, b, e, f), 10 μm (c, d), and 1 μm (g, h).

The HFF cells were also cultured in monolayers as host cells of a type of parasite, *Toxoplasma gondii* (*T. gondii*). Many strains of *T. gondii* have been studied in each laboratory, and although these differ in virulence and other respect, all strains are thought to constitute a single species. The *T. gondii* RH strain used in this study has specific characteristics: its rapid replication rate, high productivity and highly efficient lysis of host cells, which facilitates the easy isolation of tachyzoites that are relatively uncontaminated by host cell materials. The *T. gondii* RH strain was maintained by serial passage in the HFF cells. They infect monolayer cultures of HFF cells more efficiently than suspension culture such as lymphocytes or monocytes, because contact and invasion is easier. In this point, HFF cells offer several advantages: large and flat morphology provide an extensive plasma membrane to invade or egress; they are derived from human body, providing a host comparable in certain respects to a clinical infection as shown in Figure 2-11(c, d). *T. gondii* tachyzoites can be maintained indefinitely by serial passage in a HFF cell monolayer cultured in T-flask (T25, Cosmo Biosciences Inc.). The parasites were separated from the host cells by aspiration with needles (21G, Terumo Japan) and were filtered through polycarbonate membrane filters (pore size, 3 μm, Millipore). The parasites were washed with PBS containing Ca^{2+} (pH 7.2, Sigma-Aldrich, USA) and centrifuged at 400 × g for 10 min to eliminate the host cells and cell debris (Figure 2-11(e-h)). The details of culture and separation assay are described in *Appendix*.

2.5.3 Loading of adherent cells

The hydrophobic parylene surface permitted the conjugation of functionalized extracellular matrix (ECM) proteins; the surface was selectively converted to one type of ECM. The devices were rinsed with 20 μg / mL FN solution (Biomedical Technologies) by a 30-min immersion before cell seeding, to convert the surface of the microflaps selectively to FN (Figure 2-7(f), Figure 2-9(h)). The HFF cells were harvested by adding trypsin to release them from the culture

dishes; they were then loaded into a microtube and centrifuged. They were re-suspended by gently pipetting them into a petri dish with microflaps and were allowed to settle and grow at 37°C in 5% CO_2 (Figure 2-7(g, h), Figure 2-9(i, j)). The devices were immersed in the cell culture media throughout the actuation process. After half a day of incubation, cellular growth on the microflaps was observed under a microscope at varying cell densities. The cells not attached to the parylene surface were then removed by renewing the cell culture media. The number and density of the cells on the array were optimized to obtain a confluent culture onto the microflaps or single cell on each microdisk.

2.5.4 Enzymatic release

The alginate hydrogel sacrificial layer was coated underneath the array of microdisks and microflaps, and can be dissolved by adding alginate lyase. The sequential images of hydrogel dissolution were obtained under the inverted microscopes by observing fluorescent nanoparticles (YG Carboxylate Microspheres 0.20 μm, Fluoresbrite, Polysciences, Inc.) encapsulated in the sacrificial layer. The dissolved hydrogel expanded underneath the microplates, disrupting the parylene-glass substrate interface and releasing the microplates. After releasing the microflaps, we applied the magnetic field to incline the cell-laden microflaps and adjusted the inclination angles. After releasing the microdisks, we screened and collected individual cell-laden microdisks. Commercially available micromanipulators (nano-tweezers, AOI Electronics Co., Ltd., Japan) were employed to demonstrate the collection of released cell-laden microdisks.

2.6 Experimental Setup for Microscopic observation

2.6.1 Cell staining and microparticles

For immunostaining of the cells on the microflaps and microdisks, the adherent cells were

grown for 24 h, fixed with 4 wt% paraformaldehyde (Wako Pure Chemical Industries Ltd, Japan) for 30 min, permeabilized with 0.5% Triton X-100 (Alfa Aesar, UK) for 6 min, and blocked with 1% bovine serum albumin for 3 h. Immunostaining was carried out as follows: 1 μg/mL Hoechst 33528 (Sigma-Aldrich, USA) was used to stain the chromosomal DNA; actin fibers were probed with tetramethylrhodamine B isothiocyanate (TRITC)-conjugated phalloidin; α-tubulin was probed with anti-tubulin mouse monoclonal antibody (Sigma-Aldrich, USA) followed by secondary goat anti-mouse antibodies conjugated with Alexa 488 or 568 (Invitrogen, USA).

To assess the cell viability on the microflaps, living cells and non-living cells were stained with calcein-AM solution (Invitrogen, USA) and ethidium homodimer-1 (Molecular Probes, USA) following the manufacturer's protocol for live/dead assay. Polystyrene microparticles with mean diameters of 4.5 μm (Fluoresbrite BB, Polysciences, USA) were used to observe the cell membrane surface. The microbeads were coated with poly-L-lysine (Sigma-Aldrich Co., USA) and attached to the surface of cell membrane.

2.6.2 SEM analysis on cells

Adherent cells on the microdisk arrays were gently rinsed with PBS and then fixed with 2 wt% glutaraldehyde (Wako Pure Chemical Industries Ltd, Japan) in PBS for 30 min. The samples were then washed with PBS and dehydrated with a series of ethanol/water mixtures of increasing ethanol density (30, 40, 50, 60, 70, 80, 90, 95 and 100% ethanol, 10 min in each mixture). After immersing them in tert-butyl alcohol (Wako Pure Chemical Industries Ltd, Japan), they were lyophilized using freeze drier (FS-2030, Hitachi, Japan). The fixed cells were then sputtered with osmium (VIII) oxide and observed by SEM (SU-8000 FESEM; Hitachi High-Technologies Co., Japan) to obtain images of the cells on the microdisks.

2.6.3 Measurement of UV-visible spectra and thickness of parylene

To optimize the thickness of the parylene layer, the UV-visible spectrum of a parylene layer with varying thickness on a glass substrate coated with alginate hydrogel layer was measured by UV and visible spectrophotometry (V-550ST, JASCO, Japan). The thickness and surface roughness of parylene layer is measured by the Dektak profilometer (Veeco, USA) and 3D Laser Scanning Microscope (VK-X200, Keyence, Japan), respectively. Dektak profilometer measured step heights or trench depths on a surface by dragging across a surface and leveled data in the software.

2.6.4 Experimental setup for magnetic actuation

The experimental setup to test the magnetic response and observe cells consisted of the fabricated device, microscopes, magnets on a micropositioner and a gauss/tesla meter probes (MAGNA, Japan). A series of NdFeB magnets (NeoMag, Japan) were mounted on the micropositioner, which provided precise control of their magnet positions. The NdFeB magnets have two shapes: disk-shaped magnets for device actuation in response to the applied magnetic fields and ring-shaped ones for the optical measurement of cells under inverted microscopes (Figure 2-12(a-c)). The magnet was experimentally calibrated to measure the magnetic flux density as a function of distance (x) from its surface (Figure 2-12(d)). To measure the inclination angle, disk-shaped magnets were placed under the Petri dishes containing the microflaps, while dishes in which cell-laden microflaps were located were set at the center of ring-shaped magnets. For the evaluation of the vibration of the suspended microdisks, an inverted microscope IX71 (Olympus, Japan) and a high-speed CCD camera FASTCAM-1024PCI 100K (Photron, Japan) mounted on an inverted microscope (Eclipse, TE300; Nikon, Tokyo) were used.

The magnetic force generated by the magnets is able to be replaced with an electromagnet to measure the characteristics according to the magnetic field. The uniform magnetic field was

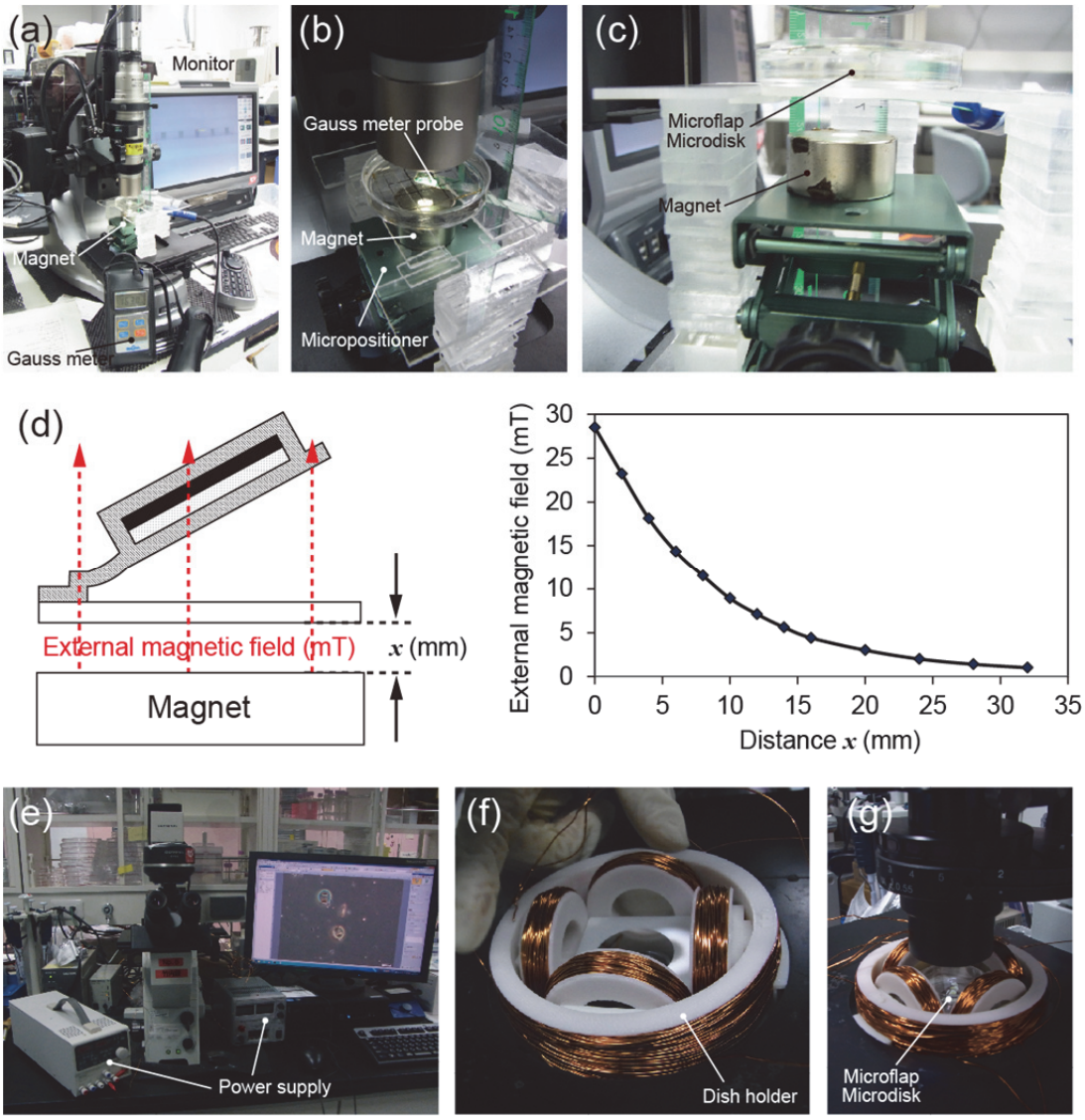

Figure 2-12. Experimental setup for magnetic actuation of microplates. (a, b) The experimental setup consisted of the fabricated device, microscopes, magnets on a micropositioner and a gauss/tesla meter probes. (c) NdFeB magnets were mounted on the micropositioner, which provided precise control of their magnet positions. (d) The magnet was experimentally calibrated to measure the magnetic flux density as a function of distance from its surface. (e) 3-axis orthogonal Helmholtz coils setup for generating a uniform rotating magnetic field. The strength of magnetic field is controlled by input current of the electromagnet. (f, g) The dish is mounted on a 2-axis dish holder and placed at the center of the coils. A dish is placed in the middle of the three orthogonal Helmholtz coil pairs.

Table 2-1. Parameters of the 3-axis orthogonal Helmholtz coils setup

Parameters	External coil (x1)	Inner coil (x4)
Mean diameter (mm)	93.5	38
Number of Turns	300	170
Wire thickness (mm)	0.65	0.65
Distance from center (mm)	-	28.5
Magnetic flux density per unit ampere (mT/A)	3.7	1.9

generated by a three-axis Helmholtz coil setup as previously described (Figure 2-12(e)) (Matsumoto et al., 2011; Petit et al., 2012; Sakar et al., 2011; Tottori et al., 2012). The experimental setup consists of five identical in-plane electromagnetic coils (Figure 2-12(f)). The coils are integrated with 3D printed solid frames that allow experimentation with both inverted and upright microscopes. Paired coils were placed 57 mm away from each other and the electromagnet has a core diameter of 93.5 mm. Uniform magnetic fields up to 7 mT were generated by a three-axis Helmholtz coil setup by adjusting the input current of the electromagnet. The details of coil parameters are described in Table 2-1. The coils are independently driven with current control electronics.

Pictures of the microflap and microdisk motion were acquired with an upright microscope (VHX-1000, Keyence, Japan) (Figure 2-12(a)), and the image was displayed on a computer screen. Bright-field and fluorescence images were obtained by a charge-coupled device camera mounted on an inverted optical microscope with 10×, 20×, 40×, 63×, and 100× objectives (IX71, Olympus, Japan; Leica DM IL LED, USA) with a charge-coupled device camera (DP72, Olympus, Japan). Confocal images of cells on the microflaps and cross section z-stack images of the cells on the microdisks were recorded using an inverted confocal laser-scanning microscope (LSM 780, Carl Zeiss, Germany). Time-lapse images of the cell behavior around

the microdisks were captured using a folded optical structured microscope system (BZ-9000, Keyence, Japan) with the stage top incubator (TOKAI HIT, Japan). Time-lapse images of the cell behavior around the microflaps were captured using a folded optical structured microscope system (BZ-9000, Keyence, Japan). The captured images were analyzed using image processing software (ImageJ, NIH). Image blurs caused by the microflap vibration were corrected by using camera shake correction function, "Warp Stabilizer" in software, Adobe After Effect CS5.5 (Adobe Systems Software Ireland Ltd., USA).

2.6.5 Introduction of microdisks into microchannels

Cell-laden microdisks were introduced into microchannels by the setup including syringe, tubes and syringe drivers. Syringe drivers (Micro 4, World Precision Instruments, USA; KDS210, KD Scientific, USA) were used to control the flow rates, and microdisks were infused into the device using 250 or 500 μL Hamilton Gastight syringes (1700 series, TLL, Hamilton GASTIGHT syringe, USA). The images of captured cells on the microdisks were captured using a charge-coupled device camera (3CCD Digital Camera C7780, Hamamatsu, Japan) with imaging software (AQUACOSMOS ver.2.6, Hamamatsu, Japan). To observe the fluorescence images, we used a CCD camera (DP72, a 12.8 megapixel cooled digital color camera, Olympus, Japan) mounted onto an inverted optical microscope (IX70, Olympus, Japan) and a CCD camera (AxioCam HRc, Carl Zeiss, Germany) with image software (AxioVision ver.4.7.1, Carl Zeiss, Germany). Video images were taken with Hamamatsu CCD camera mounted onto an inverted microscope (Eclipse, TE300, Nikon, Japan).

2.7 Magnetic property of permalloy layer

We investigated the magnetic properties of permalloy layer in order to verify whether there is a difference in magnetic response between before and after sputtering process. The magnetic properties were measured using a superconducting quantum interference device (SQUID; Quantum Design MPMS-5S), one of the facilities of the Cryogenic Research Center at the University of Tokyo, Japan. A mass of permalloy target (0.5 mg) and thin file sputtered on the parylene surface (3.5 mm×3.5 mm×100 nm) were measured by putting on the straws with an external magnetic field (*H*) applied parallel to or perpendicular to the film surface. Figure 2-13(a, b) show the magnetic field dependence of magnetization (*M*) of permalloy targets (a) and thin films (b) when the magnetic field was increased and then decreased at 0°C, 25°C, and 35°C. In both targets and thin films, few *M-H* hysteresis loops were observed at any temperature and at any magnetic field ranging from -10 to 10 kOe. There was a little gap in the magnetization between before and after sputtering (Figure 2-13(c)). These results indicated that the sputtering process completely forms the thin film composed of permalloy on the surface of polymers, parylene, and the composition of thin film is the same as permalloy targets.

Next, we measured the shape anisotropic property of thin permalloy film. Figure 2-13(d) shows the magnetization *vs.* magnetic field curves of the magnetic field applied parallel to or perpendicular to the sputtered permalloy thin film at 25°C. Compared with the permalloy thin film parallel to the magnetic field, the slope of magnetic flux density-magnetization curve of permalloy thin film perpendicular to the field is lower around 0.15 emu/kOe in a relatively low magnetic field region of <4 kOe, indicating that permalloy is highly anisotropic in terms of shape. There are two possible reasons that give rise to shape anisotropy: the effect of demagnetizing field that acts on the magnetization so as to reduce the total magnetic moment; the shape of thin films. Especially, the demagnetization coefficient is prescribed from the shape of the base material and magnet area that is directed and exposed to the magnetic field. Thus,

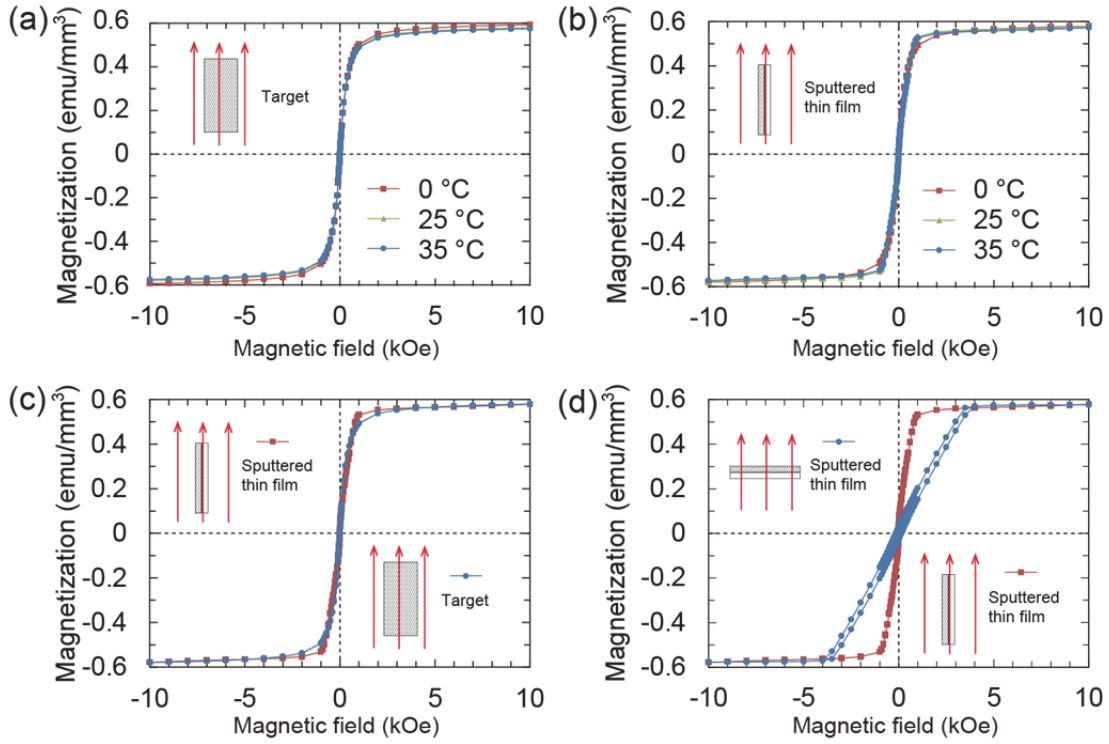

Figure 2-13. SQUID analysis of magnetic response. (a) Temperature-dependent magnetization curves as a function of the magnetic field for the permalloy target (0, 25, 35°C). (b) Temperature-dependent magnetization curves as a function of the magnetic field for the sputtered permalloy thin film (0, 25, 35°C). (c) The comparison of the magnetization for the permalloy target and sputtered permalloy thin film (25°C). (d) Magnetization vs. magnetic field curves of the magnetic field applied parallel to or perpendicular to the sputtered permalloy thin film.

ferromagnets with high magnetization including permalloy are especially influenced by the demagnetizing field. Even when subtracting the effect of the demagnetizing field, there is no coincidence in the gap of hysteresis loops between the magnetic field applied parallel to and perpendicular to the permalloy film. This phenomenon would be caused by the other except for the demagnetizing field, such as the specific characteristics of thin films. Note that the unit of kOe can be converted to A/m. However, in this study, we did not convert it since the permalloy film for measurement have different shape and magnetic environment from permalloy pieces embedded in the microplates.

CHAPTER 3

EXPERIMENTAL RESULTS & DISCUSSION OF MICROFLAP

Numerous experiments to fabricate the mobile microplates to manipulate adherent cells were conducted with two types of devices in this study. In this chapter, we will discuss the first hinged microplates, termed "microflap", toward the multi-angle observation of multiple adherent cells. Magnetically responsive microflaps were used to (i) micro-pattern multiple adherent cells on the fibronectin-coated microflap surface, (ii) verify the design criterion for inclination of cell-laden microflaps, and (iii) test the observation of inclined adherent cells. To enhance the utility and application of multi-angle observation, we demonstrate the feasibility of the observation of parasite invasion into inclined cells by using infectious parasites and their host cells cultured onto the microflaps. Another type of device is magnetically responsive microdisks, which was used to isolate and manipulate single adherent cells. The microdisk technology to manipulate single adherent cells is considered in later chapters 4. As the objective of each experiment is different, their corresponding experimental setup is also slightly different. Each experiment is arranged and presented as a separate section by itself and will begin with a magnetic actuation with an applied magnetic field, followed by results of loading cells, and finally discussion.

3.1 Loading of adherent cells onto microflaps

3.1.1 Cell attachment, migration, and patterning

We investigate how adherent cells suspended in the cell-culture media behave and adhere on the surface of microflaps. The technology to pattern cell adhesion area is critically required for the precise characterization of microflaps inclination, because adherent cells tend to exert cell traction force that is generated by actomyosin interactions and actin polymerization, and pulls toward the center of the cell body (Chen et al., 2004; Lemmon et al., 2009; Tan et al., 2003). To avoid cells settling down on the hinge and disturb the microflap inclination, we cultured adherent cells only on the microplates. We patterned an extracellular matrix protein (fibronectin, FN) and cell adhesion inhibitor (2-methacryloyloxyethyl phosphorylcholine, MPC polymer) on the parylene surface and glass surface, respectively as shown in the fabrication process in Figure 2-6(f-h). When we suspended human foreskin fibroblast (HFF) cells on the microflaps, the cells remained sphere-shaped while migrating on the MPC-polymer-coated area and then stretched after reaching the FN-coated area (Figure 3-1). The cells on the FN-coated parylene surfaces continued to stretch and proliferate, leading to confluent culture on the microflap surface due to contact inhibition of HFF cells (Figure 3-2(a)). It took approximately 24 h to culture the cells on the entire microflap area. Figure 3-2(b) shows the higher affinity of HFF cells to the FN-coated parylene surface than to the MPC-polymer-coated glass surface or FN-free parylene surface after 3 days of incubation. Throughout the incubation, the cells remained on the surface of parylene and never migrated to the MPC-polymer coated area. In addition, the alginate hydrogel layer remained under the parylene layer, and the microflaps were never released from the glass substrates. Hence, the FN and MPC polymer successfully provided a patterned cell adhesion area for the adherent cells on the microflap surface.

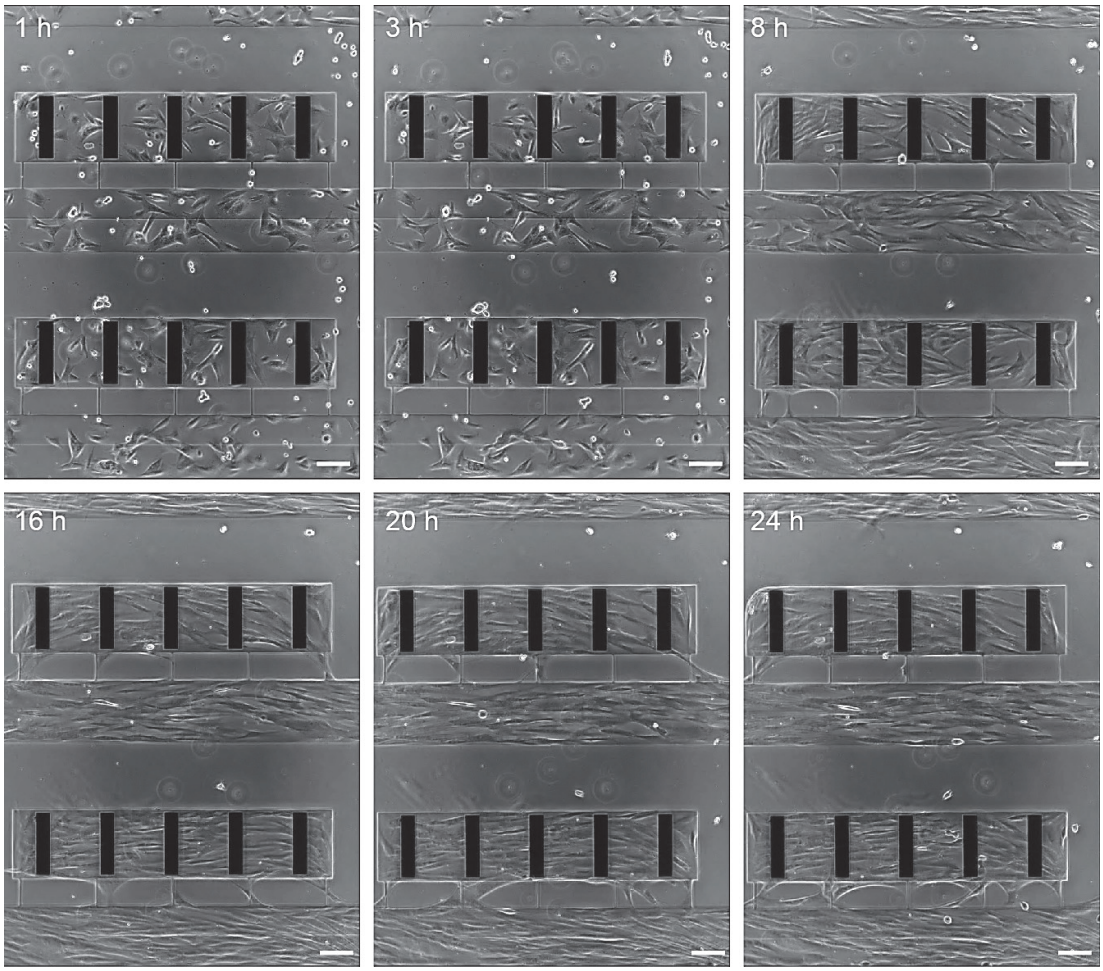

Figure 3-1. Migration of HFF cells on the surface of parylene microflaps during 1 day culture. When we suspended cells on the microflaps, the cells remained sphere-shaped while migrating on the MPC-polymer-coated area and then stretched after reaching the FN-coated area, leading to confluent culture on the microflap surface. The scale bars are 100 μm. Reprinted with permission from (Teshima, et al, Advanced Materials, 2014). Copyright 2014, Wiley.

3.1.2 Hinge length

We investigated the suitable hinge length by using the microflaps with hinge length of 20–100 μm. Although the cells did not settle on single hinges, we found that the HFF cells on the microflaps tend to migrate along the hinges during incubation and bridge between the microplate and the base when the hinge length is less than 40 μm as shown in Figure 3-2(c). We

observed that most of the bridging cells were along the hinges, but some of the cells were bridging over the gaps without hinges between microplates and bases. These bridging cells generate cell traction force, resulting in a lower yield of cell patterning and low angle tunability of microflaps. By lengthening the hinges to more than 40 μm, the average number of bridging cells per microflap decreased to <1, as shown in Figure 3-2(d). We also observed that microflaps with the hinges more than 100 μm length have a frequent vibration after inclination. In this study, we selected 80-μm hinges in length to avoid cell bridging.

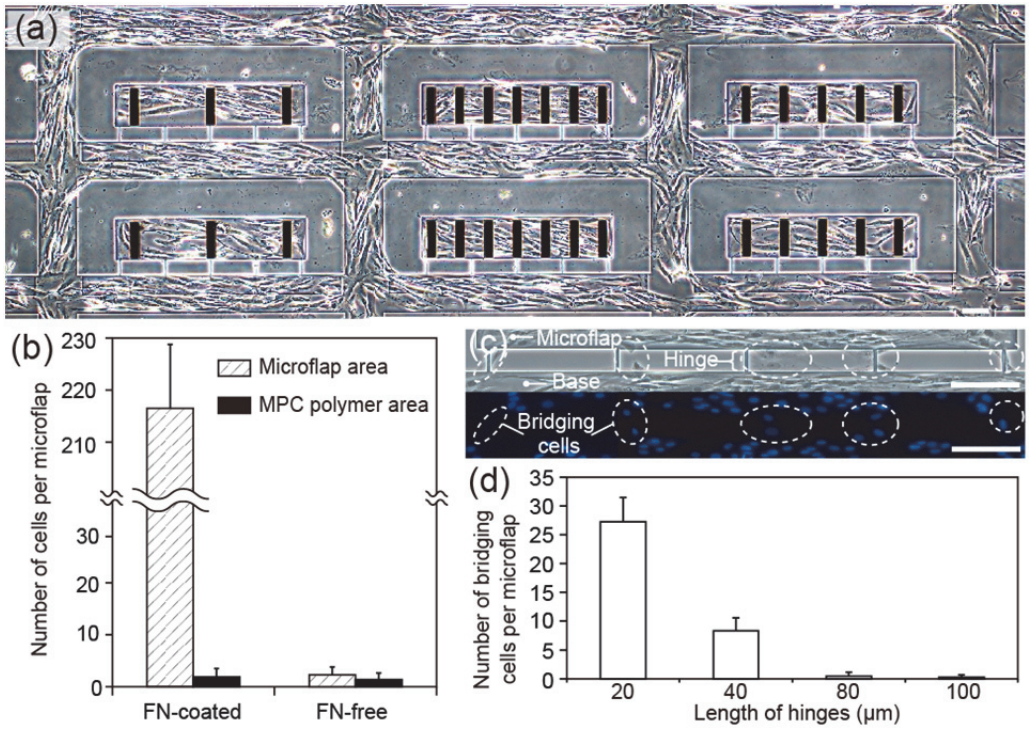

Figure 3-2. Loading of adherent cells onto the microflaps and magnetic inclination of cell-laden microflaps. (a) Phase-contrast image of HFF cells grown on an array of FN-coated parylene microflaps after 1 day of incubation. (b) After the cells were cultured, they were not patterned onto the MPC-polymer coated area, but stretched only around the microflaps. (c) Phase contrast / fluorescent images of cell bridging along the hinges. Nucleus was stained with Hoechst. (d) Extent of cell bridging decreases as hinges become longer. The scale bars are 100 μm. Reprinted with permission from (Teshima, et al, Advanced Materials, 2014). Copyright 2014, Wiley.

3.1.3 Cell morphology

To investigate the relation between the number / orientation of cells and the structure of microflaps, we cultured HFF cells on the microflaps with 1000 μm × 220 μm, 440 μm × 220 μm, 220 μm × 220 μm, 220 μm × 110 μm, 110 μm × 55 μm, and bulk petri-dishes. Figure 3-3(a-c) show the image of cells cultured on the microflaps after 3 day incubation after loading cells. The nucleus of cells on the microflaps were stained by Hoechst to count the number of cells. Figure 3-3(d) indicates that the larger the microplates become, the less the number of cells on single microflaps tended to be. This result suggests that the area of microplates regulates the number of cells, and it is possible to distinguish multi-cell assay with single cell analysis by changing the area of microflaps, the density of suspended cells, or the period to incubate the

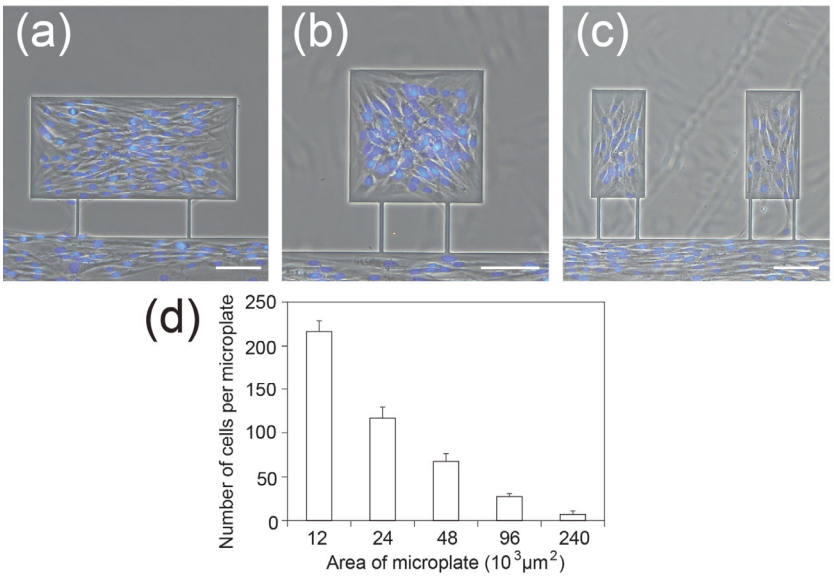

Figure 3-3. Number of cells on the single microflaps. The number of cells was counted by staining cell nucleus with Hoechst. The number of cells on the microflaps with microplates (*w*, *l*) = (440 μm, 220μm) (a), (220 μm, 220 μm) (b), (110 μm, 220 μm) (c), respectively. (d) The number of cells on the single microflaps with various shapes of microplates. The scale bars are 100 μm. Reprinted with permission from (Teshima, et al, Advanced Materials, 2014). Copyright 2014, Wiley.

cells after loading. The bright field images in Figure 3-3(a, c) show that the cells stretched in the direction of long axis of microplates, while the ones in the square-shaped microplates stretched randomly shown in Figure 3-3(b). We compared that the textiles of the actin-fibers of cells loaded onto the microflap surface with that of cells prepared on the petri dish at bulk by fluorescent microscope, and evaluated the orientation of the textiles quantitatively by the image analysis performed on the projected images using custom Fast Fourier Transform (FFT) written MATLAB code (Figure 3-4(a-f)) (Ayres et al., 2006; Kennedy et al., 2010; Kiriya et al., 2012). Briefly, randomly selected regions of cell growth were processed with a Gaussian filter in order to reduce edge effects. A 2D FFT was performed and filtered to include only frequencies from 512 pixels. Average pixel intensity was measured at every angle, and plotted with respect to the angle from horizontal. While brightness distribution of the FFT image of the actin fibers inside the cells in the bulk is isotropic, that of the actin fiber of the cells on the microflaps is sharply-peaked at the direction of long axis of microflaps. Thus, plots of the summed pixel intensity from the FFT image indicated that the textiles of the actin fiber were highly orientated to the long axis of microflaps regardless of the length and dimension of microflaps, and the orientation of actin fibers in the bulk experiments was random. These results quantitatively indicate that HFF cells on the microflaps were aligned along the long axis of the microflaps as discussed in a previous study (Wan et al., 2011). Therefore, the shape and aspect ratio of engineered microplate coated with coated ECM is a key factor for obtaining aligned cell structures and orientation. This characterization will result in the ability to observe wider area of stretching single cells in the single microscopic focus throughout the process of inclination of microflaps. In addition, it is possible to select the appropriate dimensions of microplates from the perspectives of the required number or structure of cells for the experiments.

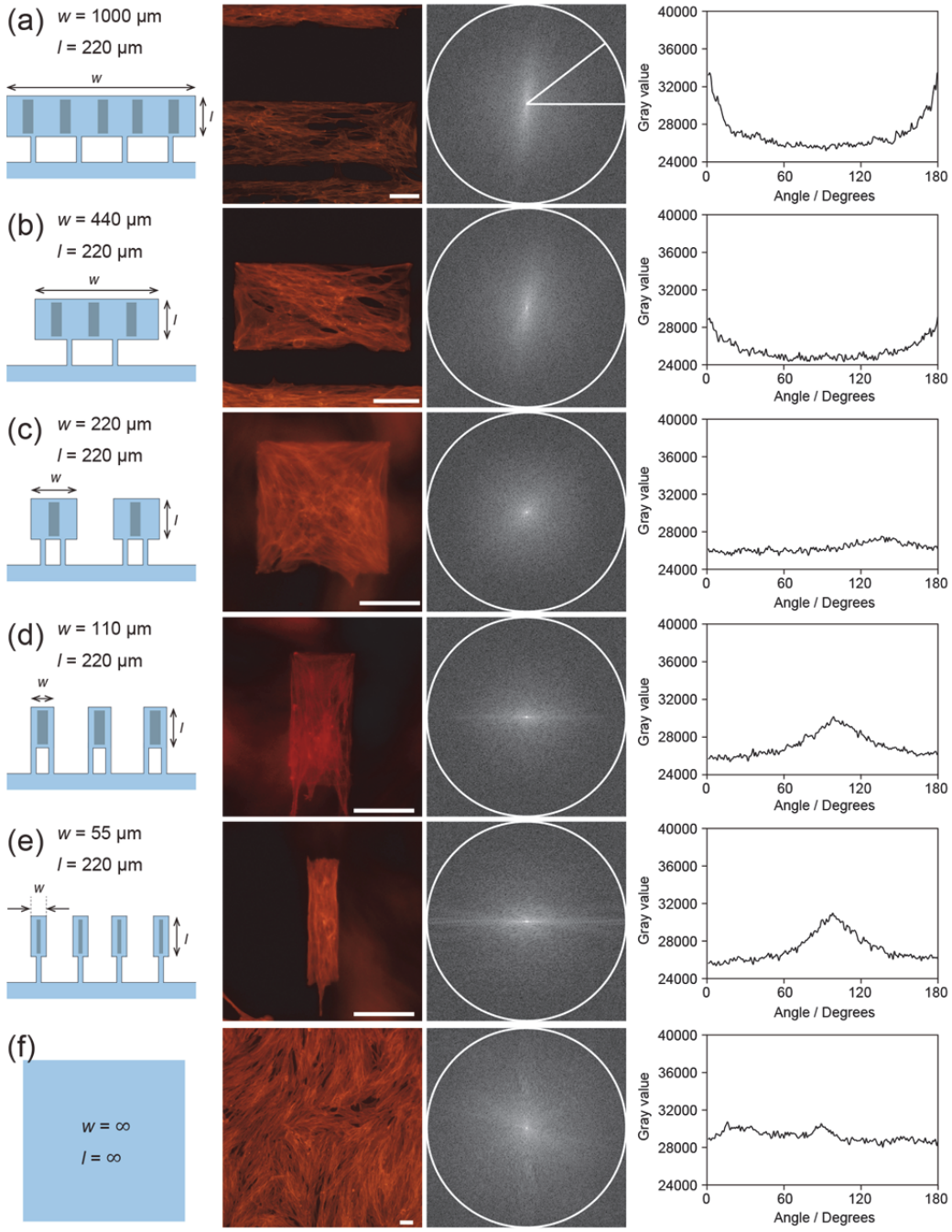

Figure 3-4. Cell orientation of actin filaments inside the cells cultured on the microflaps. Cells are tested on the microflaps with microplates (*w*, *l*) = (1000 μm, 220 μm) (a), (440 μm, 220μm) (b), (220 μm, 220 μm) (c), (110 μm, 220 μm) (d), (110 μm, 220 μm) (e), and in bulk (f), respectively. Each experimental result has a schematic image, representative fluorescent images of stained actin filamens, FFT output images and radial projection, and plots of pixel intensity against the angle of acquisition. Note the distinctive peak in the graph of pixel intensity plots produced by the image containing aligned information. The scale bars are 100 μm.

3.2 Manipulation of microflaps

We validated two microflap processes: dissolution of the sacrificial alginate hydrogel layer and magnetic inclination of the microflaps. To release the microflaps, we tested the enzymatic dissolution of the alginate hydrogel sacrificial layer using alginate lyase. After alginate lyase was added, the alginate hydrogel gradually dissolved from the edge of the microflaps to the center. Figure 3-5(a) shows sequential images of dissolution of alginate hydrogel layer under the microflaps. This dissolution can be detected by observing the interference fringes under the microflaps. During the dissolution process, the area of interference fringes gradually decreased from the edge of microflaps to the center. The yield of released microflaps did not depend on the position of the microflaps on the glass substrate, and all of the microflaps in the single glass substrate were released in an equable manner. It took approximately 15 min to release all of the arrayed microflaps from the glass substrate (Figure 3-5(b)). After the microflaps were released, a magnetic force was applied to the permalloy pieces, which causes the hinges to bend and yields a batch-scale inclination in parallel.

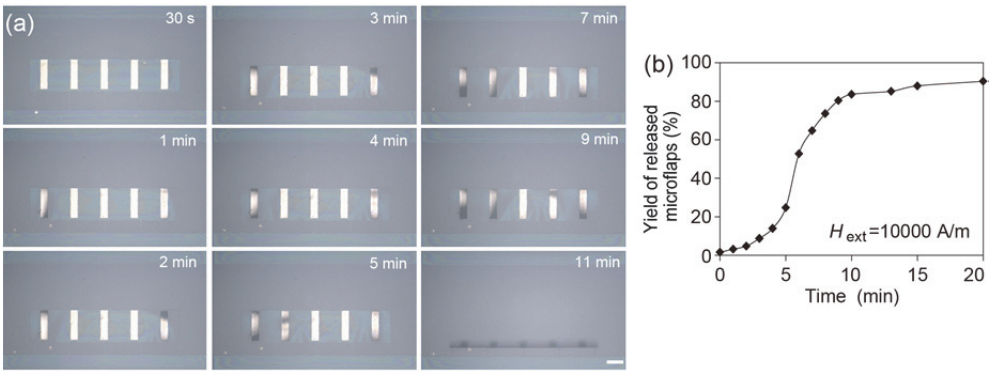

Figure 3-5. Dissolution of sacrificial alginate hydrogel layer. (a) Sequential images of dissolution of alginate hydrogel layer. (b) The graph of yield of release microflaps after addition of alginate lyase. The scale bar is 100 μm. Reprinted with permission from (Teshima, et al, Advanced Materials, 2014). Copyright 2014, Wiley.

Next, we observed the inclination motion of the microflaps tuned by a magnetic field applied perpendicularly to the glass substrate. The size of microflaps is designed in the criteria that the height of microflaps is less than the focal distance of an objective lens, and the width of microflaps is within the microscopic field of an objective lens with high magnification. In this study, we designed the microflaps to 220 μm in height and 1000 μm in width. Figure 3-6(a) shows sequential images of inclined microflaps responding to the applied magnetic field. In this case, the direction of applied magnetic field is aligned in the *z*-axis. We confirmed that the deformation of microflap hinges was elastic and hinges worked as beams as shown in Figure

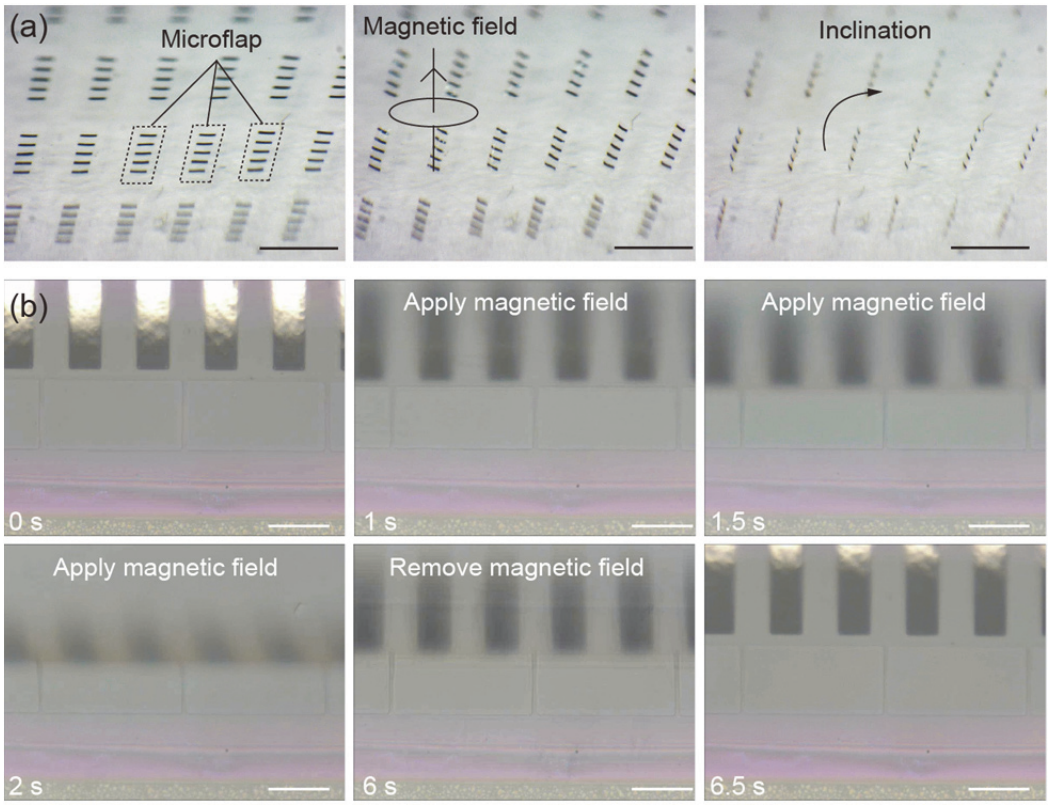

Figure 3-6. Inclination of microflaps after applying the magnetic fields. (a) Sequential bright field images of an array of microflaps in a batch inclination. (b) Phase contrast images of hinge function as a beam. The scale bars are 100 μm (a), 100 μm (b). Reprinted with permission from (Teshima, et al, Advanced Materials, 2014). Copyright 2014, Wiley.

3-6(b). While the hinges were bent, the surface of inclined microplates remained flat without deformation.

The permalloy has high magnetic susceptibility M (~1.0 T) (Donolato et al., 2010), and elastic modulus of the parylene layer E_h, as used in the hinges is about 3 GPa (Hassler et al., 2010). Therefore, the theoretical curve of the inclination angle of microflaps with four independent parameters, V_{mag} = 5000 μm^3, L_h = 80 μm, W_h = 40 μm (= 8.0 μm × 5 hinges), and T_h = 350 nm, given by Equation (2-7) is shown in Figure 3-7(b). Then, we measured the inclination angle under the microscopes and plotted the measurement data in Figure 3-7(b). The plots of measurements conform to the theoretical predictions, indicating that these values satisfy the design criterion in Equation (2-7). Note that we cannot assume the magnetization at small inclination angles is equal to the saturation magnetization (1.0 T) when a material with low coercivity such as permalloy or Ni is utilized for magnetic actuation. However, it is clear from the figure that the measurements conform to the theoretical predictions well when the inclination angles are larger than π/3. There is a slight hysteresis in inclination angles between decreasing magnetic fields from 25000 A/m to 0 A/m and increasing from 0 A/m to 25000 A/m (Figure 3-7(c)). To investigate the effects of varying external magnetic fields on the inclination angles, we measured the inclination angles of the microflaps with three different W_h, L_h, or V_{mag}. When we fabricated the microflaps with W_h (24, 40, and 72 μm) or L_h (40, 80, and 120 μm), each hinged structure has different inclination angles in the same external magnetic field. The inclination angle increased with decreasing W_h or increasing L_h (Figure 3-7(d, e)). For the microflaps with V_{mag} (3000, 5000, and 7000 μm^3), the inclination angle increased as V_{mag} became larger. These results indicated that the magnetic response of the microflap is critically regulated by the hinge width (W_h), the hinge length (L_h) and the permalloy volume (V_{mag}). After the microflaps were inclined repeatedly more than 400 times, there were few changes in the

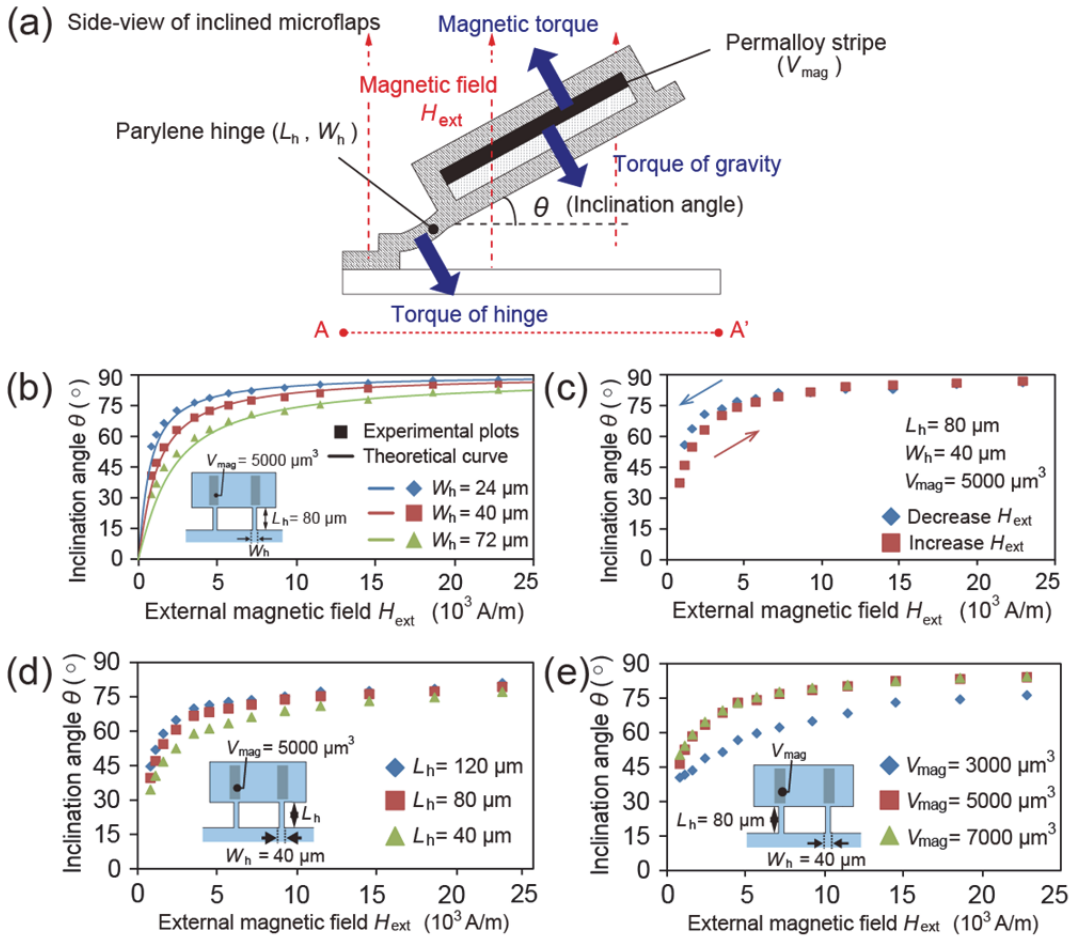

Figure 3-7. Magnetic inclination of microflaps with three different values of W_h, L_h and V_{mag}. (a) Schematic representation of torques and angles involved in applied magnetic field and parylene hinges. (b) Theoretical and experimental plots of inclination angle as function of external magnetic field (H_{ext}) for various W_h values. (c) Experimental plots of inclination angle as function of increasing or decreasing H_{ext}. (d) Graph of inclination angle *vs.* magnetic field strength for three different values of L_h. (e) Graph of inclination angle *vs.* magnetic field strength for three different values of V_{mag}. Reprinted with permission from (Teshima, et al, Advanced Materials, 2014). Copyright 2014, Wiley.

response to the applied magnetic field and little distortion in the hinge structure. These results suggest that this actuation method had high repeatability and durability.

3.3 Multi-angle observation of cell boundaries

3.3.1 Enzymatic release

In the previous sections 3.1 and 3.2, we observed that we patterned the adherent cells only onto the microplates, and the magnetic response of the microflap is critically regulated by the design of microflaps and the strength of external magnetic field. By combining these two characterizations, we conducted the experiment to incline cell-laden microflaps in the magnetic field toward the multi-angle observation of cells. To observe living cells with this method, we first examined that the cell-laden microflaps were released from the glass substrate and inclined by applying magnetic fields without cytotoxicity. The alginate hydrogel layer underneath the cell-laden microflaps with 80-μm hinges was dissolved enzymatically by alginate lyase. As shown in Figure 3-8(a), within 15 min after the addition of alginate lyase, all of the cell-laden microflaps were detached from the glass substrates at room temperature without detachment of the cells on the microflaps; the cell-laden microflaps then started to respond to the magnetic field. A live/dead assay showed that more than 95% of the cells on the microflaps were alive. We tested the dissolution of alginate hydrogel layer by using PBS^- solution. We observed that the microflaps were released from the glass substrate, and the cells on the microflaps were also detached from the surface of parylene surface. It is because of the PBS^- function to remove the Ca^{2+} or Mg^{2+} ions that is vital for cell adhesion. Therefore, in this study, we did not employ the PBS solution as the solution to release microflaps.

We observed that the surface of cell-laden microflaps remained rigid and flat without wrinkles and deformation after being released from the glass substrates. By assuming that the traction force of single cells is about 10 nN (Beningo et al., 2002; du Roure et al., 2005; Harris et al., 1980), we estimated the maximum of total traction force of cells on the microflaps to be less than 2 mN in confluent state, which induces to deform the microflaps. We considered the flexure formula about the relation between bending stress, moment and section modulus to

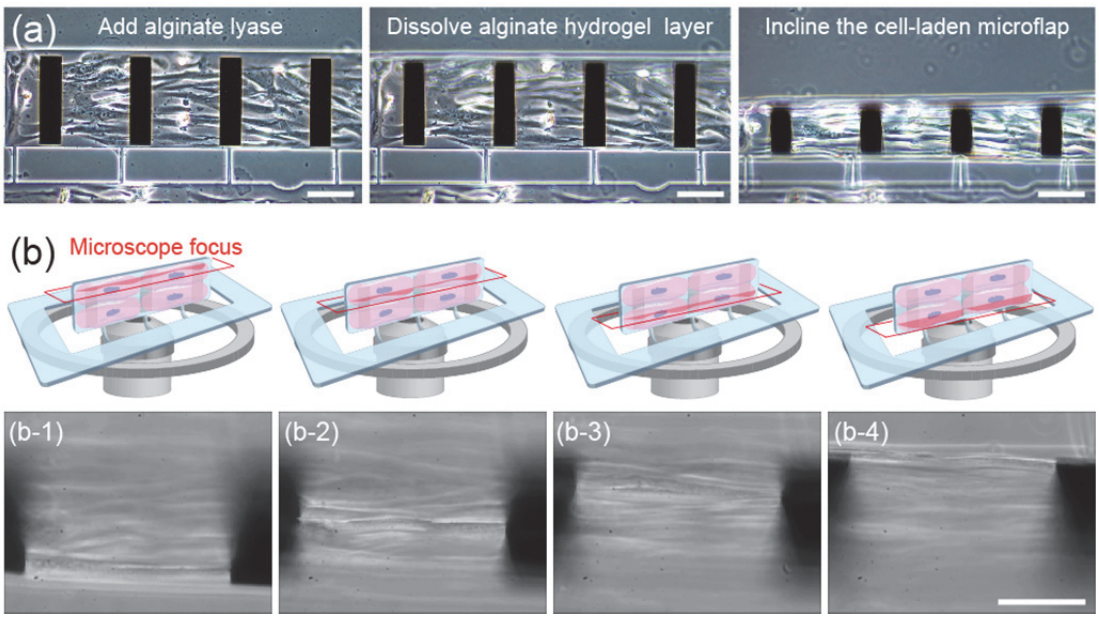

Figure 3-8. Inclination of cell-laden microflaps. (a) Sequential images of microflaps after dissolution of alginate hydrogel sacrificial layer. Cell-laden microflaps were inclined by increasing magnetic field strength. (b) Observation of HFF cells inclined at 60° on the microflaps in the applied magnetic field. We changed the microscope focus on the cells from the top of the microflaps (b-1) to the bottom (b-4). We successfully observed the membrane boundary of the cells aligned along the long axis of the microflaps. The scale bars are 100 μm. Reprinted with permission from (Teshima, et al, Advanced Materials, 2014). Copyright 2014, Wiley.

estimate the force to induce the wrinkles and deformation of microflap surface. The bending stress of cell traction force is given as follows:

$$\sigma^{+}_{\max} = \frac{F}{S} = \frac{Me_1}{I} \qquad \sigma^{-}_{\min} = -\frac{F}{S} = -\frac{Me_2}{I} \tag{3-1}$$

where F, S, M, and I are the cell traction force, the area of microflap, bending moment, and the moment of inertia of area, respectively; e_1 and e_2 are the lengths between the surface of microflaps and neutral axis of the section. Here, the curvature of neutral surface, ρ^{-1} is determined as.

$$\frac{1}{\rho} = \frac{M}{EI} \tag{3-2}$$

Thus, by substituting equation (3-2) for (3-1), the radius of curvature of deformation of microflap is obtained as:

$$\rho = \frac{EI}{M} = \frac{Ee_1}{\sigma_{\max}} \tag{3-3}$$

The radius of curvature of deformation of microflap (ρ) is estimated to be 100 mm, with high elastic modulus of parylene (E = 3 GPa) and the rectangular cross-section of 220 μm in height and 350 nm in thickness (I = 9.45 μm^4, S = 0.22 mm^2, e_1 = 175 nm). This determined value of the radius of curvature indicates that the deformation caused from cell traction forces is ignorable and parylene substrates provide adequate mechanical strength to bear the cell traction force. Furthermore, the cells were cultured on the microflaps for more than 5 days, which suggests that the ability of the MPC polymer to repel cell adhesion continued for 5 days; HFF cells exhibit contact inhibition. These results indicate that the enzymatic release and magnetic handling process employed in this study are gentle enough to circumvent cell damage, and suitable for long-term observation of living adherent cells.

3.3.2 Observation of cell membrane boundary

We verified that this microflap system enables us to observe cell boundaries from multiple angles under a conventional microscope; in this experiment, we used an inverted microscope with 40× - 60× objective lens (Figure 3-8(b)). By changing the microscopic focus from the bottom to the top, we were able to obtain the images of the cell membrane surface of all cells. The cells remained aligned along the long axis of the microflaps after inclination. To observe the boundary of the cell plasma membrane, fluorescent microparticles (blue, φ = 4.5 μm) were attached to the membrane surface of cells cultured on the microflaps (Figure 3-9(a)). By applying a magnetic field ranging from 5000 to 20000 A/m, we were able to find an appropriate inclination angle and focus on the interface between the target cells and microparticles.

Consequently, we obtained the images of the interface between the cells stained by Calcein-AM and fluorescent microparticles (Figure 3-9(b, c)). Continuous application of an optimized magnetic field held the cell-laden microflaps at a certain angle in the desired orientation and enabled us to observe the targeted microparticles from the desired angles. Since the refractive index of parylene is about 1.6 (Hubers et al., 2001), the parylene leads to the refraction of light. However, we did not observe deformation and distortion in the obtained images because the parylene layer is flat and thin. These results indicated that our method is suitable for observing the surfaces of stretched single cells from multiple angles, while maintaining cell viability and morphology. By simply combining the cell-laden microflaps in the cell culture dishes and

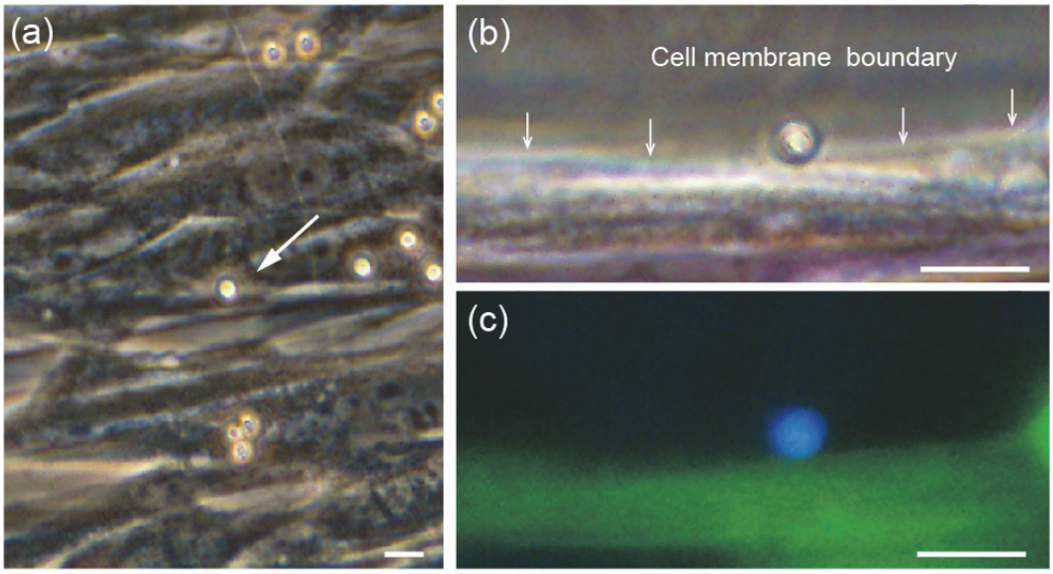

Figure 3-9. Observation of cell membrane surface after magnetic inclination. (a) Magnified image of fluorescent microparticles attached to surface of cells on non-inclined microflaps. The arrow indicates the microparticles. (b, c) Phase-contrast/fluorescent images of fluorescent microparticles (blue, ϕ= 4.5 μm) attached to surface of cells on inclined microflaps. HFF cells (green) were stained by calcein-AM. The arrows indicate the cell membrane boundary. The scale bars are 10 μm. Reprinted with permission from (Teshima, et al, Advanced Materials, 2014). Copyright 2014, Wiley.

conventional microscopes, we obtained the clear focused images of cell boundaries after inclining the microflaps with high-magnification lens. Since both the transparent parylene microflaps and ring-shaped magnets do not disturb the light path of microscopes, it is possible to apply the microflaps system to the both upright and inverted microscopes throughout inclination process.

3.3.3 Long-term cell culture on the microflaps

We investigated long-term culture of cells loaded on the surface of microflaps. When we utilized HFF cells on the microflaps, we found that the proliferation speed of HFF cells was fast compared with the other type of cells such as neural cells, and it is difficult to conduct long-term culture and observation of cellular activity in the confluent state. Thus, investigation of behavior of the cells with slow proliferation speed or the differentiated ones would provide us with the information about how long we culture and observe the cells on the microflaps, and how durable to long-term incubation the microflaps are. In this study, we tested the culture of neuron-like PC12 (rat adrenal pheochromocytoma) cells on the microflaps coated with collagen IV as the model of long-term culture and observation. PC12 cells do not proliferate and tend to extend nerve growth factor (NGF)-induced neurites after differentiation by addition of NGF (Berdichevsky et al., 2010; Bhang et al., 2009; Hsiao et al., 2011).

We verified that this microflap system enables us to observe cell boundaries of PC12 cells from multiple angles under a conventional microscope. The neural cells first attached randomly when suspended in DMEM containing FBS and Horse Serum, and then gradually moved from the MPC polymer-coated cell-repulsive area to collagen IV-coated cell-adhesive microflaps. After the cells attached on the surface of microflaps, we replaced the media with serum-free DMEM containing NGF for the neuronal differentiation, while keeping them inclined in the applied magnetic field. It took about 30 min for PC12 cells to adhere to the microflaps and start

to migrate (Figure 3-10(a)). In the same manner as HFF cells, we were able to observe PC12 cells and their cell membrane boundaries from multi-angles by optimizing the inclination angle of microflaps, even when they were not in the confluent state. By changing the microscopic focus from the bottom to the top in an inverted microscope with 20× objective lens, we were able to obtain the images of the cell membrane surface of all cells (Figure 3-10(b)). We found that the directions of both cell migration and neurite outgrowth were not dependent on the one

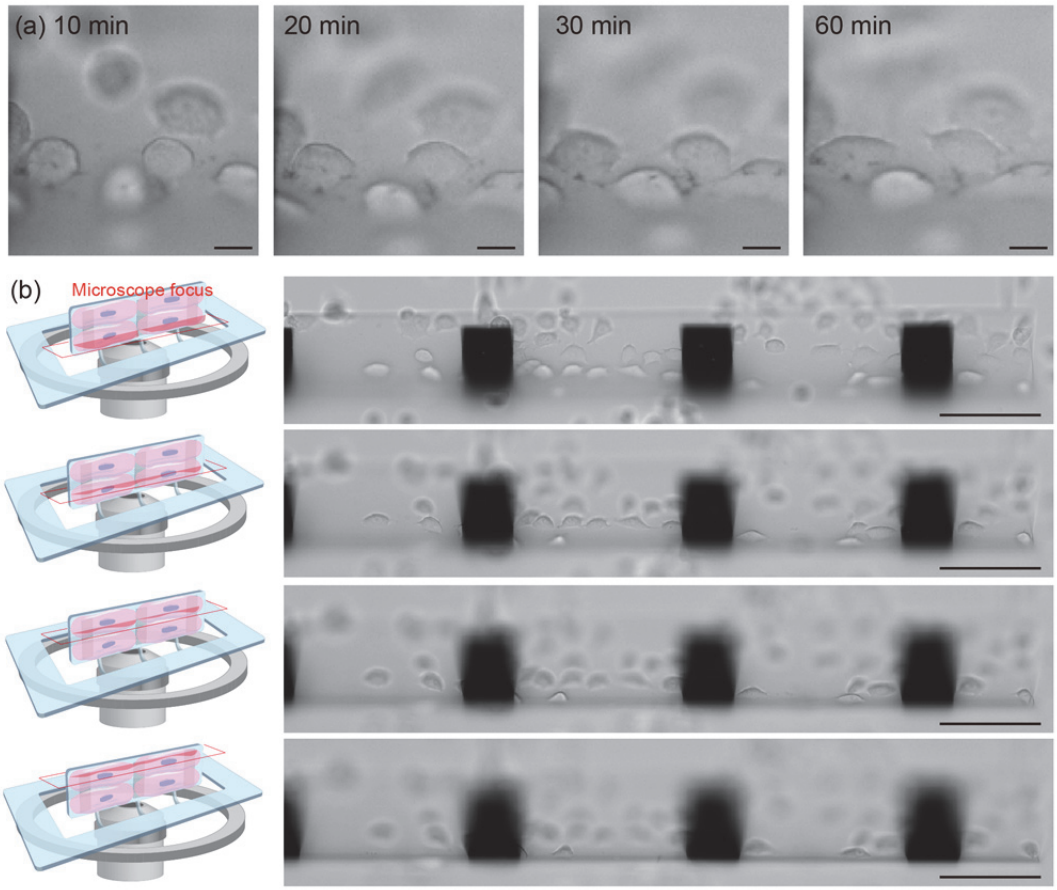

Figure 3-10. Observation of PC12 cells on the surface of inclined microflaps. (a) Time-lapsed images of cells that were adhering to the parylene surface. (b) Observation of HFF cells inclined at about 63° on the microflaps in the applied magnetic field. We changed the microscope focus on the cells from the bottom of the microflaps to the top. The scale bars are 10 μm (a), and 100 μm (b).

of gravity, which indicates that there were few influence of gravity on the behavior of inclined cells. The inclined microflaps helped us to understand the cell morphology including the shape of cell membrane at the timing of elongation and shortening of neurites, and the angle from the top of PC12 soma to the edge of neurites (Figure 3-11(a)). More than approximately 70% of somas of single PC12 continued the cells exhibited elongation and shortening of neurites for more than one week. The inclination angles of microflaps were ranged from 63 to 65 degree with few vibrations, which is constant enough to observe cell behavior form more than one week in the stable substrates (Figure 3-11(b)). In 6 days after incubation, however, the cells on the microflaps turned to be sphere-shaped, though they continued elongation and shortening of neurites. As shown in Figure 3-11(c), the average radius of curvature of PC12 cells increased from 6.6 μm to 28.2 μm after suspending cell, and decreased from 30.3 μm to 10.4 μm in 6 day

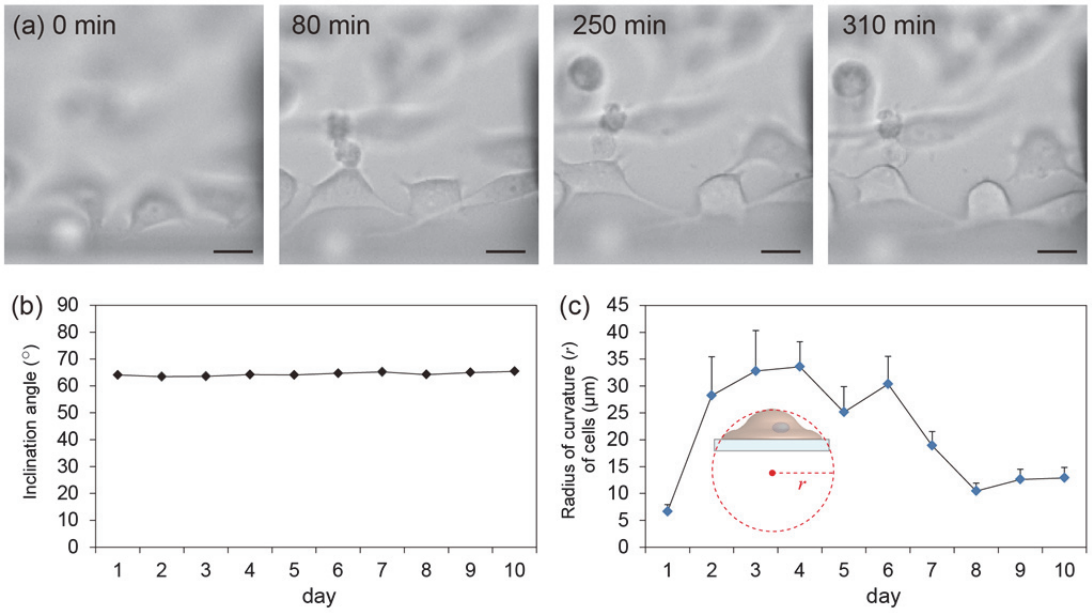

Figure 3-11. Long-term culture of PC12 cells on the surface of inclined microflaps. (a) PC 12 continued elongation and shortening of neurites. (b) The inclination angle of cell-laden microflaps during long term incubation. (c) Change in radius of curvature of cells loaded on the microflaps during long term incubation. The scale bars are 10 μm.

culture. Since this cell detachment from the microflap surface was observed in the cells cultured on the microflaps that were not inclined, it is expected that the cell detachment is caused by the effect of inclination or gravity, but the consumption of collagen IV coated on the microflaps. Eventually, the temperature of media or cellular activity such as adhesion and migration would require ECM coated on the microplates and spend all of them. These results indicate that we can perform long-term culture and observation of loaded adherent cells on the microflaps for less than one week, and maximum term is totally dependent on the existence of ECM on the surface of microplates. To realize the longer time observation of cells, it is required to establish the technology to compensate for the consumed ECM on the microflaps and replace with new one.

3.3.4 Observation of parasite infection into cells on microflaps

To demonstrate the ability to observe the plasma membrane boundary, we traced microbial infection of the host cells (HFF) by a species of parasites, *Toxoplasma gondii* (*T. gondii*). A detailed analysis of the microbe motility during the invasion process through the host cell membrane provides essential information regarding the exact timing and location of protein expression (Carruthers et al., 2007; Tonkin et al., 2011). The invasion direction into 2D cultured cells and the optical path for the observation are along the same axis, as illustrated in Figure 3-12(a). In this case, because the sole evidence for determining the parasite invasion is the slight difference in the image contrast, it is difficult to capture the moment of parasite invasion and confirm whether parasites are located inside or outside the host cells (Figure 3-12(b)). This difficulty also hampers the comprehension of parasite behavior at each stage of infection: attachment, invasion, and sealing (Alexander et al., 2005; Boothroyd et al., 2008; Handa et al., 2007; Sweeney et al., 2010). In the following experiments, we addressed these challenges by using the inclined microflaps to observe the interface between parasites and the inclined host cell membrane from multiple angles (Figure 3-13(a)).

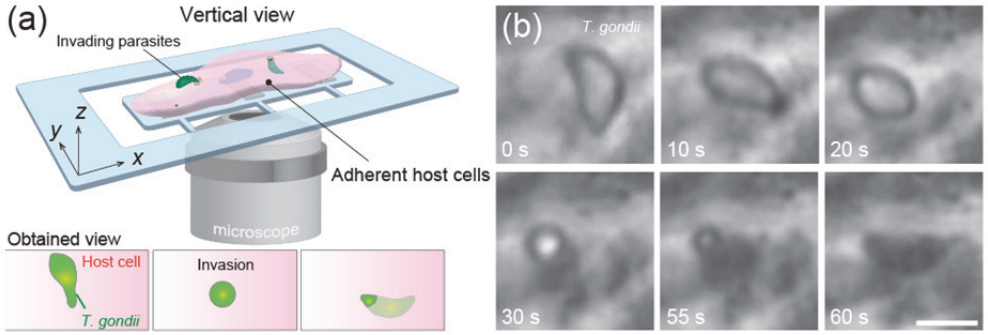

Figure 3-12. Observation of parasite behavior on their host cells before inclining the microflaps. (a) Schematic image of magnetically responsive microflaps for inclining host HFF cells infected by *T. gondii*. (b) Time-lapse images of *T. gondii* invasion into 2D-cultured host HFF cells. Because the sole evidence for determining the parasite invasion is the slight difference in the image contrast, it is difficult to capture the moment of parasite invasion and confirm whether parasites are located inside or outside the host cells. The scale bar is 5 μm. Reprinted with permission from (Teshima, et al, Advanced Materials, 2014). Copyright 2014, Wiley.

We first examined two steps in motion of the parasites: gliding and invasion. Time-lapse sequences showed that *T. gondii* gradually approached the inclined HFF cells and exhibited gliding motility to prepare for invasion. When *T. gondii* performed the gliding motion, we observed two distinct forms: helical gliding and upright twirling that are shown in Figure 3-13(c, e). After they attached their entire bodies to the host cell membrane by bringing their tails down as shown in Figure 3-13(b), helical gliding commenced while the parasites are rubbing their bodies against the host cell in forward and backward motion as shown in Figure 3-13(c). During helical gliding, the parasites paused and moved with a variety of velocities ranging from 0 to 1.4 μm/sec. They then exhibited upright twirling attaching their anterior side to the host cell membrane vertically (Figure 3-13(e)). The upright twirling had random speed of rotation, estimated to be from 0 to approximately 40 rpm, and unstable angle from host cell membrane boundaries, ranging from <10° to 90°. In the transition from helical gliding to upright twirling, we found that they exhibited a bending motion (Figure 3-13(d)). During the bending motion, the

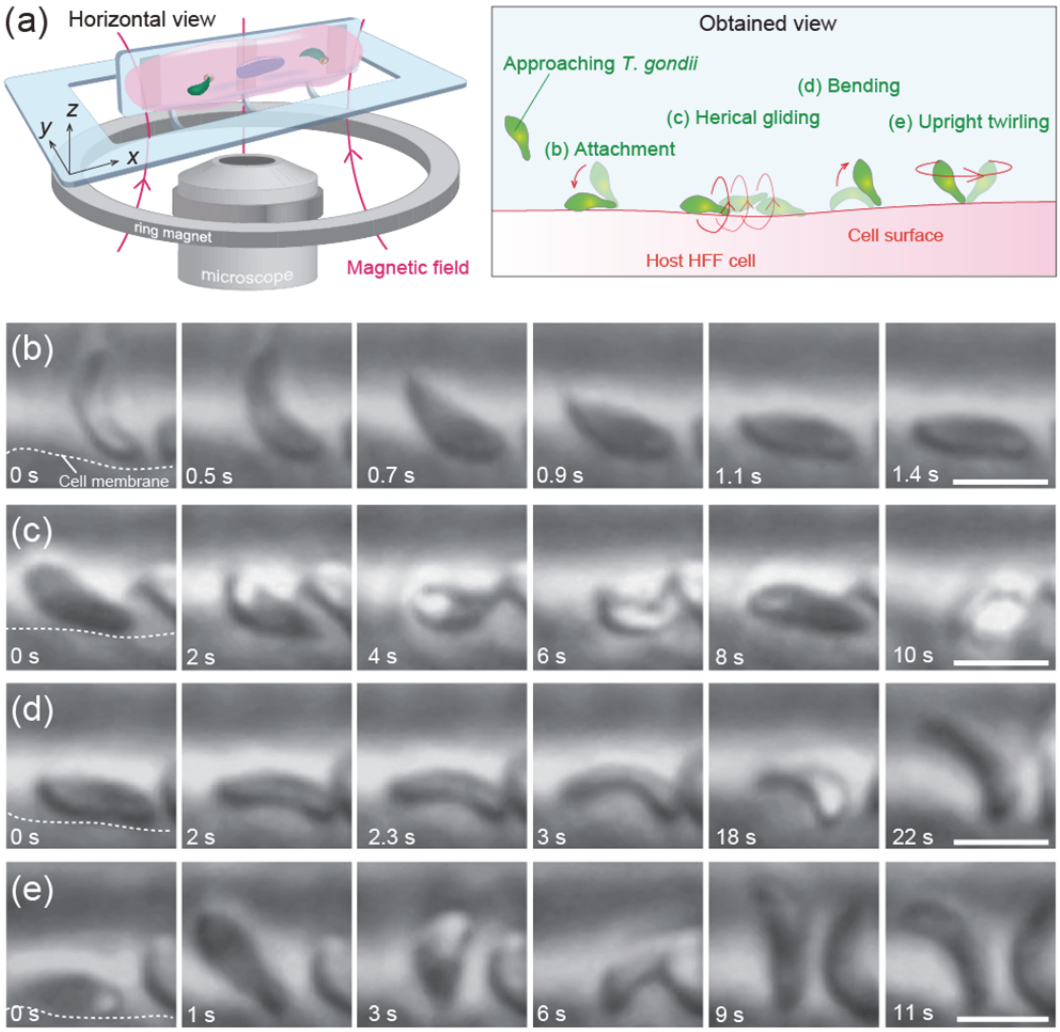

Figure 3-13. Observation of parasite behavior on their host cells inclined by the microflaps. (a) Schematic image of the microflaps for inclining host cells infected by *T. gondii* and obtained cross-sectional view of gliding parasite body on the surface of host cell membrane. (b) Time-lapsed images of parasite attachment to the host cell membrane. They attached their entire bodies to the host cell membrane by bringing their tails down to commence helical gliding. (c) Time-lapsed images of helical gliding motility. Helical gliding commenced while *T. gondii* were rubbing their bodies against the host cell in forward and backward motion. (d) Bending motion of *T. gondii* to commence upright twirling. During the bending motion, the parasites paused and moved while maintaining a concave shape. (e) Upright twirling of *T. gondii*. After helical gliding, *T. gondii* exhibited upright twirling attaching their anterior side to the host cell membrane vertically. The scale bars are 5 μm. Reprinted with permission from (Teshima, et al, Advanced Materials, 2014). Copyright 2014, Wiley.

parasites paused, span their bodies, and moved while maintaining a concave shape; the radius of curvature of the concave shape is approximately 3 μm. These measurement values regarding two gliding motilities and bending motions have never been reported by previous studies using conventional microscope observation. Accordingly, observation of the cell membrane surface of the cells inclined on the microflaps enabled the detailed analysis of the motility and trajectory of invading parasites.

Next, we traced the time-scale of parasite invasion into the host cells in real-time movies as shown in in Figure 3-14(a). The time-lapse images in Figure 3-14(b) indicate that after pause gliding for more than 1 min, it was less than 1 min to totally invade the host cells. During invasion, the parasites proceeded along the host cell surface, rubbing their bodies against the host cell membrane. Interestingly, the trajectory of the invasion described an arc along a circle, and the velocity of invasion was almost constant, which is different from the gliding motility. The invasion angle of *T. gondii* gradually increased from 10° up to 105° (Figure 3-14(c)). In the final step of invasion, they raised their tails to dive into the host cells. These sequential images of the motility with frequent changes, including gliding, bending and invasion, have never been acquired in previous works (Hakansson et al., 1999). Compared with the conventional observation shown in Figure 3-12(b), the microflaps enabled us not only to determine the moments at which the invasion began and ended, but also to obtain detailed information about the trajectory at sub-micron scales, invasion angle, and adhesion area between two cells. As a result, this method offers newly obtained information on three different modes of parasite invasion: upright twirling, helical rotation, and invasion. The clear images of invading parasites at the interface of host cell membrane were taken under the inverted microscopes with an inverted microscope with 60× objective lens, which enabled us to obtain the high resolution images at sub-micron scales.

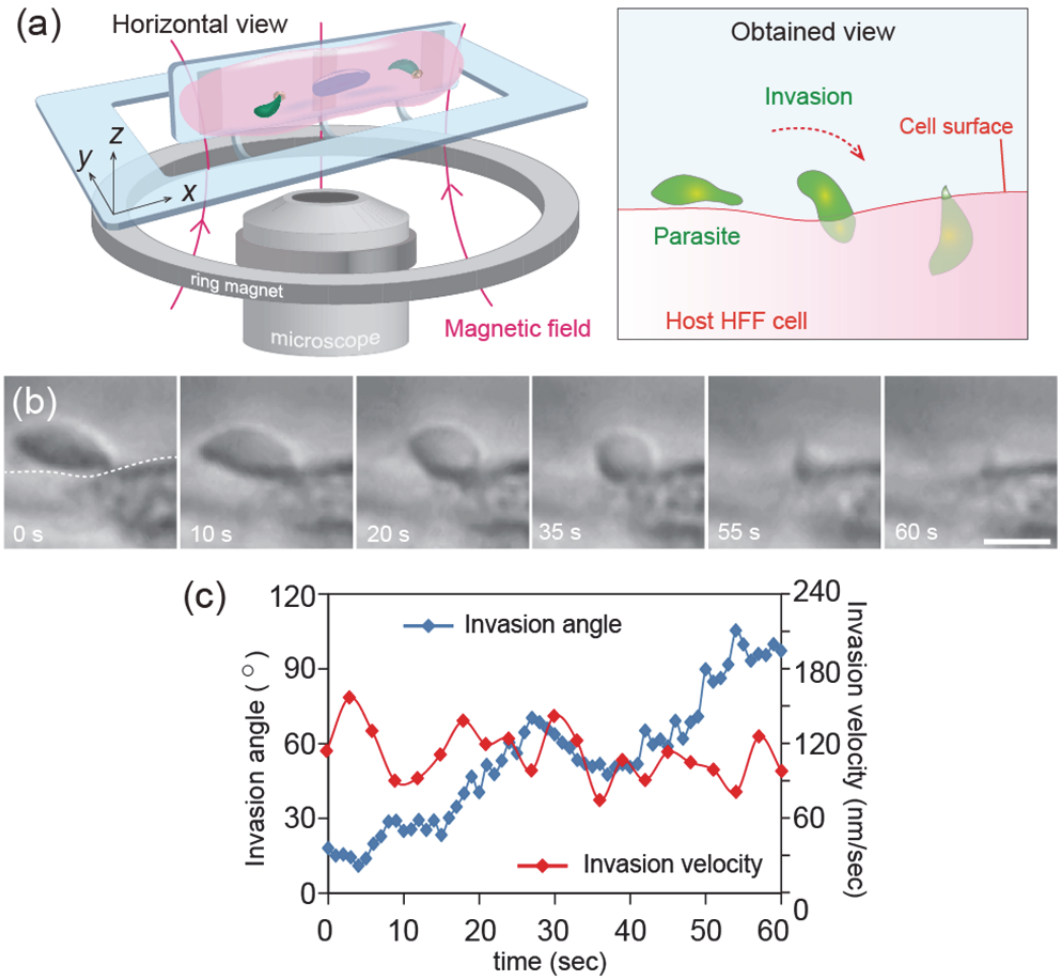

Figure 3-14. Observation of parasite invasion into their host cells inclined by the microflaps. (a) Schematic image and obtained cross-sectional view of the microflaps for inclining host cells infected by *T. gondii*. (b) Time-lapsed images of parasite invasion into HFF cells inclined on the microflaps. (c) Angle and velocity of *T. gondii* during the invasion into HFF cells. The scale bar is 5 μm. Reprinted with permission from (Teshima, et al, Advanced Materials, 2014). Copyright 2014, Wiley.

3.3.5 Confocal observation of parasites

In the section 3.3.4, we discussed the bright-filed image of cell membrane of cells inclined on the microflaps. In the cell biological field, however, it is necessary to obtain high resolution images of detailed cellular structure inside, intra-membrane, and outside the cells. To realize the

high resolution images, the confocal observation is commonly conducted to obtain the scanned images that show the localization and deformation of fluorescent-tagged multiple cellular components. By applying confocal microscopy to the microflap system, we obtained clear cross-sectional image of the cell plasma membrane after parasite infection. First, we reconstructed the cross-sectional image from three-dimensional stacked *x-y* images of parasite-infected cells (Figure 3-15(a, b)). The resolution of Figure 3-15(b) is too low to comprehend the location of parasite and the membrane boundary of host cells. When we inclined the microflaps up to 90° under an applied magnetic field, we obtained cross-sectional images during a single scanning of *x–y* plane without reconstructing images into three-dimensional stacked images. The confocal *x–y* plane image shown in Figure 3-15(c)

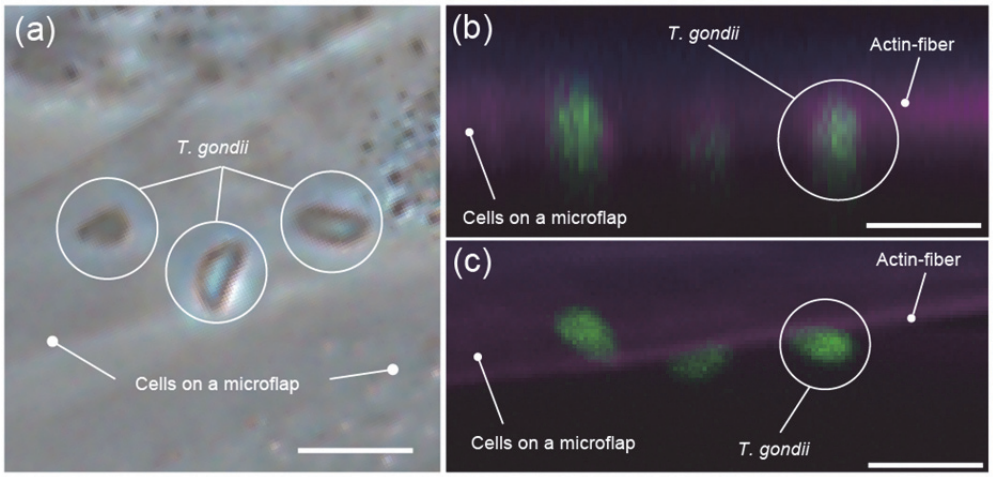

Figure 3-15. Confocal observation of parasite behavior on their host cells before and after inclining the microflaps. (a) Phase-contrast image of *T. gondii* around plasma membrane of HFF cells on microflaps before inclination. (b) Confocal observation of HFF cell stained for actin filament (magenta) and green fluorescent protein expressing *T. gondii* (green). Scanned lateral images were stacked and the cross-sectional image of cells was reconstructed. (c) Confocal observation of HFF cell invaded by *T. gondii*. The scale bars are 10 μm. Reprinted with permission from (Teshima, et al, Advanced Materials, 2014). Copyright 2014, Wiley.

critically shows not only that only the leftmost of three parasites was located under the TRITC-phalloidin-labeled cells, indicating that it totally invaded the host cells, but also the imaging with real-time observation shown in Figure 3-13(b-e) and Figure 3-14(b), this intracellular molecules (GFP) of parasites before and after invasion. By combining confocal technique has the potential to reveal distinct sets of proteins involved in attachment, gliding motility, invasion, closure and separation (Carruthers et al., 2007), and to elucidate the mechanisms that drive microbial infection.

3.4 Discussion

The materials we used for the microflap have three advantages: biocompatibility, transparency and high magnetic permeability. The biocompatibility of parylene and embedding permalloy in parylene ensured long-term culture (>1 week) and observation of seeded adherent cells without cytotoxicity, while the conventional microflaps made of metals such as nickel (Chang et al., 2009; Judy et al., 1997), Si/phosphorus-doped SiO_2 (Robaina et al., 2011), Epoxy/Ge/Si (Schmidt et al., 2002), Ti/ carbon nanotube (De Volder et al., 2012), and permalloy (Fan et al., 2002; Zou et al., 2001) have never achieved culture of adherent cells. Although recently mobile substrates to manipulate adherent cells magnetically by using biocompatible materials (Gach et al., 2010; Kim et al., 2011b) have been fabricated, they lack angle-tunability in inclination. While some reports recently added the biocompatibility characteristic to magnetically responsive microflaps by using photocurable resin (Kim et al., 2013; Kim et al., 2011a) or photoresists (Sakar et al., 2010), there are still few approaches to utilize the microflaps for biomedical applications such as cell handling technologies. In this study, the biocompatibility of parylene (Khodagholy et al., 2011) and embedding permalloy in parylene ensured long-term culture (>1 week) and observation of seeded adherent cells without cytotoxicity. Since high transparency of parylene does not disturb the light path of microscopes,

it is possible to equip the microflap system to both upright and inverted microscopes. Although, conventionally, physical obstruction of microscope components have resulted in technical limitations on inclination of the optical pathway (Charriere et al., 2006; Dormann et al., 2006; Ewanowich et al., 1989; Huisken et al., 2004; Toomre et al., 2010), the ability of microflaps to "add-on" to any types of conventional microscopy including phase contrast, differential interference contrast, fluorescence, and confocal microscopes, allows multi-angle real-time observation of inclined cells with high magnification throughout the inclination and cell-culture process. Finally, high magnetic permeability of permalloy facilitates easy control of inclination angle of cell-laden microflaps by controlling the strength of the applied magnetic field as well as the metal microflaps reported previously (Chang et al., 2009; Iwase et al., 2006). Unlike electrically (Jager et al., 2000) or thermo-kinetically (Kaajakari et al., 2003) actuated microflaps, magnetically responsive microflap does not require electric wiring, and allows remote actuation of cell-laden microflaps from the outside of culture dishes, which enables us to avoid the risk of contamination and exposure to infectious microbes. The transparent polymers and magnetic materials that are compatible with MPC polymers and are resistance to chemical etching in the fabrication process are able to be utilized as the materials of microflaps such as magnetic polymer composite materials. As one of these materials, we specifically selected parylene as the transparent polymer with high elastic modulus (3 GPa), (Hassler et al., 2010) and permalloy as the magnetic material with high magnetic susceptibility (1.0 T) (Donolato et al., 2010) in this study. Although the magnetic manipulation of cell-laden microflaps demonstrated here was all manually operated, they can be improved by incorporating the fast, reliable and fully automated system to regulate the strength and orientation of applied magnetic field toward auto-focus live-cell imaging with feedback control of obtained images (Petit et al., 2012).

Multi-angle observation of parasite invasion showed that *T. gondii* exhibited a distinctive pattern of behaviors, especially the bending motion that has not yet been observed by previous

approaches (Hakansson et al., 1999; Sweeney et al., 2010). When we observed the bending motion under conventional microscopes, the obtained images showed that the parasites got shortened along the long axis because motions and deformations in *z* axis cannot be traced. Herein, multi-angle snapshots of bending motion obtained by the microflap system provide biologically fundamental information to confirm which part of the parasite attached to the surface of host cells for migration, estimate the physical forces, and understand the exact timing and location of protein expression corresponding to their behaviors. Since infectious microbes, including parasites and bacteria, generally behave with motions in *x*-*y*, *y*-*z* and *x*-*z* plane, multi-angle observation on the microflaps is a promising method for detailed analysis of the microbial motility.

High angle-tunability and experimental versatility of the microflaps are critically important for applications to a wide range of biological studies. The combination of two materials, parylene and permalloy, provides a unique concept for handling adherent cells while maintaining their viability and morphology. Here, if the following two additional requirements were realized, the microflaps would become more attractive tools for biologists: the ability to pick up specific cell-laden microplates among all microflaps, and availability to the microscopic lens with shorter focal length. These two points are not achieved in this chapter mainly due to the existence of hinges. In this study, the microdisks have a potential to fulfill these two requirements, since they have no hinges and achieve high mobility during manipulation that is discussed in the chapter 4.

This microflap system has no limits on the types of adherent cells seeded, such as primary neuronal cells or stem cell, by coating the appropriate ECM on the microflap surface for each type of cells. There are also demands from biologists to investigate the effects of vibrations (Nikolaev et al., 2012; Park et al., 2010), gravity (Ma et al., 2013), and shear stress (Ueki et al., 2010) on morphology, proliferation and differentiation of adherent cells. The microflap

proposed here would be useful for such studies by culturing the cells on the microflap oscillating in the certain frequency. Multi-angle observation of cell plasma membrane is highly required for many biological studies such as not only microbial infection into host cells (Bargieri et al., 2013), but also protein secretion (An et al., 2010; Rappoport et al., 2003), migration (Fraley et al., 2012; Shulman et al., 2012), membrane budding (Hurley et al., 2010), and cell division (Hesse et al., 2012) at plasma membrane boundaries. This observation technique is thus broadly applicable for monitoring the plasma membrane dynamics.

CHAPTER 4

EXPERIMENTAL RESULTS & DISCUSSION OF MICRODISK

An approach for manipulating single adherent cells magnetically is developed that is integrated with an enzymatic batch release. This strategy uses an array of releasable microfabricated mobile microplates without hinges, termed microdisks, formed from a biocompatible polymer, parylene. A parylene microdisk array of 10–70 μm in diameter can be formed on an alginate hydrogel sacrificial layer by using a standard photolithographic process. The microdisks with micro-sized optimal diameters are able to provide a limited area for single adherent cells to be isolated and sorted, while the single microflaps handle multiple adherent cells. In addition, the parylene surfaces are modified with fibronectin to enhance attachment, growth, and stretching of loaded single adherent cells. To load single cells onto these microdisks, cells are initially placed in suspension at an optimized seeding density and are allowed to settle, stretch, and grow on individual microdisks. The sacrificial layer underneath the microdisk array can be dissolved on a time-scale of several seconds without cytotoxicity. Release of single cell-laden microdisks allows higher degree of freedom in microdisk mobility than microflaps, resulting in the multi-angle observation of single cells loaded on microdisks. Each experiment is arranged and presented as a separate section by itself and will begin with single cell loading onto parylene microdisks without permalloy, followed by manipulation of single cell-laden microdisks with embedded permalloy pieces with manipulators or an applied magnetic field, the

observation of *T. gondii* invasion into single host cells cultured on the microdisks, and finally discussion.

4.1 Loading of Single Adherent Cells onto Microdisks

4.1.1 Optical characteristics of parylene films

The thickness of microdisks and the roughness of parylene surface were measured by using Laser Scanning Microscope (VK-X200, Keyence, Japan). To measure the thickness of transparent parylene surface, we deposited the Al layer on the surface of whole area. Figure 4-1(a-b) shows the surface of parylene microdisk with embedded permalloy layer, and indicates that the diameter of microdisk is estimated to 48 μm. Since the diameter of microdisk in the mask design is just 50 μm, it shows that O_2 plasma over-etched the parylene layer form the edge of microdisks into 48 μm. The aggregated fragment of MPC polymer is observed on the surface of glass substrates. Figure 4-1(c) shows the measured thickness of the diameter region of microdisk surface by laser-based scanning. This result indicates that the roughness is ranged from 10 to 35 nm, and the thickness of permalloy layer is about 100 nm. Since the microdisks have sacrificial alginate hydrogel layer underneath it, the roughness of the parylene microdisks is dependent on that of alginate hydrogel layer.

To optimize the thickness of the parylene layer, the UV-visible spectrum of a parylene layer with varying thickness on a glass substrate coated with alginate hydrogel layer was measured by UV and visible spectrophotometry (V-550ST, JASCO, Japan). Figure 4-1(d) indicates the optical transparency in the presence and absence of a parylene layer, with thicknesses of 2 μm or 12 μm, on a glass substrate coated with the alginate hydrogel layer under UV light. The glass substrate and alginate hydrogel layer transmitted UV light above 270 nm. In contrast, the parylene layer with a thickness of 12 μm exhibited high optical transparency at wavelengths above 350 nm and became opaque at wavelengths below 350 nm. The parylene layer with a

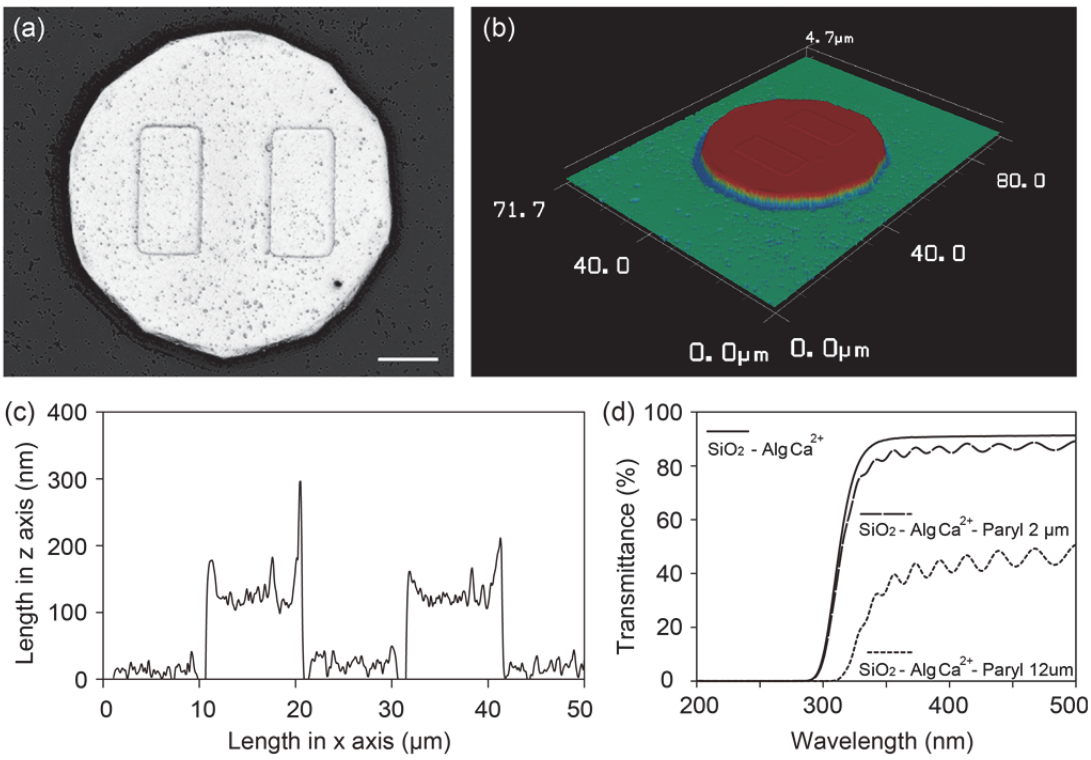

Figure 4-1. Parylene microdisks with embedded permalloy pieces. (a, b) Top view and reconstructed 3D images of parylene microdisks obtained by laser scanning microscope. (c) The graph of roughness of microdisk surface measured by laser scanning microscopes. (d) The UV-visible spectra of a glass slide coated with alginate hydrogel (Alg Ca^{2+}) (solid line) and a 2-μm- or 12-μm-thick parylene (Paryl) layer on a glass slide coated with alginate hydrogel (dashed and dotted line). The scale bars represent 10 μm.

thickness of 2 μm was less opaque in the UV region. In order to count the number of cells on the microdisks, we stained the nucleus by using Hoechst 33528 (λ_{ex} = 350 nm–360 nm). These results indicate that the 2-μm-thick parylene layer will not degrade images of cells stained by Hoechst 33528 or DAPI under a fluorescent microscope and also that 350-nm-thick microflap will not degrade it shown in Chapter.3. Furthermore, since the permalloy layer blocks the light pathway from the microscopic light sources, the area of permalloy pieces must be designed not to disturbs the observation of cells that are stretching on the microplates.

4.1.2 Diameter of microdisks

An array of parylene microdisks was fabricated on a glass substrate. To investigate cell number, morphology, and behavior, we first tried to culture a variety of cells onto the planar microdisk without permalloy layer, because the permalloy pieces disturb the optical pathway under the inverted microscopes and the observation of cells. The fabricated device comprises two areas: an array of fibronectin-coated parylene microdisks and a non-cell-adhesive glass surface coated with 2-methacryloyloxyethyl phosphorylcholine (MPC) polymer as shown in Figure 2-9(h-j). For single-cell loading, the diameter of microdisks is desired to be approximately the same as the size of single adherent cells; the microdisks ranged in size from 5 to 70 μm. The modifications in cell morphology are further investigated in Section "Observation of Cell Behavior on the Microdisks". In this experiment, we selected the standard diameter of microdisks to be 50 μm, because a diameter of less than 50 μm may cause nuclear deformation (Versaevel et al., 2012), apoptosis (Chen et al., 1997; Thery, 2010), and cell proliferative disorder (Thery, 2010; Thery et al., 2006) in long-term cultivation; this standard diameter is appropriate to endothelial, epidermal, or fibroblast cells, and can be changed according to the cell type. We seeded human foreskin fibroblast (HFF) cells onto an array of fibronectin-coated circular microdisks. After seeding, the cells on the MPC polymer-coated area remained spherical and gradually migrated to reach the microdisks. The cells then began to stretch around the microdisk surface (Figure 4-2(a)). The live/dead assay showed that almost all spherical cells that were not migrating and those that cultured outside of the microdisks eventually died. It took several hours to load all of the suspended cells onto an array of microdisks coated with fibronectin. Figure 4-2(b) show the single-cell laden microdisks whose nuclei were stained by Hoechst 33528.

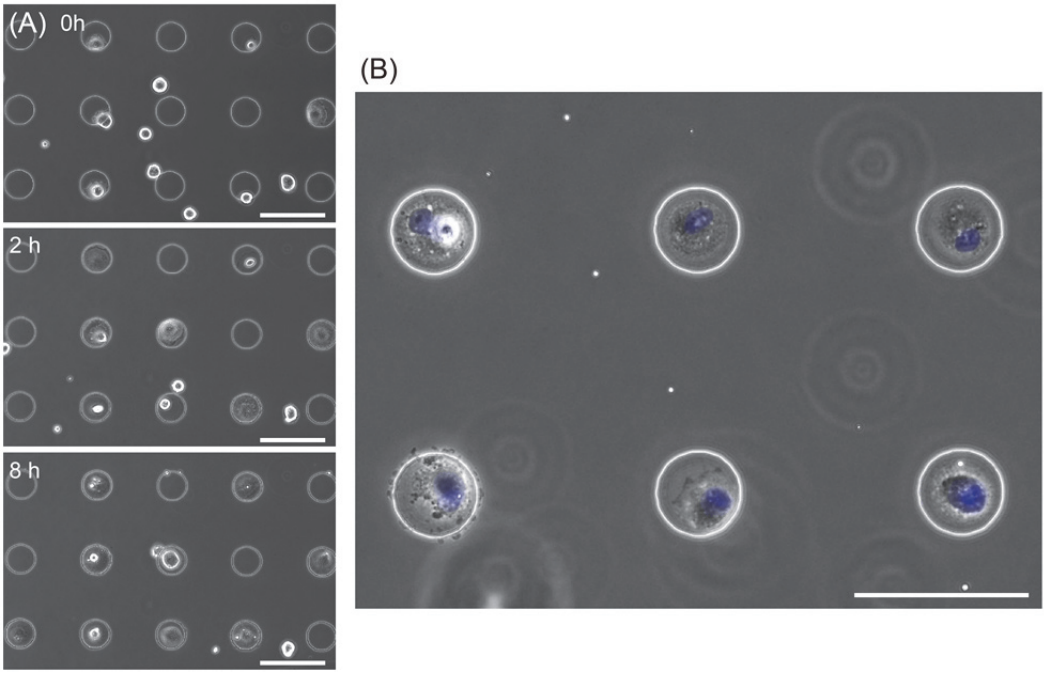

Figure 4-2. Cell culture on the microdisks. (a) Sequential phase-contrast images of HFF cells migrating around the microdisks. Images are taken at 0 h, 2 h, and 8 h after cell suspension. (b) An overlay of bright-field and fluorescent images of the HFF cells on the microdisks. Nucleus was stained with Hoechst 33528. The scale bars represent 100 μm. Reprinted with permission from (Teshima, et al, Small, 2014). Copyright 2014, Wiley.

4.1.3 Gap distance and seeding density

In addition to the diameter of the microdisks, we also found that two parameters strongly regulate the single-cell loading: the gap between adjacent microdisks and the seeding density. First, to investigate the effects of the distance between adjacent microdisks, we cultured cells on 50 μm microdisks with 10- to 75-μm gaps. As shown in Figure 4-3(a), we observed that the HFF cells on the microdisks formed bridges between pairs of microdisks on 50 μm microdisks with a 30 μm gap, which resulted in a low yield of single-cell loading onto single microdisks. The cells on the microdisks migrated only on the microdisk surface; however, their pseudopodia randomly distributed beyond the microdisk surfaces to reach neighboring microdisks. By increasing the gap between microdisks to more than 75 μm, the number of bridging cells was

made to decrease to less than 5%, as shown in Figure 4-3(b).

Second, the number of cells on microdisks was controlled by changing the seeding density of suspended cells to obtain a single cell per microdisk. After we suspended the HFF cells at various densities ranging from 20 to 200 cells/mm^2 on an array of microdisks with diameters of 50 μm and gaps of 75 μm, the number of single cells was counted by staining nuclei. Figure 4-3(c) shows the number of counted cells on the microdisks. The number of microdisks with multiple cells increased with increasing seeding density of suspended cells. W thus selected the

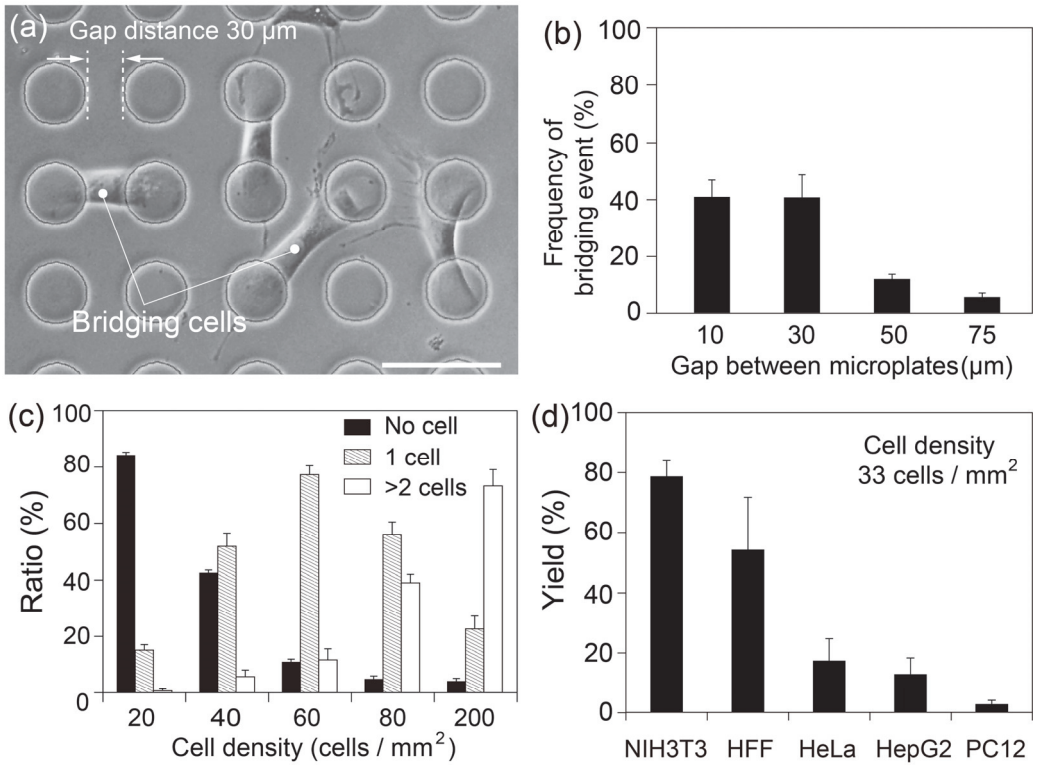

Figure 4-3. Loading of single adherent cells on the microdisks. (a) HFF cells bridging two neighboring microdisks. (b) A graph of cell-bridging events of HFF cells per single microdisk *v.s.* the gap between two microdisks. (c) A graph of the number of HFF cells on single microdisks vs. the seeding density of suspended cells. (d) The yield of cell adhesion onto the fibronectin-coated microdisks is plotted against cell type. The scale bars represent 100 μm. Reprinted with permission from (Teshima, et al, Small, 2014). Copyright 2014, Wiley.

seeding density to be 60 cells/mm^2 to achieve a single HFF cell per microdisk. Since the area of a single microdisk is about 2000 μm^2, the expected number of cells per microdisk is estimated to be 0.12 cells per microdisk when the seeding density is 60 cells/mm^2. Because this probability is calculated for the condition of non-migrating cells, the difference between the probable (12%) and experimental (80%) number of loaded cells is mainly caused by the effect of cell migration on the MPC polymer-coated surface; the cells initially placed on the MPC surface migrate, and eventually reach and settle on the microdisks. This effect would increase the number of cells on single microdisks by about seven times.

4.1.4 Cell type

We tested the culturing of various types of adherent cells on the array of microdisks with diameters of 50 μm and gaps of 75 μm: fibroblast cell lines (HFF, NIH/3T3) and non-fibroblast

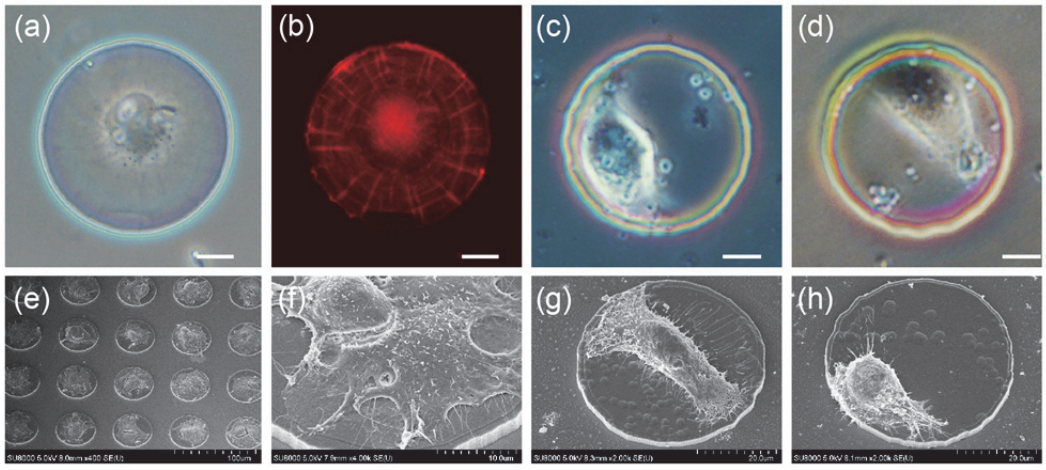

Figure 4-4. Culture of four types of adherent cells on the microdisks. (a) Bright-field and (b) fluorescent images of single HFF cells at 12 h after cell incubation. Red-stained actin fibers indicate that cells are stretching over the entire area of the microdisks. The HepG2 cells (c) and HeLa (d) cells did not completely cover the microdisk areas. A SEM image of (e,f) HFF cells, (g) HeLa cells, and (h) HepG2 cells. The scale bars represent 10 μm. Reprinted with permission from (Teshima, et al, Small, 2014). Copyright 2014, Wiley.

cell lines (HeLa, HepG2, PC12) (Figure 4-4(a-d)). The HFF and NIH/3T3 cells attached to more than half the arrayed microdisks after they were suspended. In contrast, the HeLa, HepG2 and PC12 cells attached to the less than 20% of the arrayed microdisks (Figure 4-3(d)). This difference can presumably be attributed to the differences in cell mobility between the different cell types and affinity to the substrate coated with fibronectin. SEM images in Figure 4-4(e-h) show that fibroblast cells were attaching and stretching to the whole area of microdisks, and non-fibroblast cells including HeLa, HepG2, and PC12 cells were attaching to a part of microdisk area.

4.1.5 Observation of cell behavior on the microdisks

The behavior of cells on microdisks was monitored by observing their cell cycle, proliferation, and morphology. The cell cycle was observed after loading the cells onto the microdisks using Fucci-gene-transfected HeLa cells (Sakaue-Sawano et al., 2008). We

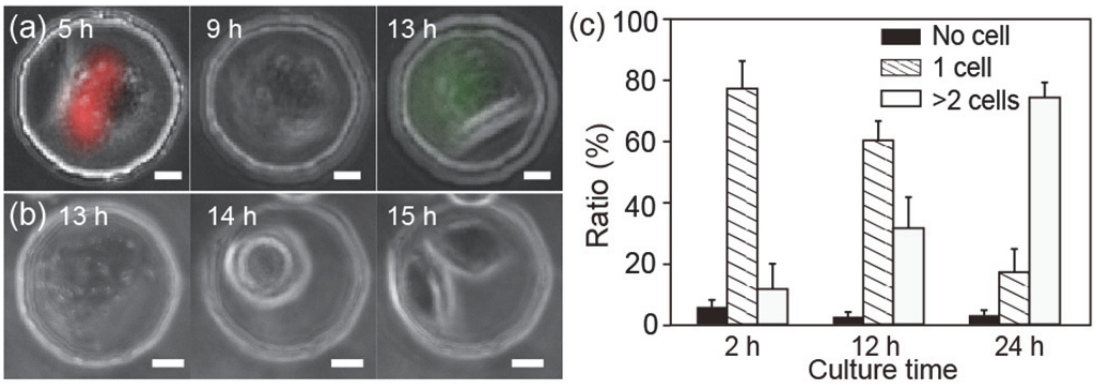

Figure 4-5. Single-cell behavior on the microdisks. (a) A single Fucci-transfected HeLa cell showing its cell cycle by fluorescence in its nucleus. (b) Sequential images of cell division on the microdisks. (C) Single cells proliferated only on the microdisk surface. At 12 h after cell incubation, more than 80% of the single microdisks held multiple cells. The scale bars represent 10 μm. Reprinted with permission from (Teshima, et al, Small, 2014). Copyright 2014, Wiley.

monitored changes in cell cycle during culture by detecting a fluorescence marker in the nuclei by means of fluorescent microscopy, as shown in Figure 4-5(a). As the cells modified their shape, the cell cycle turned from the growth phase (G1 period, red) to the synthesis phase (S/G2 period, green). After verifying the state of each cell cycle (M period), we observed that cell proliferation occurred only on the microdisk surface (Figure 4-5(b)). The cells on microdisks with diameters greater than 40 μm divided into two cells horizontally. As a result, two cells shared the same microdisk area. The percentage of single-cell-laden microdisks was greater than 60 % within a 12 h incubation. After a 24 h of incubation, approximately 80% of the microdisks had more than two cells (Figure 4-5(c)). These results suggest that cells on the microdisks undergo normal cell-cycle progression and also provide information about how they proliferate in the micropatterned area. When we kept single HFF cells on each microdisk for a single-cell survey, the assay duration was optimized to less than 24 h.

The morphology of the cells cultured on the 50 μm microdisks was investigated by observing the stretching area and immunostained cytoskeleton. After 6 h incubation, the HFF cells stretched over the whole microdisk area. The immunostained actin fibers inside single HFF cells extended in a radial pattern from the nuclei and reached the edge of the microdisks, as shown in Figure 4-4(a, b); in contrast, HeLa and HepG2 cells attached to less than half the microdisk surface when microdisks of 50 μm diameter were used (Figure 4-4(c, d)). We found that even when the microdisk diameter was changed from 5 to 70 μm, the HFF cells stretched all over the microdisks (Figure 4-6(a)). Confocal microscopic images of the tetramethylrhodamine B isothiocyanate (TRITC)-phalloidin-labeled cytoskeleton of the cells on various diameters of microdisks in (Figure 4-6(b)) represent cross-sectional images of cell morphology. While cells on microdisks with diameter of 5–20 μm partly attached to the limited microdisk area and formed spheres, the microdisks with around 40 μm diameter made cells dome-shaped. The larger the microdisk area (over 70 μm diameter), the more the cells spread

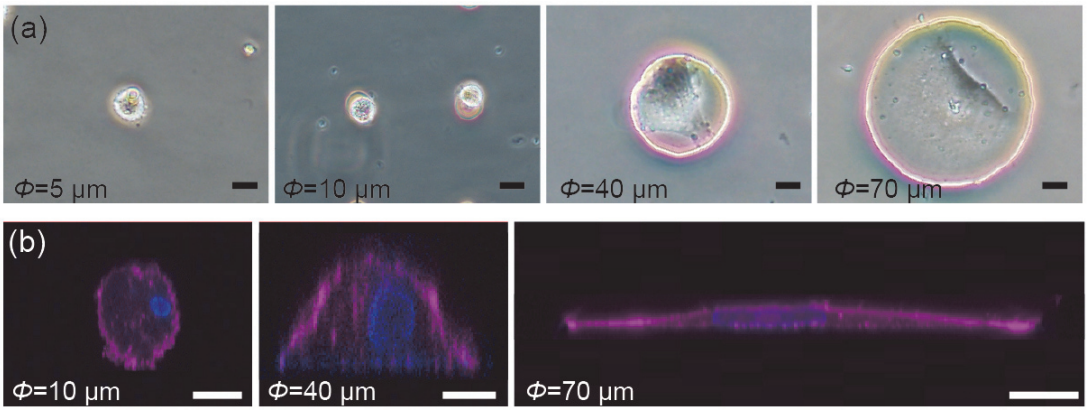

Figure 4-6. Morphology of single cells on the microdisks. (a) Top-view bright-field images of adherent cells on the microdisks. The size of the microdisk limited the area for single-cell location. (b) *x–z* cross-sectional confocal microscopic images of single adherent cells (red actin, blue nucleus). The scale bars represent 10 μm. Reprinted with permission from (Teshima, et al, Small, 2014). Copyright 2014, Wiley.

horizontally and formed flat shapes. These images indicate that the shape of adherent cells is highly dependent on the diameter of the microdisks. The microdisks with more than 40 μm diameter provided cells with space for single-cell stretching. Previous studies reported that the differences in cell morphology that trigger various cell growth or viability are controlled through modulation of the area of extracellular matrix (ECM) to which the cells bind (Chen et al., 1997; Vogel et al., 2006; Zhou et al., 2011). Their results indicate that the morphologies of adherent cells cultured on 2D-patterned ECMs are the same as those on microdisks. However, the previously reported block-shaped microcarriers (Onoe et al., 2008; Salazar et al., 2007; Wang et al., 2010; Wang et al., 2008) cannot regulate the adhesion area to control the cell morphology because cells tend to migrate to not only the top surface but also the side wall. This disk-shaped microdisk system possesses the same precision in modifying cell structure at the single-cell level as 2D cell patterning that is previously reported (Tseng et al., 2012; Vogel et al., 2006; Zhou et al., 2011).

We examined the biocompatibility of the microdisks to introduce adherent cells toward the long-term cell culture. We checked cell proliferation during culture by counting the number of DAPI stained nuclei. At first, single cells attached to the surface of single microdisks. By incubating cells on the microdisks for two days, any types of cells tended to migrate and proliferate only to the area of microdisks. When we focused on single HFF cell survey with this microdisk system, the assay duration is optimized about for less than 24 hours. In addition, the size of microdisks controls the direction of cell division. Single cells on microdisks with more than 40 μm diameter divided into two cells horizontally, and as a result, two cells shared the same microdisk area and horizontally divided cells attaching to the parylene surface remained alive. On the other hand, microdisks with less than 30 μm diameter force cells to divide vertically because the surrounding area of microdisks are modified by MPC polymers, and proliferated cells are located on the cells already attaching to the microdisk. After 1 day incubation, cell apoptosis assay showed that vertically piled-up cells induced cell apoptosis.

4.1.6 Loading single cell onto the microdisks with embedded permalloy

To demonstrate the single cell culture on the microdisks with embedded permalloy layer, we cultured four types of cells: HFF cells, PC12 cells, HeLa cells and HepG2 cells. HFF cells suspended in the media remained spherical on the surface of MPC polymer-coated surface and gradually migrated to reach the microdisks with permalloy bars. The cells then began to stretch around the microdisk surface, which leaded to the cell patterning only onto the microdisks (Figure 4-7(a)). As well as discussed in 4.1.5, all types of cells attached to the fibronectin-coated surface of microdisks (Figure 4-7(b-e)). There were no differences in cell morphology, migration speed, and ratio of cell attachment to the fibronectin surface between the microdisks with embedded permalloy layer and planar microdisks. Besides, the adhesion between parylene layer and glass substrate via alginate hydrogel layer was tight enough not to release the

microdisks with embedded permalloy during cell culture. We could culture the cells only onto the microdisks and confirm the proliferation of cells in the same way as microflaps and planar microdisks. There are some previous reports of the effect of magnetic field to down-regulate cell activities (Liburdy, 2000; Liburdy et al., 1993). To investigate the effect of magnetic field and embedded permalloy on the culture cells, the expression of Cx43 on each cell type was examined by western blot with or without the existence of magnetic field (Figure 4-7(f)). Connexins are a critical component of cellular gap junctions (GJs), forming structures that mediate intercellular communication (Bruzzone et al., 1996; Kim et al., 2002; Kumar and Gilula, 1996). Here, we checked the expression of one of the Connexins subtypes, Cx43, as the index of activity of adherent cells. While the amount of Cx43 in the neuronal cells or HeLa cells is comparatively little, fibroblast cells constantly expressed it in larger quantities, localized within their cell membrane. In this study, we measured the expression level of Cx43 in the one type of fibroblast cells, NIH/3T3, and non-fibroblast cells, (PC12 and HeLa) cells with and without applied magnetic field (100 mT). It is found that the expression level of Cx43 in non-fibroblast cells was low regardless of the existence of magnets. When we compared the NIH/3T3 cell cultured on the magnets with the ones without magnets, there was no difference in the expression amount of Cx43. This result indicates that there are few influences of magnetic field on cell morphology and the efficiency of loading cells. Besides, the microdisks with permalloy layer was gentle enough to circumvent cytotoxicity because permalloy layer were encapsulated by parylene, and suitable for long-term observation of living adherent cells. When we observed the cells on the microdisks under the inverted microscopes, the permalloy pieces tends to obscure light from light sources of microscopes and disturb the optical pathway for the observation. Therefore, to escape the light disturbance, the permalloy bar should be located on the edge of microdisks during the design and fabrication process, or we should employ the upright microscope for the observation of whole cell bodies.

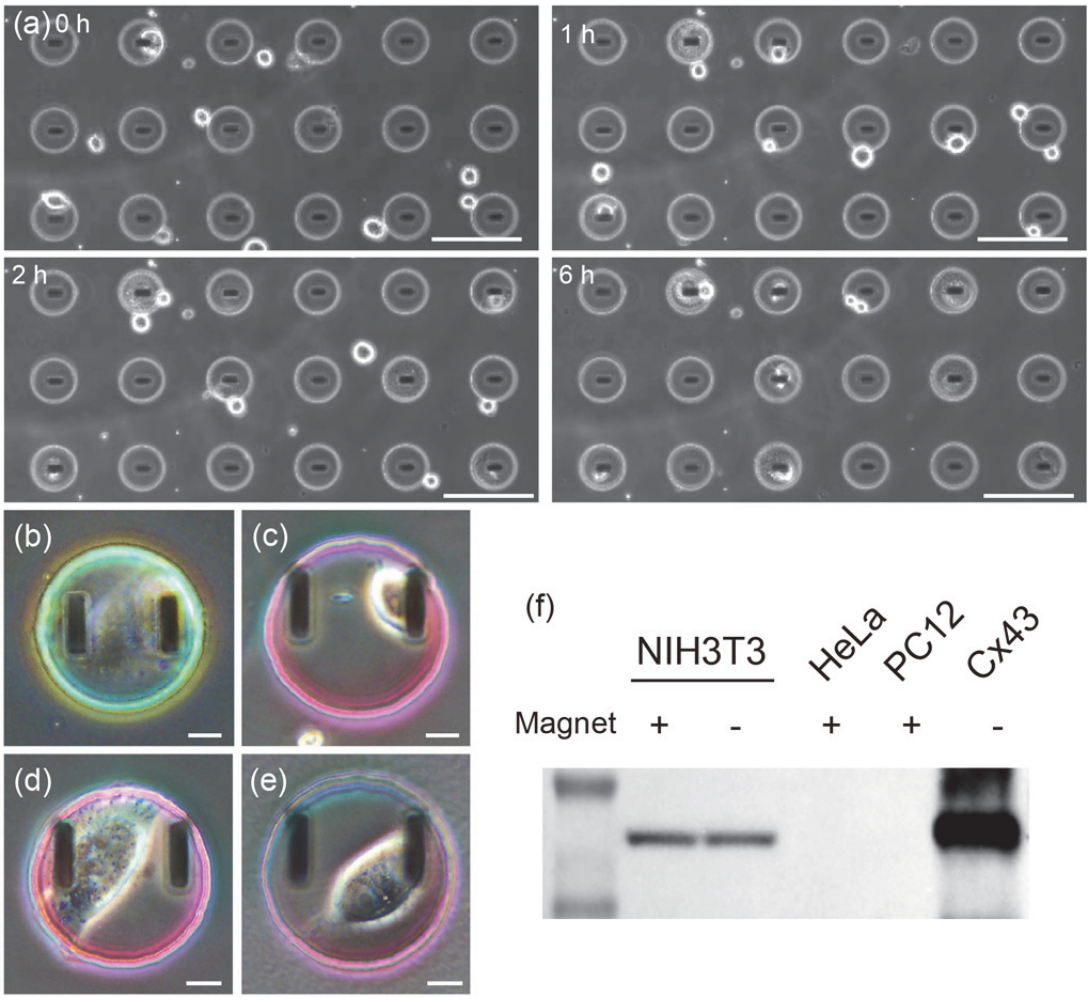

Figure 4-7. Loading of single adherent cells onto the microdisks with embedded permalloy layer. (a) Sequential images of cells migrating on the surface parylene and MPC-polymer coated area (0h, 1h, 2h, and 6h). (b) Bright-field images of single cells on the microdisks at 12 h after cell incubation. (b) HFF cell, (c) PC12 cells, (d) HeLa cells, and (e) HepG2 cells. (f) Western blot analyses of Cx43expressed on each cell type and Cx43. The blotted membrane was immunostained with either anti-Cx43. The scale bars represent 100 μm (a), 10 μm (b-e).

4.2 Manipulation of cell-laden microdisks

4.2.1 Enzymatic release of cell-laden microdisks

The dissolution of the alginate hydrogel sacrificial layer that connects the glass substrate and

the parylene microdisks was examined. Herein, we employed the gel–sol transition in the sacrificial layer connecting the glass substrate and the parylene layer. In general, sodium alginate solution becomes a hydrogel after combination with calcium ions (Ca^{2+}), and the alginate hydrogel layer could be immediately removed by introducing phosphate-buffered saline (PBS) without Ca^{2+} ions or a chelating agent such as ethylene diamine tetra-acetic acid (EDTA). By using these solutions, however, adherent cells would be detached from the microdisks, as reported previously (Gutwein et al., 2000; Li et al., 2008). Herein, we employed the enzymatic reaction of alginate lyase to dissolve the hydrogel, in order to prevent cellular detachment, because alginate lyase does not chelate Ca^{2+}. To visualize the dissolution of alginate hydrogel, we encapsulated green fluorescent nanometer-sized particles in the alginate hydrogel that were located and fixed only under the microdisk layer. Figure 4-8 shows the sequential overlay of bright-field and fluorescent images of cells on microdisks before and after dissolving the sacrificial alginate hydrogel layer. Just after adding alginate lyase, the color of the obtained image turned into orange due to the light reflection. Seven seconds after adding the alginate lyase, the green particles diffused out from under the microdisks, and the arrayed microdisks started to float around in the media. We traced the microdisks for 1 min after dissolving alginate hydrogel layer by using COSMOS software (SolidWorks Simulation Solutions) (Figure 4-9(a, b)). The measured displacement of microdisks after enzymatic dissolution is totally dependent on the flow in the media, and average displacement for 1 min is about 75 μm. The scanning electron microscopy (SEM) image in Figure 4-9(c) shows that the back of the microdisk surface was totally flat after enzymatic release. The alginate hydrogel sacrificial layer was completely dissolved and removed by enzymatic digestion. Consequently, all of the microdisks were detached from the glass substrates at room temperature. These results indicate that the precise sequence of enzymatic release facilitated the efficient collection of the objective population of cells with the desired characteristics.

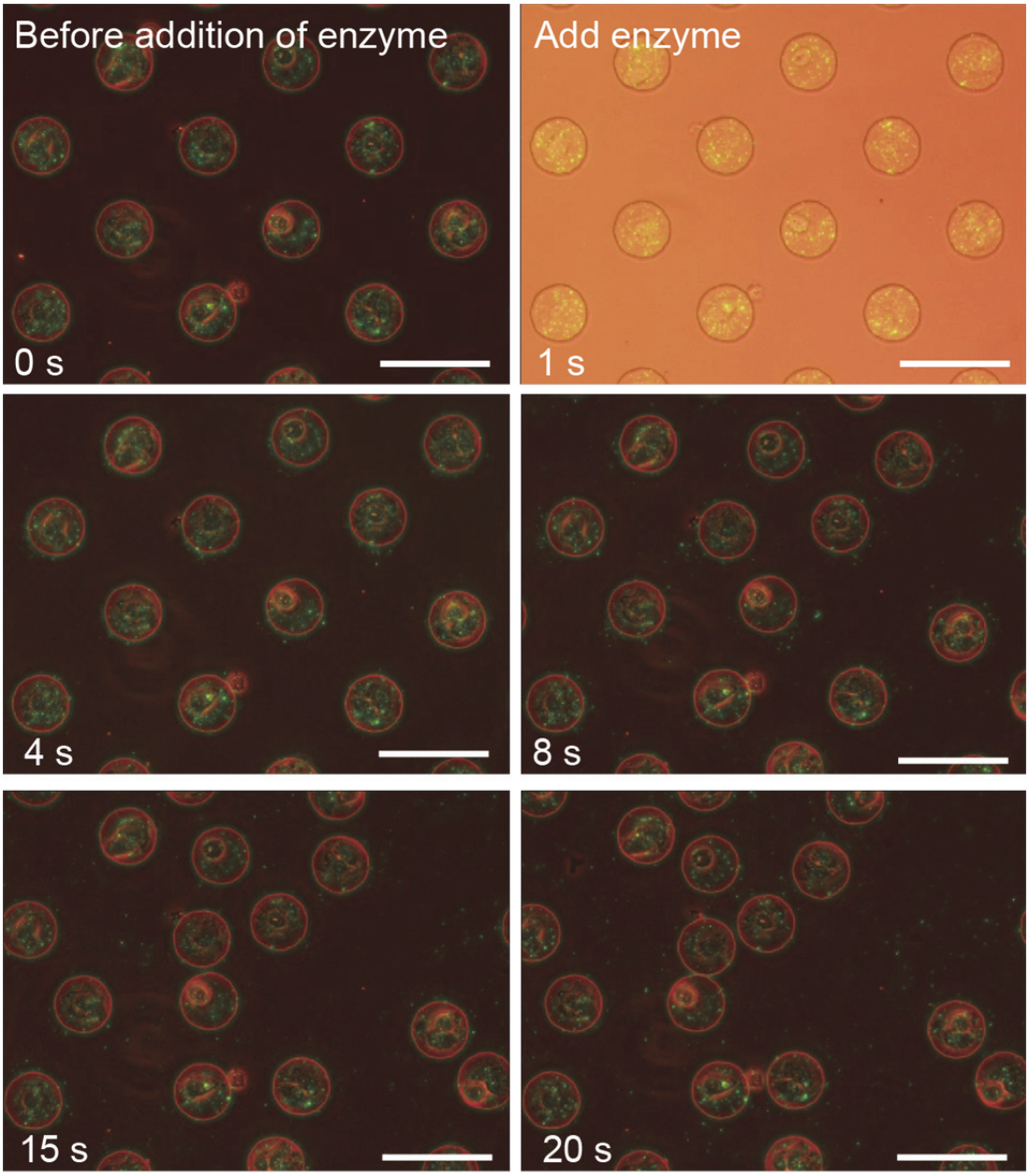

Figure 4-8. Enzymatic release of single-cell-laden microdisks. Sequential overlay of bright-field and fluorescent images of cells on microdisks before and after dissolving the sacrificial alginate hydrogel layer. The scale bars represent 100 μm. Reprinted with permission from (Teshima, et al, Small, 2014). Copyright 2014, Wiley.

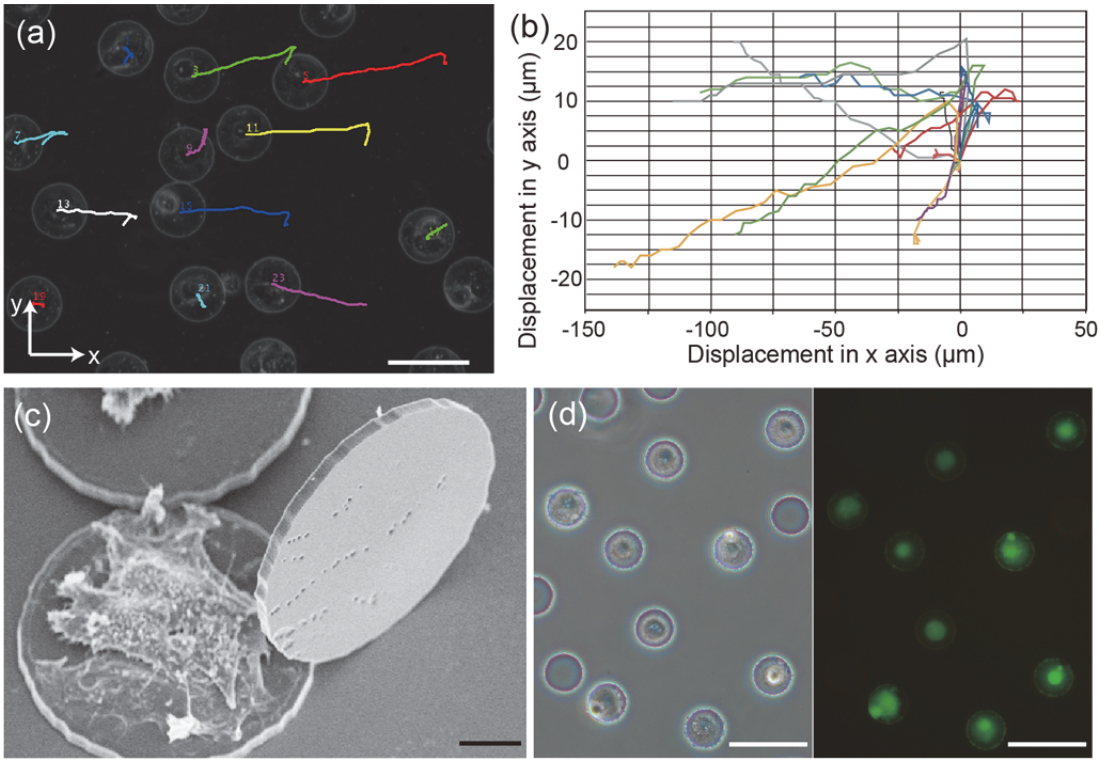

Figure 4-9. Single-cell-laden microdisks released after enzymatic dissolution. (a, b) Floating movement and displacement of microdisks after dissolving alginate hydrogel layer. (c) An SEM image of the released microdisks with attached cells, side and bottom views. (d) Overlay of phase contrast and fluorescent images of live-dead assay of single cells on microplates before and after dissolving the sacrificial alginate hydrogel layer. Cell viability was examined after dissolving the sacrificial layer. The scale bars represent 100 μm (a, d) and 10 μm (c). Reprinted with permission from (Teshima, et al, Small, 2014). Copyright 2014, Wiley.

The adherent cells on the floating microdisks maintained their adhesive structures, which indicates that the HFF cells established proper connections with the microdisk surface. A live/dead assay verified that more than 99% of the cells on the microdisks were alive both before and after the release process (Figure 4-9(d)), and that cells can be cultured on the microdisks for more than two days. Therefore, the enzymatic release employed in this study is gentle enough to prevent cell damage as ensured in the previous study (Wong et al., 2000).

4.2.2 Manipulation of cell-laden microdisks

After release of the microdisks with cells from the glass surface, detached microdisks with specific cells were collected to be relocated and rearranged. The detached microdisks with loading cells settle to the bottom in the culture dishes without any flow, but with the introduction of fluid flow, microdisks with cells can be handled smoothly. During the handling procedure, we did not observe any cell–cell adhesion or aggregation of cells on the microdisks in the culture media, thus we had expedient manipulation of single cells.

Figure 4-10(a, b) show the handling single adherent cells on the microdisks by using commercially available micromanipulators. This process consists of three procedures: holding the edge of the microdisks, picking them up from the substrate to change their positions, and setting them down again. Collected single cells on the microdisks were successfully relocated into the desired position to induce cell–cell contact as shown in Figure 4-10(c-f). We were also able to culture multiple single cell-laden microdisks in the state of cell-cell contact in the long term (form more than 2 days). Note that the microdisks were freely floating in the cell-culture media because the light source from the microscopes or movement of dishes cause a convection current; thus, the substrates to capture and immobilize each microdisk is needed to analyze cell-cell interaction between paired two single cells for long-term culture. Importantly, the cells on microdisks were manipulated without stripping them from their growth surfaces, which allows the adhesive state of the manipulated cells to be preserved.

After the cells are released and picked up from the substrate, a platform for immobilizing specific microdisks is needed. For rapid manipulation and efficient observation, a microfluidic platform will create an array of collected cells toward high through-put and efficient manipulation. Herein, we utilized a dynamic microarray system to make an array of the cells on the microdisks (Tan et al., 2007; Tan et al., 2008; Teshima et al., 2010). This system, previously proposed by our group, is a flow-through device configured as an array of hydrodynamic

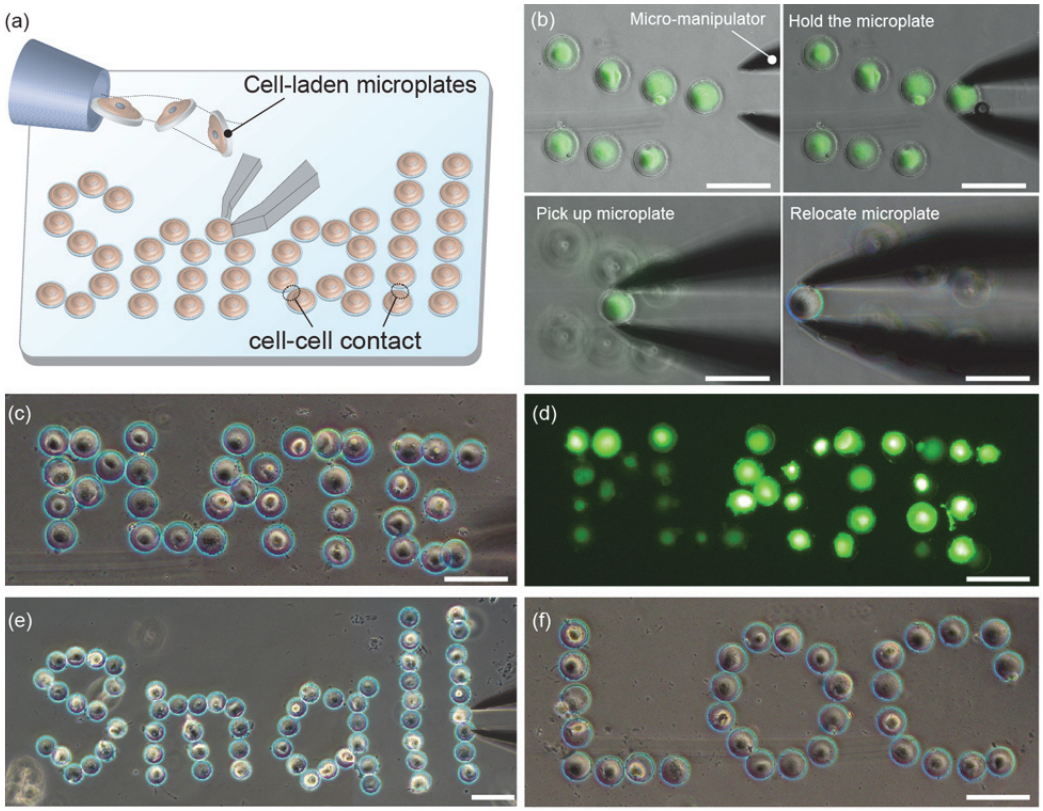

Figure 4-10. Manipulation of cell-laden microplates by using micromanipulators. (a) Schematic illustration of manipulation. (b) Sequential image of manipulated cell-laden microplates; we held, picked, and relocate single cell. (c-f) Demonstration of picked-up and rearrangement of cells to induce cell-cell contact. The scale bars are 100 μm. Reprinted with permission from (Teshima, et al, Small, 2014). Copyright 2014, Wiley.

trapping sites along meander-shaped channels (Figures 4-11(a)). Using this method, it is possible to observe single microbeads and to reduce sample volume since all of the introduced beads can be trapped at each site sequentially. Figures 4-11(b, c) shows the experimental setup of dynamic microarray that is composed of syringe, syringe pumps, tubes, PDMS microchannels, microscopes, and incubation system. After the cell-laden microdisks were collected with the micromanipulators, they were gently aspirated by using micropipettes and introduced into the inlets of microchannels via tubes from syringes. Figures 4-11(d, e) shows an

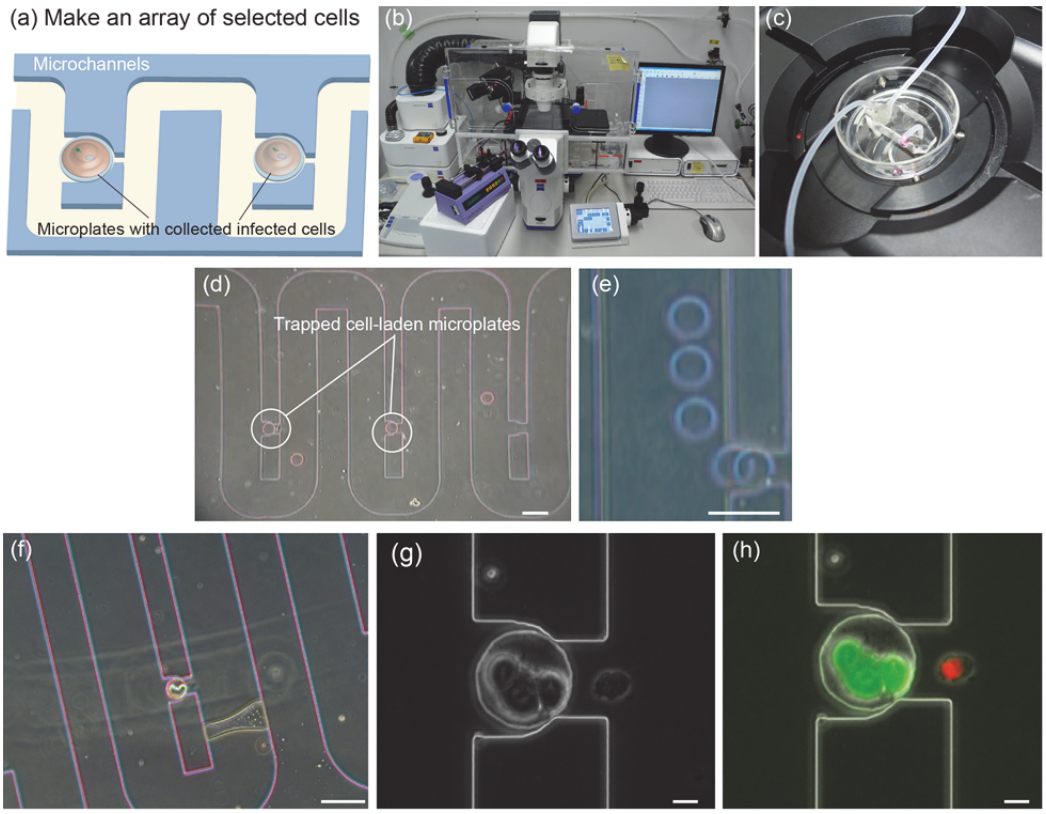

Figure 4-11. Microfluidic manipulation of cell-laden microdisks. (a) Schematic illustration of manipulation of single cell-laden microdisks in the dynamic microarray. (b, c) Experimental setup of microfluidic channels integrated with incubation system. (d, e) The cell-laden microdisks are introduced into microchannels and sequentially trapped and immobilized in the trapping sites. (f, g) The phase-contrast image of single adherent cells on the microdisks trapped in the trapping sites. (h) The live/dead assay distinguishes live cells on the microdisks from dead cells. The scale bars are (d-f) 100 μm and (g, h) 10 μm. Reprinted with permission from (Teshima, et al, Small, 2014). Copyright 2014, Wiley.

array of cells on the microdisks and the sequential images of trapping a planar-shaped single adherent cell on the microdisk, respectively. The velocities of the microdisks in the microchannels were estimated to be approximately 50 μm/s. We confirmed that this velocity was gentle enough to avoid damage to the cells, because we were able to incubate the cells on the microdisks and observe cell proliferation by the stationary cell-media flow (Figures 4-11(f,

g)). As with spherical cells or microbeads (Tan et al., 2007; Tan et al., 2008; Teshima et al., 2010), the trapping sites tightly capture disk-shaped microdisks in the flow, so that a multistep flow can be induced into the microchannels without detaching the samples from the trapping sites. By using multistep flow, we conducted a live/dead assay to test cell viability in the microchannels by washing with buffer (PBS), calcein-AM, ethidium homodimer-1 (EthD-1), and Dulbecco's modified Eagle's medium (DMEM). This assay successfully distinguished live cells on microdisks from dead cells as shown in Figure 4-11(h). By combining various cell-imaging techniques, this array system has the potential to allow further observation of single-cell behavior such as the long-term culture or induction of specific gene expression, in the state in which cells are immobilized in the microchannels.

4.2.3 Handling of parasite-infected single host cells

To demonstrate the versatility and applicability of the microdisk system for preserving cell adhesive properties, we applied this system to sorting and collection of parasite-infected or uninfected host cells while maintaining infective morphologies at a single-cell level. The conventional method for releasing cells from culture substrates involves the use of trypsin; therefore, the parasites located inside the host cells egress from the cells during trypsin digestion. Furthermore, the addition of reagents such as trypsin can influence the infection phenomena because cell morphological changes affect cell and microbe activity. Our microdisk system can resolve these problems because this system does not require additional reagents to strip cells during the release process.

First, we tested infection assay of *T. gondii* and various host cells cultured on microdisks. The parasites invade and replicate in host cells *in vitro*. We could obtain the time-lapse images of parasite motion and invasion. During cell culture, we observed the real-time parasite invasion and egression at the interface of host cell membrane. *T. gondii* could invade all types of

mammalian adherent cells including cells derived from human (HFF, HeLa, HepG2), ones derived from mouse (NIH3T3), and ones from rat (PC12). Furthermore, *T. gondii* invaded non-specifically the cells regardless of derived organ and tissues. On the other hand, there was no invasion into Sf9 insect cells (Table 4-1). This result suggests that they recognize the membrane protein or lipid molecules that are specifically located in not insect cells but mammalian cells when they invade the host cells.

Second, we tested the infection assay to investigate the relation between infection rate and the morphology of host cells. The diameter of microdisks ranged from 10 μm to 70 μm controlled cell stretching area and height of cultured cells as shown in Figure 4-6(b). In microdisks with 10-30 μm diameter, single adherent cells formed sphere-shaped, and the cross-sectional shape of single adherent cells is circle. On the other hand, in microdisks with 40-70 μm diameter, cells formed dome-shaped and the cross-sectional shape of single adherent cells is triangle. When we suspended the parasites onto the morphologically-controlled single adherent cells on the microdisks, they could invade cells with any types of shapes. Three-dimensional reconstruction image of confocal x-y scanning multi-layered images clearly shows parasite existence inside host cells. This result indicates that there is no relation between infection rate and the shape of cellular membrane or the curvature of cells (Table 4-2). In addition, the microdisks are able to handle cos-Fucci cells expressing the fluorescent marker of cell cycle. The single Fucci-cells with both M phase and S phase on the microdisks verify that there is no relation between host cell morphology / cycle and parasite invasion efficiency (Table 4-3). Although these assays are able to be performed in the conventional bulk experiments, there was limitation in the difficulty in observing the specific host adherent cells because we could not detect the membrane boundaries between paired cells. The microdisk technologies we proposed in this study show the cell membrane boundaries of the single adherent cells, and facilitate to understanding the dimension, the intracellular structure, and the edge of host cells.

Table 4-1. Relation of *T. gondii* infection rate *v.s.* host cell type.

Cell behavior	**Cell type**					
	HFF	NIH/3T3	HeLa	HepG2	PC12	Sf9
Invasion	○	○	○	○	○	×
Egression	○	low	low	○	○	×

○ : success of invasion

× : failure of invasion

Table 4-2. Relation of *T. gondii* infection *v.s.* the diameter of microdisks (Cell shape)

Cell behavior	Diameter of microdisks				
	5 μm	10 μm	20 μm	40 μm	70 μm
Invasion	○	○	○	○	○

○ : success of invasion

× : failure of invasion

Table 4-3. Relation of *T. gondii* infection *v.s.* host cell cycle

Cell behavior	Cell cycle	
	S-M phase	G1 phase
Invasion	○	○

○ : success of invasion

Finally, we performed the manipulation of single HFF cells infected by *T. gondii*. In conventional infection assay, it is still difficult to detect the boundaries of paired cells that are cultured randomly in the culture dishes and grasp where or which host cells the parasites are infecting or located in as shown in Figure 4-12(a). On the other hand, the microdisks are able to isolate single adherent host cells, define the edge of single adherent cells, and regulate the morphology of them by optimizing the diameter or shape of microdisks (Figure 4-12(b)). Thus, this technology helps us to understand the edge of isolated and morphologically controlled single host cells and understand where the parasites are located around the host cells. The versatility of our method to manipulate single adherent cells was also examined by collecting and sorting only parasite-containing cells. During cell culture, we obtained time-lapse images of

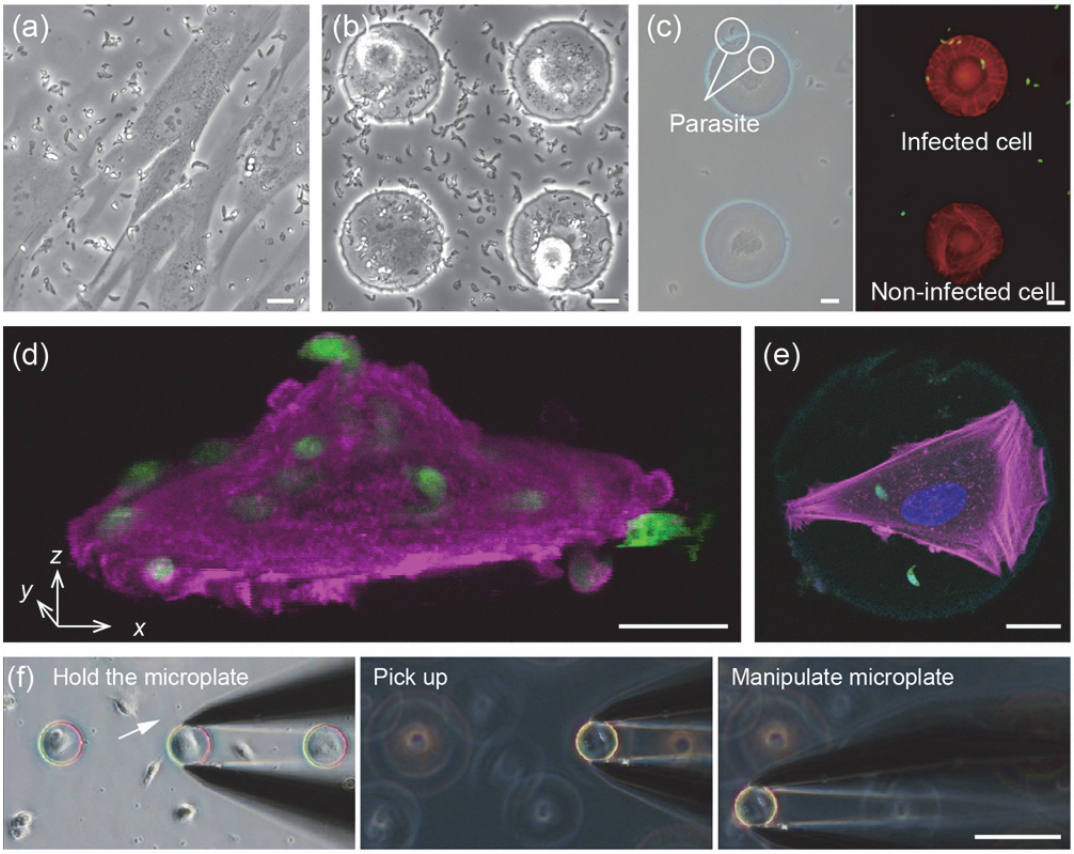

Figure 4-12. Single host cells infected by *T. gondii* on the microdisks. (a) A bright-field image of HFF cells cultured on the culture dishes and infected by *T. gondii*. (b) A bright-field image of single HFF cells cultured on the microdisks and infected by *T. gondii*. (c) A set of bright-field and fluorescent images of single cell infected by parasites. (d) 3D reconstructed confocal images of single host cells infected by *T. gondii.* (e) A scanned confocal image of single host cells infected by *T. gondii.* (f) Sequential images of the manipulation of parasite-infected single adherent cells with the assistance of micromanipulators. The microdisk with a single parasite-infected cell (white arrow) was selected for release. During the handling procedure, the infected cells remained on the surface of the microdisks and retained their adhesive properties. The scale bars are (b, c, g) 100 μm and (d, f) 10 μm. Reprinted with permission from (Teshima, et al, Small, 2014). Copyright 2014, Wiley.

parasite motion and invasion at the single-cell level. We successfully observed real-time parasite invasion into the host HFF cells and distinguished infected cells from uninfected cells (Figure

4-12(c)). In addition, by combining with the confocal observation, we were able to obtain the three-dimensional information about the location of infecting parasites and invasion angle from the 3D reconstructed fluorescent scanned images (Figure 4-12(d)). The single scanned images also provided us the detailed position of parasites inside the cells after invasion (Figure 4-12(e)). This image is helpful enough to analyze the specific invasion points of single cells and the interaction between invasion efficiency and host cell cytoskeleton. After the parasite infection, we released the laden host cell on the microdisks from the glass substrate. The microdisk system successfully retained adhesive properties of both the parasite-infected and uninfected host cells, which allowed us to manipulate, sort, and collect the cells without changing the cell morphology as shown in Figure 4-12(f). In addition, we confirmed that the parasite inside the host cells did not egress, thus sustaining the infection during the procedure. The ability to retain cell morphology throughout this process can lead to further cellular analysis after the collection of specific targeted cells, including the investigation of microbe–host cell interactions in invaded host cells or microbe behavior inside host cells (Charron et al., 2002; Morisaki et al., 1995; Sweeney et al., 2010).

4.2.4 Magnetic manipulation of microdisks

We fabricated the microdisk with embedded rectangular shaped permalloy bars to manipulate single adherent cells. To manipulate microdisks magnetically, fabricated devices were set and suspended in Petri dishes, and neodymium magnets were put under the dishes to apply magnetic fields. When we apply external magnetic field, the permalloy is induced to have magnetic dipole moment. Since the interaction between the external magnetic field and the magnetic dipole moment causes the microdisks to move along with the applied magnetic field. In consequence, the long axis of permalloy bars were aligned to the direction of magnetic fields (Figure 4-13(a)). We found that both the response speed to align and magnetic force to incline

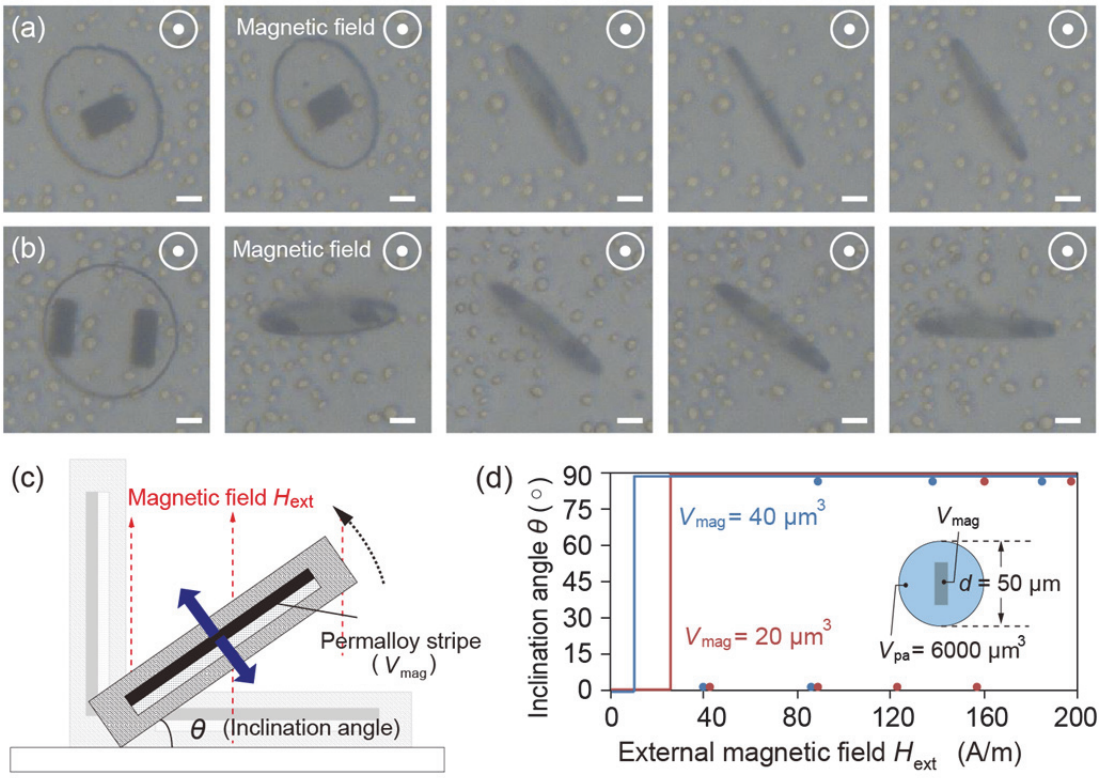

Figure 4-13. Magnetic inclination of the microdisks with embedded permalloy layer. (a-b) Magnetic inclination of microdisks with 20 μm^3 permalloy pieces (a) and microdisks with 40 μm^3 permalloy pieces (b) after applying magnetic fields. (c) A schematic illustration of inclined microdisks. (d) Theoretical and experimental plots of inclination angle as function of external magnetic field (H_{ext}) for two V_{mag} values: red, V_{mag} = 20 μm^3; blue, V_{mag} = 40 μm^3. The scale bars represent 10 μm

were totally dependent on the volume of permalloy pieces (Figure 4-13(b)). Theoretically, the magnetic strength to incline microdisks with 20 μm^3 (20 μm × 10 μm × 100 nm) in volume to 90 degree discussed in Chapter 2 is estimated to 23.1 A/m. In the experimental results, the magnetic strength to incline microdisks was 158 A/m that is 7 times more than theoretical force, 23.1 A/m (Figure 4-13(c, d)). The magnetic strength to incline microdisks with 40 μm^3 (20 μm^3 × 2 pieces) to 90 degree was 93 A/m, that is 7 times more than 12.5 A/m. This result indicated that the difference between experimental results and theoretical estimation is caused by the fluid

viscosity of suspension media, low response speed to the direction of magnetic field, and adhesion forces between parylene microdisks and glass substrates. Compared with the magnetic strength to microflap was about 20000 A/m, the inclination of microdisks was achieved by small magnetic strength. This difference attributes the lack of hinges that introduce the larger torque than that of gravity.

Once the microdisks were inclined in the magnetic field, the vibration of the microdisk in the media appears to be remarkable during the observation under the microscopes. This vibration should be reduced during manipulation process, because it will give rise to the deformation and distortion in the obtained microscopic images. The vibration of the microdisk would results from the convection current that is generated by microscopic light sources and the vibration of microscope itself. The fictitious force from the external environments including microscope vibration and convection current would be conducted to the media and forces the microdisks to be oscillated, which leads to the difficulty in the steady observation of position fixed samples. Here, we focused on the following two approaches to reduce the vibration: (i) the increase in viscosity and (ii) isolation of media space by cover glass (Figure 4-14(a)). First, we tried to change the type of solution for suspension of microdisks to the one with higher viscosity. Viscosity of the glycerol is dependent on its concentration, and the viscosity of 100% glycerol is 60 times more than 50% glycerol (Figure 4-14(b)). Compared with PBS, the glycerol solution reduced the amplitude of vibration and increased the vibration period (Figure 4-14(c, d)). Accordingly, it is found that the vibration is mainly caused by Mechanical stability was achieved most by increasing the viscosity of solution such as glycerol, since the fictitious force generated from the solution and external environment.

Next, we tried to cover the PBS solution by glass substrates to isolate it inside the dishes. This cover glass also down-regulated the amplitude of vibration and increased the vibration period (Figure 4-14(c, d)). However, the effect to reduce vibration motion is less than the use of

glycerol. Finally, to combine these two trials, we tried to cover the glycerol solution by glass substrate and observe the vibration. In consequence, the amplitude of vibration is ranged in the undetectable region, and the microdisks appeared to be fixed even when we used high-speed cameras. When we perform the immunostaining assays of the cells, the use of both glycerol and cover glass is the most appropriate due to no influence on the fixed samples. In contrast, since cells cannot live in glycerol solution, the use of only cover glass with as a few amount of solution as possible is better suited for real-time imaging of living cells.

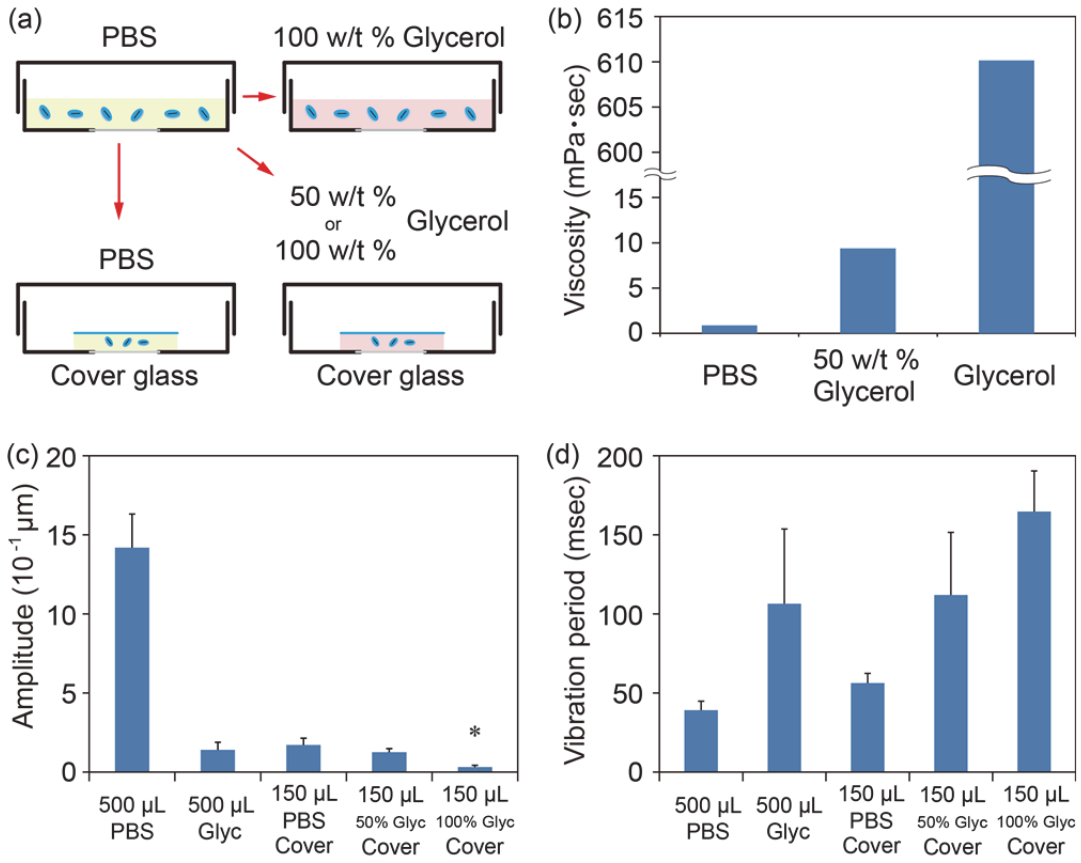

Figure 4-14. Mechanical stability of inclined microdisks in the applied magnetic field. (a) To increase the mechanical stability of microdisks, we replaced the PBS solution with glycerol, or covered the solution by glass substrates. (b) Measured viscosity of three types of solution. (c) Amplitude of the microdisk vibration. (d) Vibration period of inclined microdisks.

4.2.5 Magnetic manipulation of cell-laden microdisks

Due to the lack of hinges, microdisks acquired higher degree-of-freedom than microflaps that is fixed to the glass substrates. After dissolution of sacrificial alginate hydrogel layer, cell-laden microflaps started to float around in the cell-culture media and respond to the applied magnetic field. In the magnetic field with more than 200 A/m, all the cell-laden microdisks were

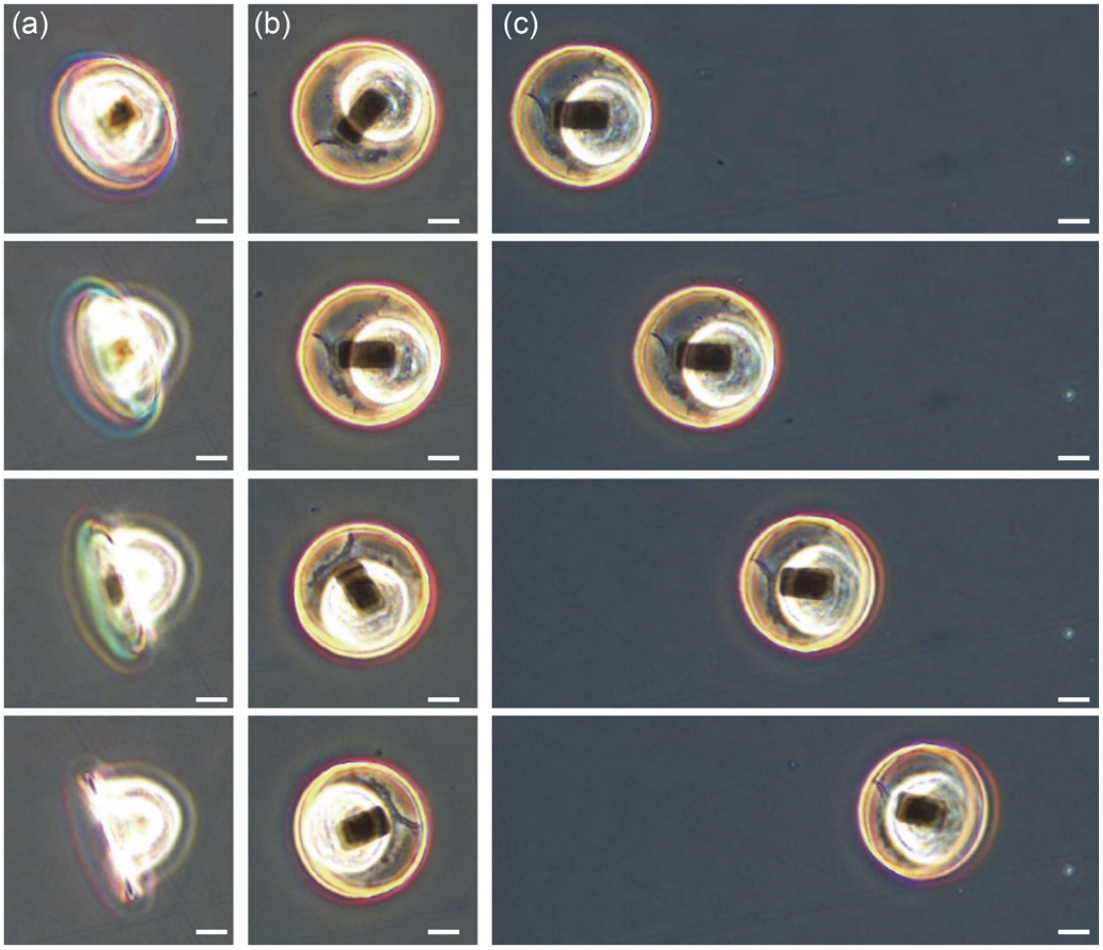

Figure 4-15. Magnetic manipulation of cell-laden microdisks. (a) Single cells were inclined and aligned to the applied magnetic field. (b) By changing the position of magnets in the lateral field, cells were rotated in x-y layer. (c) By making magnets close to the culture dishes, cells moved horizontally while being attracted to the magnets. The scale bars are 10 μm.

smoothly aligned to the magnetic direction. Since the change in the position of magnets leads to the changing in the direction of magnetic field, applied magnetic field could easily manipulate the cell-laden microflaps. The motion of manipulation is mainly composed of three parts: inclination, rotation, and translational motion. Inclination can be achieved the magnetic field that is perpendicular to the glass substrates (Figure 4-15). By making the magnetic field vertical to the microdisks, the microdisks tend to flip upside down. By keeping this magnet direction, we could keep the microdisks inclined and observe the cell membrane boundaries of apical side (Figure 4-15(a)). Then, by rotating magnetic field under the condition that the field is horizontal to the microdisks, the microdisks are forced to be rotated and aligned parallel to the magnetic field (Figure 4-15(b)). The success rate of rotating microdisks is dependent on the magnetic strength, and exceeding a certain threshold value of magnetic strength will succeed in rotating all the microdisks. Under the magnetic field more than about 0.4 mT, all of the microdisks in the media are successfully tilted or rotated simultaneously. By fixing the magnet location to keep applying magnetic field with more than 1.5×10^4 A/m, the microdisks behave in translational motion (Figure 4-15(c)). The average velocity of translational motion is about 300 μm/ min. The combination of three magnetic motions enables us to freely manipulate, immobilize, and rearrange the targeted cells even under the microscopes. In addition, magnetic manipulation can be achieved while culture-dishes remain closed, resulting in the lower risk of contamination and exposure to the infection microbes during experiments.

Conventional magnets made single cell-laden microdisks inclined only at 90 degrees, because the applied magnetic field is aligned only perpendicular to the culture dishes. Figure 4-13(d) shows the angle of inclined microdisks, indicating the lower angle tunability ranging from 0 to 90 degrees, when compared with microflaps shown in Figure 3-7(b-e). Automatically manipulating system is required for providing the angle-tunability with microdisks toward the multi-angle bright-field observation of cell membrane boundaries. In this study, we focused on

the electromagnetic actuation that is composed of five coils (*x*-*y* (×1), *y*-*z* (×2), *x*-*z* (×2)), three-axis Helmholtz coils to generate uniform magnetic field (the details of experimental setups is describes in the section 2.6.4). Horizontal magnetic field generated by two faced *x*-*z* / *y*-*z* coils rotate cell-laden microdisks in the applied filed direction, and the response speed to the field depended on the power current (Figure 4-16(a)). Lateral magnetic field generated by single *x*-*y* coil tilted cell-laden microdisks perpendicular to the culture dishes. By decreasing the power current in the coils, the inclination angles also decreased to 0 degree. However, the inclination of microdisk by the single *x*-*y* coil showed less angle tunability because this coil generated only one directional (lateral) magnetic field (Figure 4-16(b)).

By combining the horizontal field with the lateral one, angle tunable actuation was achieved as shown in Figure 4-16(c). Unless the actuation by magnets in which the inclination angle is limited to unless 90 degrees, three-axis Helmholtz coils omnidirectionally generate the magnetic field (all directions in *x*, *y*, and *z*), so that we are able to flip single adherent cells to their back without using both inverted and upright microscopes (Figure 4-16(d)). After flipping them, single adherent cells are in the state to be attached to both the surface of culture-dishes and microdisks. The direction of magnetic field is estimated by composition of vectors of horizontal or lateral magnetic strength. Figure 4-16(e) shows the relation between the direction of applied magnetic field and the inclination angle of microdisks. The experimental measurements conformed to the theoretical inclination angle of magnetic field well when the inclination angles are less than $\pi/2$. Actual measured values of inclination angle of microdisks had a margin of error from the theoretical value that is ranged from 3% to 16%. The shape anisotropic property of thin permalloy film is determined to be a cause this margin of error as discussed in the section 2-7. The other possibility is the actual magnetic field in discord with theoretical direction that is determined by simple composition of vectors. Compared with the actuation by magnets, the electromagnets control the inclination angle more precisely, and manipulate the microdisks in

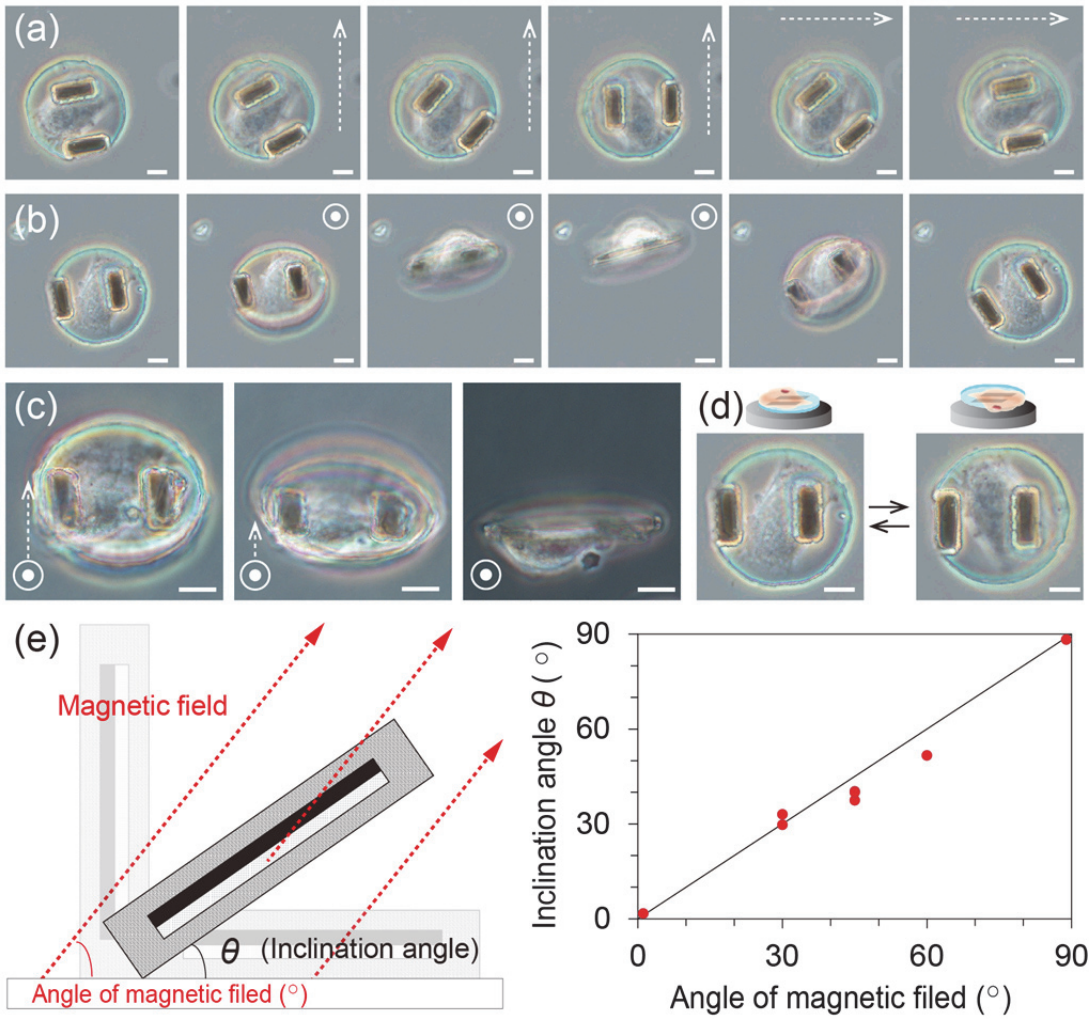

Figure 4-16. Magnetic manipulation of single cell-laden microdisks in three-axis Helmholtz coils. (a) Cell-laden microdisks were rotated parallel to the culture dishes by using two faced *x-z* / *y-z* coils. (b) Cell-laden microdisks were tilted perpendicular to the culture dishes by using single *x-y* coil. (c) Inclination angle of tilted cell-laden microdisks was maintained to be constant by using *x-y* and *x-z* (or, *x-y* and *y-z*) coils that generate inclined magnetic field. (d) Flipping motion of cell-laden microdisks. (e) Relation between the direction of applied magnetic field and the inclination angle of microdisks. The scale bars are 10 μm.

the desired orientation. Besides, when we set the current of all coils to 1 A, the temperature of cell media was kept at 35 degrees throughout the manipulation. On the other hand, when we increased the current to more than 1 A, the temperature of cell media became higher than 40

degrees. Although the temperature in the media rests on the seasons or the room temperature, it is found that this actuation holds the features to keep an appropriate temperature to culture the cells.

4.3 Multi-angle observation of single cell-laden microdisks

4.3.1 Long-term culture of single cells

We investigated the long-term culture of single cells on the microdisk with embedded permalloy bars in the applied magnetic field. After inclining single cell-laden microdisks in the magnetic field perpendicular to the culture dishes, we kept to apply magnetic fields by putting neodymium magnets under the dishes in the incubator system. We prepared the culture dishes coated with fibronectin or MPC polymer. Figure 4-17(a) shows the sequential images of single cell-laden microdisks inclined on the fibronectin-coated bottom substrates. In 5 min, the cells on microdisks started to migrate to the bottom substrate, and bridge between the bottom substrate and microdisks. During cell migration, the microdisks were not aligned perpendicular to the applied magnetic field, and tilted due to the cell traction forces. Within 60 minutes, the cells completely moved to the bottom substrate and the microdisks without loaded cells floated away in the cell-culture media.

In contrast, when we cultured cell-laden microdisks on the MPC polymer-coated surface, the cells stayed only on the microdisk and the height of cells from the microdisk surface changed within 6 h as shown in Figure 4-17(b). As discussed in Figure 4-12, cell-laden microdisks moved floating in the convection current of cell culture media, which made long-term observation for more than 1 day difficult. This difficulty was settled by decreasing the amount of media to about 150 μL and covering it with slide glass to reduce the inertial force. It took around 24 h for more than 50% for single cells to proliferate and share the single microdisk area in the same way as the cells on microdisks before magnetic inclination shown in Figure

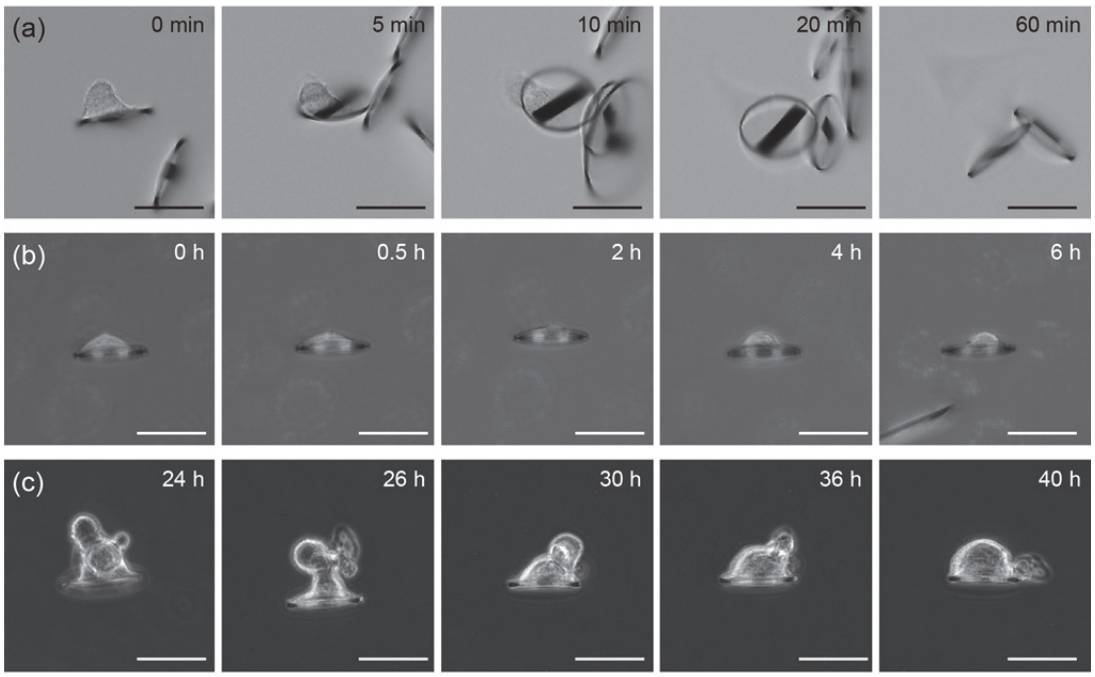

Figure 4-17. Long-term cell culture of single cells on the microdisks after inclination. (a) Single HFF cell on the microdisk moved and migrated to fibronectin-coated glass substrates. (b) Single HFF cell on the microdisk stayed onto the microdisks, and did not move to MPC polymer-coated glass substrates. (c) HFF cells proliferated only on the microdisk when they were cultured on the MPC polymer-coated glass substrates. The scale bars are 50 μm.

4-5(a-c). We observed that cells proliferated in the direction perpendicular to the microdisk surface, and a part of cells continued to attach and detach the MPC polymer-coated bottom surface. In 40 h, the cells formed cell-cell adhesion and cell-microdisk adhesion, which results in dome-shaped spheroid as shown in Figure 4-17(c). After 2 day incubation, there were no cell migration and deformation of dome-shaped spheroids. These results suggest that MPC polymer-coated substrates successfully repelled cell adhesion, and enabled us to maintain the morphology of cells on the microdisks and observe single cell behavior without migration, which provides us with information about how they proliferate in the micropatterned area in a stable manner. Furthermore, it is possible to conduct a single-cell survey even after inclining

cells on the microdisks in the magnetic field, and in is proved that the assay duration is optimized to less than 24 h.

By using the magnet-active microdisks, we conducted the experiments to observe parasite behaviors on the surface of single host cells. The diameter of microdisks is critically able to control the morphology: thus, we used the microdisks with 50 μm diameter and made the cells on the microdisks domed-shaped. Suspended *T. gondii* attached to the cell surface of microdisks and prepared for the invasion process. As we discussed in the 3.4.1 and 3.4.2, we not only detected the cell membrane interface between the parasites and their host cells, but also observed two types of gliding: helical gliding and upright twirling. Figure 4-18(a, b) shows the helical gliding and upright twirling, respectively. Compared with the parasites on the microflaps, the displacement of gliding motility of the parasites on the microdisks looked shorter, because the cell surface of host cells on the microdisks is with markedly uneven and shorter than on the

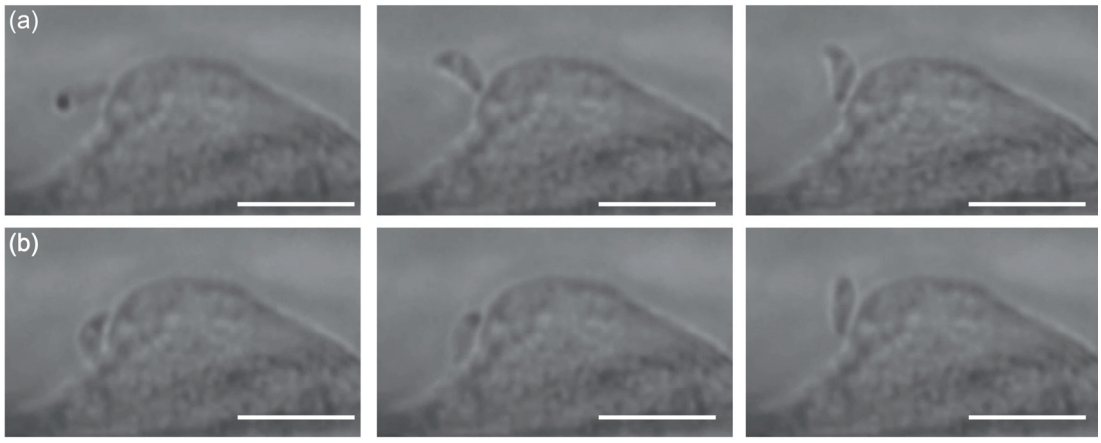

Figure 4-18. Bright-field observation of parasites on the cell membrane boundaries of HFF cells. (a) Upright twirling of *T. gondii*. After helical gliding, *T. gondii* exhibited upright twirling attaching their anterior side to the host cell membrane vertically. (b) Time-lapsed images of helical gliding motility. Helical gliding commenced while *T. gondii* were rubbing their bodies against the single host cell in forward and backward motion. The scale bars are 10 μm.

microflaps. The parasites continued to attaching to the specific area with limited dimension at the slopes of single host cells. By using the microdisks, we could obtain detailed information about the trajectory at sub-micron scales, invasion angle, and adhesion area between single parasites and single host cells. This method would facilitate to understanding the host cell-microbe interaction at single cell level without the host cell adhesion.

4.3.2 Confocal observation of intracellular structure

For the multi-angle observation, the confocal microscopy has been widely employed because it can stack the scanned *x*-*y* images to reconstruct the 3D and cross-sectional artificial images (Figure 4-19(a, b)). However, there is limitation in the resolution in *z*-axis, resulting in blurred 3D images that hamper the detailed analysis of intracellular structures (Figure 4-19(c)). By equipping the microdisk technologies to incline the cells with the conventional confocal microscopy, we were capable of obtaining scanned *x*-*y* images of intracellular structures (Figure 4-19(d)). Since we can incline the cells on the microdisks in the desired orientation, this system enables higher-resolution cross-sectional imaging with single-molecule sensitivity at single image scanning than conventional methods of reconstruction and deconvolution. In this system, we successfully observed the intracellular structure composed of immune-stained actin fibers and microtubules inside single adherent cells (Figure 4-19(e)). Compared with the images taken by conventional confocal microscopy, we could detect the cross-sectional image of each fiber of microtubules inside the cells (Figure 4-19(f)). Furthermore, because this image can be taken at single scanning, it is possible to escape the following considerations: (i) long term scanning leads to photobleaching and phototoxicity; (ii) multiple focal planes lead to dominating depth-induced spherical aberration.

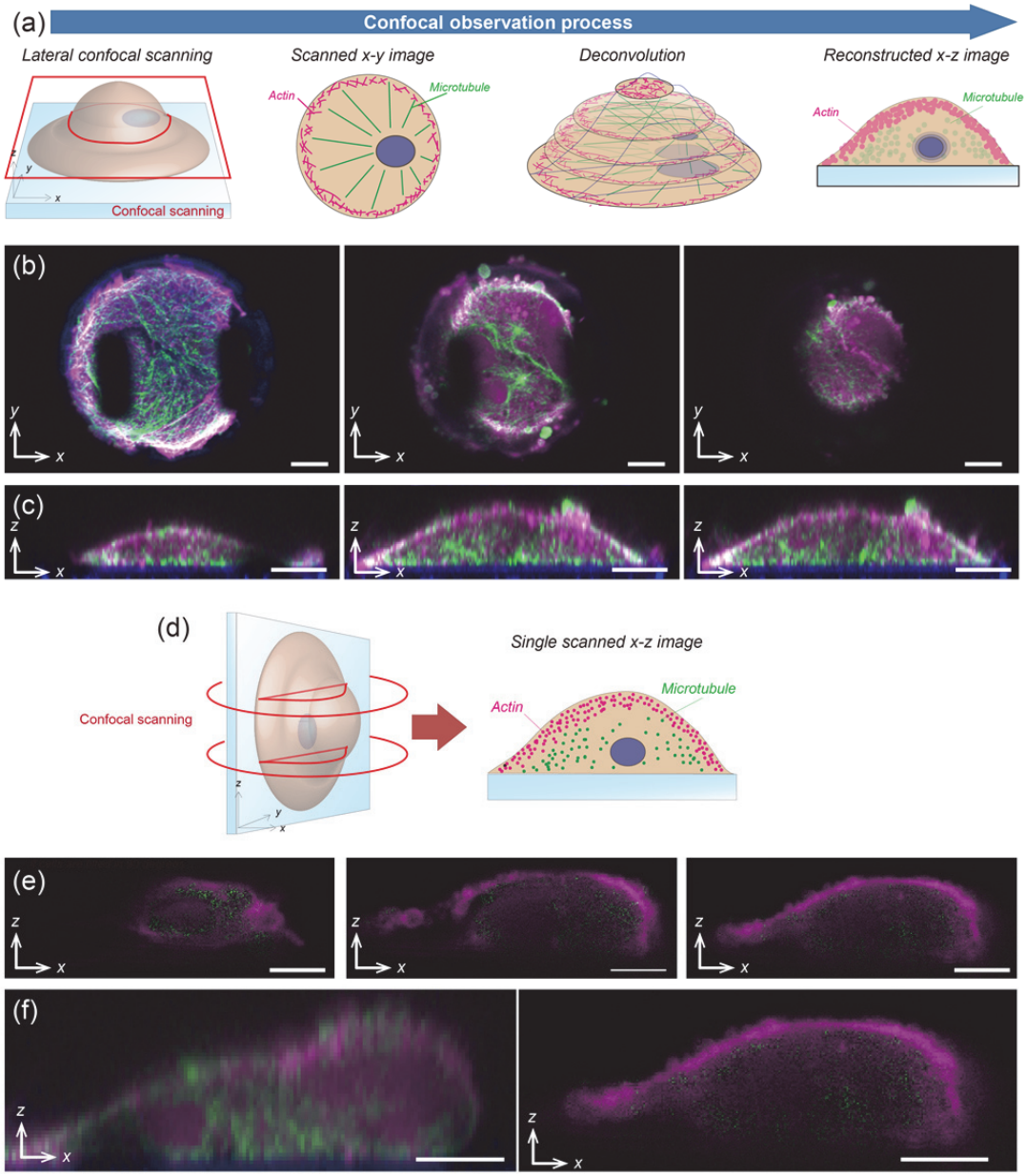

Figure 4-19. Confocal observation of intracellular structure. (a) Stack of scanned x-y images into 3D information and reconstruction of artificial cross-sectional images. (b) Scanned x-y images at each eight of adherent cells. (c) Reconstruction of cross-sectional intracellular images. (d) Single scanning of inclined cells to obtain the cross-sectional intracellular images. (e) Single scanned images of the cross-sectional intracellular structure. (f) Comparison of conventional reconstructed image (Left) with single scanned image (Right). The scale bars represent 10 μm.

4.3.3 Confocal observation of intracellular structure

For the study of parasite detection, the analysis with high resolution images is highly required to detect cell membrane boundary. As the demonstration of high resolution observation, we applied this microdisk handling technology to analyze the parasite invasion into host cells. We tested infection assay by using *T. gondii* and their host HFF cells cultured on microdisks. By using microdisks, the single host cells were inclined at 90 degrees and observed with confocal microscopy. This enables us to obtain the cross-sectional images scanned in *x*-*y* layer as well as Figure 4-20. Compared with confocal microscopic reconstructed *z*-axis images in conventional two-dimensionally cultured cells in petri dishes (Figure 4-20(a)), the confocal *x*-*y* scanning

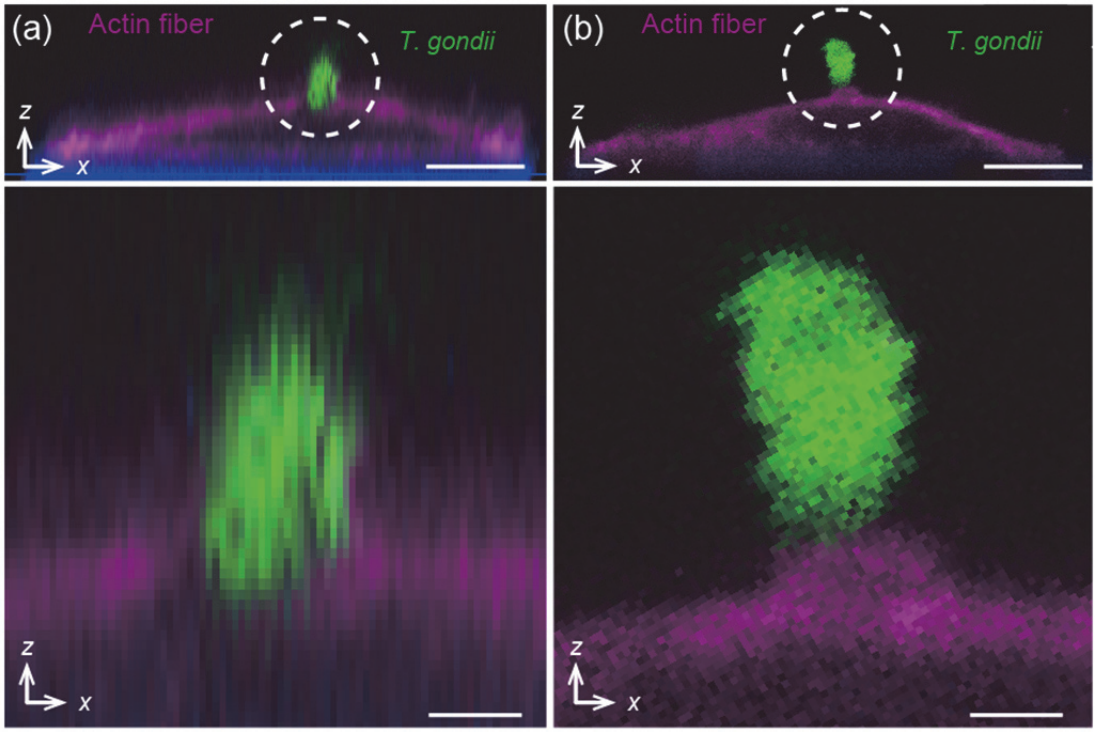

Figure 4-20. Confocal observation of parasite-infected host cells with stained actin fibers. (a) Reconstruction of artificial stacked images of intracellular structures. (b) Single scanning of inclined host cells. The scale bars represent 10 μm (a, b, above), and 1 μm (a, b, below).

image of 90° rotated single host cells clearly show the cell membrane boundary between host cells and parasites. Here, we found that during the parasite invasion process, cytoskeleton inside the host cells, especially actin fibers, were dynamically moved and deformed. Figure 4-20(b) indicates that the parasites harness the actin fibers inside the host cells to migrate and invaginate the host cell membrane. This deformation is attributed to either active induction of the replacement of actin fibers by *T. gondii* or passive deformation of host cell cytoskeleton. Figure 4-21(b) indicate that during the parasite invasion, they are encapsulated by microtubules derived from host cells. Since the invasion process is completed within one minute, the deformation and displacement of microtubules might be processed in such a short term.

Many studies have focused on understanding host cell invasion by *Toxoplasma* with a long-term goal of developing novel therapeutics. The images in Figure 4-20 and 4-21 clearly show that host microtubules and actin-fibers are localized at the interface with the interactions, unlike their previously described role in pathogen invasion. While the researchers have reported so many factors inside *T. gondii* such as motor system for intercellular transmission and active cell invasion, there are few studies that showed the host cell is not entirely passive during *Toxoplasma* invasion and that host actin and microtubules contribute to entry. Besides, not much is known about the contribution of the host factors to cell invasion. This state is similar to that of the research about malaria invasion and the other parasites. Therefore, the founding obtained by integration of microdisks with confocal microscopy would broad the new scientific field and reveal the relation between host cell morphology / cycle and parasite invasion efficiency. This method can be an attractive platform for the manipulation of host cells, the observation of invading microbes and the analysis of microbe-host cell interaction

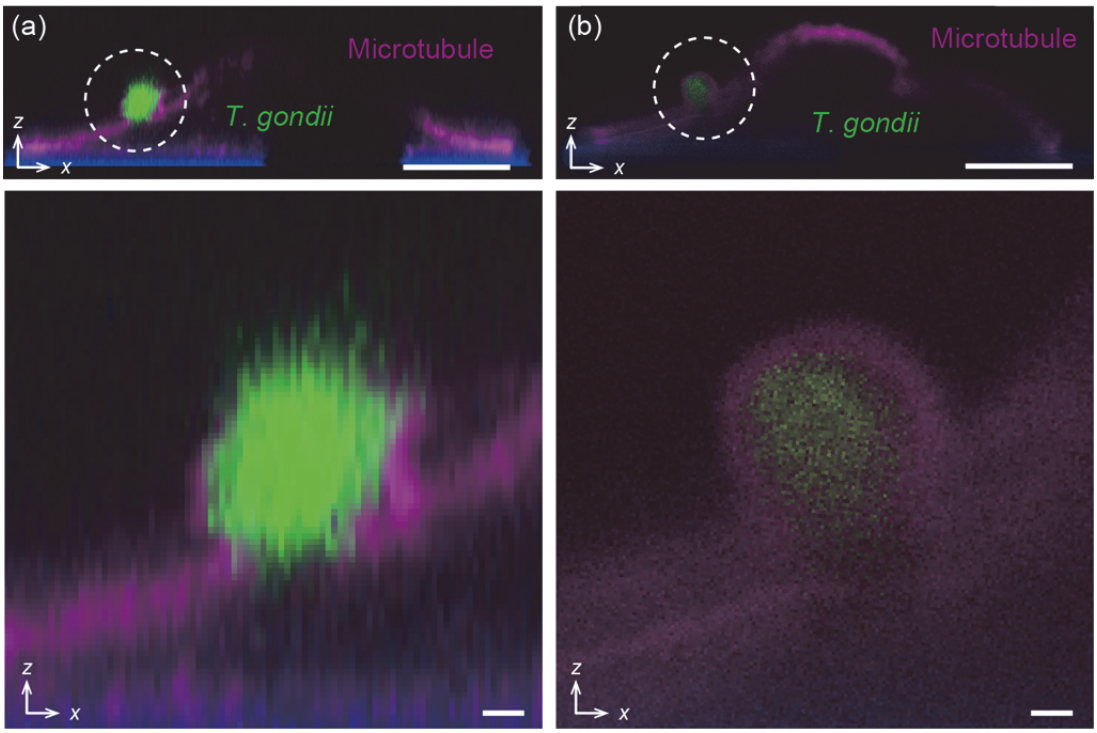

Figure 4-21. Confocal observation of parasite-infected host cells with stained microtubules. (a) Reconstruction of artificial stacked images of intracellular structures. (b) Single scanning of inclined host cells. The scale bars represent 10 μm (a, b, above), and 1 μm (a, b, below).

4.4 Discussion

In this study, we demonstrated a microdisk array for culturing, releasing, manipulating and immobilizing single adherent cells. Single-cell-laden microdisks were releasable by an enzymatic dissolution of an alginate hydrogel sacrificial layer without cell toxicity in a batch process, thereby realizing the collection and manipulation of adherent cells with micromanipulators or microfluidic devices. Importantly, the single cells remain adherent to the growth substrate throughout the releasing, handling and collection process; thus, this method can significantly enhance the handling process and viability of single live adherent cells. Accordingly, by harnessing the microdisks as building components, we would perform

multi-cell docking or assembly for the analysis of cell-cell communication or for tissue engineering (Teshima et al., 2011a; Teshima et al., 2011b). This system also provides a new approach for the positive selection of specific parasite-infected cells, which indicates significant benefits to biomedical investigations based on single adherent cells and infectious microbes, including parasites, bacteria and viruses. Furthermore, additional functions for microdisks including holes or microgrooves would yield the modification of cellular shape, morphological activities, and cytoskeletal properties. For example, neuronal cells have their specific morphology composed of somas and neuritis; thus, the well-defined microstructure of additional paths attached to microdisks will enable us to control somato-neuritic growth (Yoshida et al., 2013). This technology is applicable to assembly of multiple single neuronal cells by pick-and-place of microplates and constructing neural circuits with desired geometry. Since the microdisks were fabricated by micropatterning, lithography technology, and thin film procedure, the desired shapes and additional function can be added to the microdisks.

We also demonstrated the microdisk system to manipulate single adherent cells for multi-angle observation by applying magnetic field. Fabricated microdisks have magnet-active function, which enables them to tilt in desired orientation. We handled single adherent cells under applied magnetic fields. Controlling the magnetic field enables to achieve handling adherent cells on microdisks while keeping adherent property and to obtain the high resolution images of the cell membrane. This method can be an attractive tool for manipulation single adherent cells and observing the interaction between infectious microbes not only parasites but also bacteria and virus, and single host cells by equipping to the conventional confocal microscopy due to the ability to obtain high resolution images <400 nm. Since microdisks are inclined to 90 degrees by magnet field perpendicular to the substrates, it is possible to observe the change in cellular shape or proliferation speed under the influence of the gravitational pull by keeping cells inclined. Furthermore, by continuing to rotate the cells on the microdisks in the

magnetic field parallel to culture dishes, we will be able to trace the cellular behavior at constant revolutions per minute while maintaining the adhesive properties, toward the creation of new cell-biological experiments such as astrobiology (King, 2004; Thomas et al., 2007) or gravitational biology (Qian et al., 2009; Tabony et al., 1992).

Compared with microflap for handling multiple cells, the angle tunability of microdisk inclination is lower because the angle of inclination can be tuned only at 0 degree and 90 degree when we use the magnets for actuation. This lower angle tunability was successfully improved by the addition of automatically manipulating system including electromagnetic actuation, because a three-axis Helmholtz coil setup generate the uniform magnetic field in the desired orientation with high angle precision. They can be further improved by integrating with the fast, reliable and fully automated system to regulate the strength and orientation of applied magnetic field toward auto-focus live-cell imaging with feedback control of obtained images. We expect that these mobile microdisks can be further developed to provide a platform for manipulating and observing any type of adherent cell at the single-cell level while maintaining their adhesive properties in micro-sized areas.

CHAPTER 5

CONCLUSIONS

5.1 Conclusions

This dissertation describes the mobile microplate technologies to manipulate adherent cells for multi-angle observation of cell membrane boundaries. We proposed two types of mobile microplate structure: hinged microplates, termed microflaps; microplates without hinges to increase the degree of freedom in location and motility, termed microdisks. These mobile microplates have the flat surface to load adherent cells at both single cell level and multiple cell level. In the applied magnetic field, they can be inclined in the desired orientation and equipped on the conventional microscopies including bright-field and confocal microscopes. The magnetic manipulation enables us to observe the cells loaded onto the microplates from desired angles, which realizes the multi-angle observation.

The multi-angle observation of cells provides us with much detailed information about the activity at cell membrane boundary and change in cell morphology. Conventionally, the researchers have developed the platform for inclining the culture-dishes on the stages or optical pathway of microscopes toward the multi-angel observation. Although these methods have succeeded in observing cells form multiple angles, there is still limitation in inclination angles due to the physical obstruction of microscopic components, resulting in the difficulty in obtaining high resolution images with high magnification. On the other hand, microfabrication technologies hold great promise for advancing the methodologies to manipulate, sort and

immobilize adherent cells while maintaining their adhesive property, termed mobile microplates. However, these potentials have yet to be fully applied to the multi-angle observation of adherent cells due to the lack of angle-tunability and function to control of inclination angle. In this study, we developed the mobile microplate system to fulfill these additional requirements. Mobile microplate technology is fabricated of biocompatible and transparent polymers with embedded magnet-active metal layer, onto which adherent cells are loaded. In addition to the ability to control the number of cells precisely, this system make it possible to incline loaded adherent cells in the desired orientation ranged from 0 to 90 degrees while preserving their cell morphologies. The core of the technology is the magnetic actuation by applying magnetic fields that allows the remote and batch manipulation of cells from outside the culture dishes. With this system, we could achieve not only high angle tunability in inclination angles, but also the ability to “add-on” to any types of microscopy. These two characteristics of the proposed device enable us to observe cell membrane boundaries from the desired angles under the inverted microscopes. Due to the simply designed architecture, it was easily fabricated using standard photolithography and soft lithography methods. The device is also highly amenable to automatic processing, and can be easily scaled up to cater for fast, high- throughput, and highly parallel screening

Our device consists of essentially two key strategies: (i) the combination of two biocompatible and transparent materials, parylene and alginate hydrogel, and (ii) magnetic actuation with embedded permalloy layer. The biocompatibility of parylene and sacrificial alginate hydrogel ensured long-term handling, culture, and observation of seeded adherent cells without cytotoxicity. Furthermore, high magnetic permeability of Permalloy facilitates easy control of inclination angle of cell-laden microflaps by controlling the strength of the applied magnetic field. Although we integrated both of these two components in single device, they are by no means limited to be used jointly, nor are they limited to microarray applications. For

example, in the case of isolation technique of single cells such as the integration with conventional flow-cytometry, where the function for inclination is not necessary, an array of engineered planar microplates without permalloy layer will be sufficient for isolation purposes. As for the magnetic actuation technique developed here, we believe that it has many other potential uses beyond the observation of parasite infection; it can be applied to observation of various types of microbial infection including bacteria and virus. Unlike electrically or thermo-kinetically actuated microflaps, this approach does away with complicated electric wiring, greatly simplifying both fabrication, packaging, and control.

By using this system, we revealed two behaviors of one types of parasites, *T. gondii*. Firstly, we found that *T. gondii* exhibited a distinctive pattern of behaviors, especially the bending motion that has not yet been observed by previous approaches. Multi-angle snapshots of bending motion obtained by the microflap system provide biologically fundamental information to confirm which part of the parasite attached to the surface of host cells for migration, estimate the physical forces, and understand the exact timing and location of protein expression corresponding to their behaviors. Since infectious microbes, including parasites and bacteria, generally behave with motions in *x*-*y*, *y*-*z* and *x*-*z* plane, multi-angle observation on the microflaps is a promising method for real-time detailed analysis of the microbial motility under the conventional optical microscopes. Secondly, we obtained the single scanned image that indicates the dynamic deformation of host cell cytoskeleton during parasite invasion under the confocal microscopes. This image has never been available because the reconstruction of cross-sectional image of cells has much lower resolution than lateral scanned images. This new and detailed knowledge of parasite motion during infection into their host cells cannot be accomplished without high angle-tunability and experimental versatility of this mobile microplate.

5. 2 Perspectives

Our approach is unique in offering multidisciplinary perspectives. We tried to approach to the problem that originates from cell biology by the means to combine the microfabrication technologies, mechanics of materials, and microscopic optics, and finally extended the application to the biomedical assay. In future, we hope the applications of this user-friendly platform to a wide range of biological studies. The developed platforms allow for accurate, efficient, and effective analysis of various types interaction between infectious microbes and their host cells, which will eventually lead to advancements in fundamental medical biology and anti-microbe drug development. This microplate system also has no limits on the types of adherent cells seeded, such as primary neuronal cells or stem cell, by coating the appropriate ECM on the microplate surface for each type of cells. By making the fullest possible use of microplate actuation system, we will be able to trace the specific cellular behavior of cells exposed to various external stimulus such as revolutions, vibrations, gravity, and shear stress while maintaining the adhesive properties, toward the creation of new cell-biological experiments such as astrobiology. Furthermore, there may be some applications to reconstruct the artificial cells such as liposomes embedding membrane proteins or cytoskeletons that mimic the adherent cells. This technology has a potential to open up a new realm of the exploration of origin of life and system biology. Multi-angle observation of cell plasma membrane is highly required for many biological studies such as not only microbial infection into host cells, but also protein secretion, migration, membrane budding, and cell division at plasma membrane boundaries. This observation technique is thus broadly applicable for monitoring the plasma membrane dynamics. Eventually, my goal is to introduce this easy observation system to a wide range of researchers, especially biologists or medical investigators, to establish the efficient and reliable experimental setup.

REFERENCES

Akiyama, T., Collard, D., and Fujita, H. Scratch drive actuator with mechanical links for self-assembly of three-dimensional MEMS. *Journal of Microelectromechanical Systems* **6**, 10-17 (1997)

Alexander, D. L., Mital, J., Ward, G. E., Bradley, P., and Boothroyd, J. C. Identification of the moving junction complex of Toxoplasma gondii: a collaboration between distinct secretory organelles. *PLoS Pathogens* **1**, e17 (2005)

Ali, B. S., Sewani, A., Vasquez, C., Akoum, N., Momin, I., and Moreno, A. P. Gap junction channels: Coexpression of cardiac connexins restricts communication pathways that modulate cell growth but not membrane potential. *Journal of the American College of Cardiology* **43**, 129a-129a (2004)

An, S. J., Grabner, C. P., and Zenisek, D. Real-time visualization of complexin during single exocytic events. *Nature Neuroscience* **13**, 577-U583 (2010)

Ashton, R. S., Banerjee, A., Punyani, S., Schaffer, D. V., and Kane, R. S. Scaffolds based on degradable alginate hydrogels and poly(lactide-co-glycolide) microspheres for stem cell culture. *Biomaterials* **28**, 5518-5525 (2007)

Ayres, C., Bowlin, G. L., Henderson, S. C., Taylor, L., Shultz, J., Alexander, J., Telemeco, T. A., and Simpson, D. G. Modulation of anisotropy in electrospun tissue-engineering scaffolds: Analysis of fiber alignment by the fast Fourier transform. *Biomaterials* **27**, 5524-5534 (2006)

Bargieri, D. Y., Andenmatten, N., Lagal, V., Thiberge, S., Whitelaw, J. A., Tardieux, I., Meissner, M., and Ménard, R. Apical membrane antigen 1 mediates apicomplexan parasite attachment but is dispensable for host cell invasion. *Nature Communications* **4**, 2552 (2013)

Beningo, K. A., and Wang, Y. L. Flexible substrata for the detection of cellular traction forces. *Trends in Cell Biology* **12**, 79-84 (2002)

Berdichevsky, Y., Staley, K. J., and Yarmush, M. L. Building and manipulating neural pathways with microfluidics. *Lab on a Chip* **10**, 999-1004 (2010)

Bhang, S. H., Lee, T. J., Lim, J. M., Lim, J. S., Han, A. M., Cho, C. Y., Kwonc, Y. H. K., and Kim, B. S. The effect of the controlled release of nerve growth factor from collagen gel on the efficiency of neural cell culture. *Biomaterials* **30**, 126-132 (2009)

Boothroyd, J. C., and Dubremetz, J. F. Kiss and spit: the dual roles of Toxoplasma rhoptries. *Nature Review Microbiology* **6**, 79-88 (2008)

Brandenburg, B., and Zhuang, X. W. Virus trafficking - learning from single-virus tracking. *Nature Reviews Microbiology* **5**, 197-208 (2007)

Breguet, V., von Stockar, U., and Marison, I. W. Characterization of alginate lyase activity on liquid, gelled, and complexed states of alginate. *Biotechnology Progress* **23**, 1223-1230 (2007)

Carlson, K., Chidley, M., Sung, K. B., Descour, M., Gillenwater, A., Follen, M., and Richards-Kortum, R. In vivo fiber-optic confocal reflectance microscope with an injection-molded plastic miniature objective lens. *Applied Optics* **44**, 1792-1797 (2005)

Carruthers, V., and Boothroyd, J. C. Pulling together: an integrated model of Toxoplasma cell invasion. *Current Opinion in Microbiology* **10**, 83-89 (2007)

Cavey, M., Rauzi, M., Lenne, P. F., and Lecuit, T. A two-tiered mechanism for stabilization and immobilization of E-cadherin. *Nature* **453**, 751-756 (2008)

Chang, C. W., and Hsu, W. Y. Three-dimensional micro assembly of a hinged nickel micro device by magnetic lifting and micro resistance welding. *Journal of Micromechanics and Microengineering* **19**, 105026 (2009)

Chang, T. Y., Yadav, V. G., De Leo, S., Mohedas, A., Rajalingam, B., Chen, C. L., Selvarasah, S., Dokmeci, M. R., and Khademhosseini, A. Cell and protein compatibility of parylene-C surfaces. *Langmuir* **23**, 11718-11725 (2007)

Charriere, F., Pavillon, N., Colomb, T., Depeursinge, C., Heger, T. J., Mitchell, E. A., Marquet, P., and Rappaz, B. Living specimen tomography by digital holographic microscopy: morphometry of testate amoeba. *Optics Express* **14**, 7005-7013 (2006)

Charron, A. J., and Sibley, L. D. Host cells: mobilizable lipid resources for the intracellular parasite Toxoplasma gondii. *Journal of Cell Science* **115**, 3049-3059 (2002)

Chen, C. S., Mrksich, M., Huang, S., Whitesides, G. M., and Ingber, D. E. Geometric control of cell life and death. *Science* **276**, 1425-1428 (1997)

Chen, C. S., Tan, J., and Tien, J. Mechanotransduction at cell-matrix and cell-cell contacts. *Annual*

Review of Biomedical Engineering **6**, 275-302 (2004)

Chen, X. M., O'Hara, S. P., Huang, B. Q., Splinter, P. L., Nelson, J. B., and LaRusso, N. F. Localized glucose and water influx facilitates Cryptosporidium parvum cellular invasion by means of modulation of host-cell membrane protrusion. *Proceedings of the National Academy of Sciences of the United States of America* **102**, 6338-6343 (2005)

Chung, S. E., Kim, J., Choi, S. E., Kim, L. N., and Kwon, S. In Situ Fabrication and Actuation of Polymer Magnetic Microstructures. *Journal of Microelectromechanical Systems* **20**, 785-787 (2011)

Cowman, A. F., and Crabb, B. S. Invasion of red blood cells by malaria parasites. *Cell* **124**, 755-766 (2006)

Daneman, M. J., Tien, N. C., Solgaard, O., Pisano, A. P., Lau, K. Y., and Muller, R. S. Linear microvibromotor for positioning optical components. *Journal of Microelectromechanical Systems* **5**, 159-165 (1996)

De Volder, M. F. L., De Coster, J., Reynaerts, D., Van Hoof, C., and Kim, S. G. High-Damping Carbon Nanotube Hinged Micromirrors. *Small* **8**, 2006-2010 (2012)

Delivopoulos, E., Murray, A. F., MacLeod, N. K., and Curtis, J. C. Guided growth of neurons and glia using microfabricated patterns of parylene-C on a SiO2 background. *Biomaterials* **30**, 2048-2058 (2009)

Delivopoulos, E., and Murray, A. F. Controlled adhesion and growth of long term glial and neuronal cultures on Parylene-C. *PLoS One* **6**, e25411 (2011)

Deutsch, A., Zurgil, N., Hurevich, I., Shafran, Y., Afrimzon, E., Lebovich, P., and Deutsch, M. Microplate cell-retaining methodology for high-content analysis of individual non-adherent unanchored cells in a population. *Biomedical Microdevices* **8**, 361-374 (2006)

Di Carlo, D., Aghdam, N., and Lee, L. P. Single-cell enzyme concentrations, kinetics, and inhibition analysis using high-density hydrodynamic cell isolation arrays. *Analytical Chemistry* **78**, 4925-4930 (2006)

Di Carlo, D., Wu, L. Y., and Lee, L. P. Dynamic single cell culture array. *Lab on a Chip* **6**, 1445-1449 (2006)

Di Carlo, D., and Lee, L. P. Dynamic single-cell analysis for quantitative biology. *Analytical Chemistry* **78**, 7918-7925 (2006)

Doherty, G. J., and McMahon, H. T. Mechanisms of endocytosis. *Annual Review of Biochemistry* **78**,

857-902 (2009)

Donolato, M., Tollan, C., Porro, J. M., Berger, A., and Vavassori, P. Flexible and Stretchable Polymers with Embedded Magnetic Nanostructures. *Advanced Materials* **25**, 623-629 (2013)

Donolato, M., Vavassori, P., Gobbi, M., Deryabina, M., Hansen, M. F., Metlushko, V., Ilic, B., Cantoni, M., Petti, D., Brivio, S., and Bertacco, R. On-Chip Manipulation of Protein-Coated Magnetic Beads via Domain-Wall Conduits. *Advanced Materials* **22**, 2706 (2010)

Dormann, D., and Weijer, C. J. Imaging of cell migration. *EMBO Journal* **25**, 3480-3493 (2006)

Drotlef, D. M., Blumler, P., and Del Campo, A. Magnetically Actuated Patterns for Bioinspired Reversible Adhesion (Dry and Wet). *Advanced Materials* **26**, 775 (2014)

El-Ali, J., Sorger, P. K., and Jensen, K. F. Cells on chips. *Nature* **442**, 403-411 (2006)

Etienne-Manneville, S., and Hall, A. Rho GTPases in cell biology. *Nature* **420**, 629-635 (2002)

Ewanowich, C. A., Sherburne, R. K., Man, S. F., and Peppler, M. S. Bordetella parapertussis invasion of HeLa 229 cells and human respiratory epithelial cells in primary culture. *Infection and Immunity* **57**, 1240-1247 (1989)

Fan, Z. F., Chen, J., Zou, J., Bullen, D., Liu, C., and Delcomyn, F. Design and fabrication of artificial lateral line flow sensors. *Journal of Micromechanics and Microengineering* **12**, 655-661 (2002)

Fang, W. L., Chu, H. Y., Hsu, W. K., Cheng, T. W., and Tai, N. H. Polymer-reinforced, aligned multiwalled carbon nanotube composites for microelectromechanical systems applications. *Advanced Materials* **17**, 2987 (2005)

Felsenfeld, D. P., Schwartzberg, P. L., Venegas, A., Tse, R., and Sheetz, M. P. Selective regulation of integrin--cytoskeleton interactions by the tyrosine kinase Src. *Nature Cell Biology* **1**, 200-206 (1999)

Fraley, S. I., Feng, Y., Giri, A., Longmore, G. D., and Wirtz, D. Dimensional and temporal controls of three-dimensional cell migration by zyxin and binding partners. *Nature Communications* **3**, 719 (2012)

Fu, J., Wang, Y. K., Yang, M. T., Desai, R. A., Yu, X., Liu, Z., and Chen, C. S. Mechanical regulation of cell function with geometrically modulated elastomeric substrates. *Nature Methods* **7**, 733-736 (2010)

Gach, P. C., Sims, C. E., and Allbritton, N. L. Transparent magnetic photoresists for bioanalytical applications. *Biomaterials* **31**, 8810-8817 (2010)

Grauw, C. J., Sijtsema, N. M., Otto C., and Greve, J. Axial resolution of confocal Raman microscopes: Gaussian beam theory and practice. *Journal of Microscopy* **188**, 273-279 (1997)

Gundelfinger, E. D., Kessels, M. M., and Qualmann, B. Temporal and spatial coordination of exocytosis and endocytosis. *Nature Reviews Molecular Cell Biology* **4**, 127-139 (2003)

Gunn, N. M., Chang, R., Westerhof, T., Li, G. P., Bachman, M., and Nelson, E. L. Ferromagnetic micropallets for magnetic capture of single adherent cells. *Langmuir* **26**, 17703-17711 (2010)

Gutwein, P., Oleszewski, M., Mechtersheimer, S., Agmon-Levin, N., Krauss, K., and Altevogt, P. Role of Src kinases in the ADAM-mediated release of L1 adhesion molecule from human tumor cells. *Journal of Biological Chemistry* **275**, 15490-15497 (2000)

Hakansson, S., Morisaki, H., Heuser, J., and Sibley, L. D. Time-lapse video microscopy of gliding motility in Toxoplasma gondii reveals a novel, biphasic mechanism of cell locomotion. *Molecular Biology of the Cell* **10**, 3539-3547 (1999)

Handa, Y., Suzuki, M., Ohya, K., Iwai, H., Ishijima, N., Koleske, A. J., Fukui, Y., and Sasakawa, C. Shigella IpgB1 promotes bacterial entry through the ELMO-Dock180 machinery. *Nature Cell Biology* **9**, 121-U165 (2007)

Harris, A. K., Wild, P., and Stopak, D. Silicone-Rubber Substrata - New Wrinkle in the Study of Cell Locomotion. *Science* **208**, 177-179 (1980)

Hassler, C., von Metzen, R. P., Ruther, P., and Stieglitz, T. Characterization of parylene C as an encapsulation material for implanted neural prostheses. *Journal of Biomedical Materials Research Part B-Applied Biomaterials* **93B**, 266-274 (2010)

Hesse, M., Raulf, A., Pilz, G. A., Haberlandt, C., Klein, A. M., Jabs, R., Zaehres, H., Fugemann, C. J., Zimmermann, K., Trebicka, J., *et al.* Direct visualization of cell division using high-resolution imaging of M-phase of the cell cycle. *Nature Communications* **3**, 1076 (2012)

Hsiao, Y. S., Lin, C. C., Hsieh, H. J., Tsai, S. M., Kuo, C. W., Chu, C. W., and Chen, P. L. Manipulating location, polarity, and outgrowth length of neuron-like pheochromocytoma (PC-12) cells on patterned organic electrode arrays. *Lab on a Chip* **11**, 3674-3680 (2011)

Hubers, H. W., Schubert, J., Krabbe, A., Birk, M., Wagner, G., Semenov, A., Gol'tsman, G., Voronov, B., and Gershenzon, E. Parylene anti-reflection coating of a quasi-optical hot-electron-bolometric mixer at terahertz frequencies. *Infrared Physics & Technology* **42**, 41-47 (2001)

Hui, E. E., and Bhatia, S. N. Micromechanical control of cell-cell interactions. *Proceedings of the National Academy of Sciences of the United States of America* **104**, 5722-5726 (2007)

Huisken, J., Swoger, J., Del Bene, F., Wittbrodt, J., and Stelzer, E. H. K. Optical sectioning deep inside live embryos by selective plane illumination microscopy. *Science* **305**, 1007-1009 (2004)

Hurley, J. H., and Hanson, P. I. Membrane budding and scission by the ESCRT machinery: it's all in the neck. *Nature Reviews Molecular Cell Biology* **11**, 556-566 (2010)

Ikonen, E. Cellular cholesterol trafficking and compartmentalization. *Nature Reviews Molecular Cell Biology* **9**, 125-138 (2008)

Ishihara, K., Fujiike, A., Iwasaki, Y., Kurita, K., and Nakabayashi, N. Synthesis of polymers having a phospholipid polar group connected to a poly(oxyethylene) chain and their protein adsorption-resistance properties. *Journal of Polymer Science Part a-Polymer Chemistry* **34**, 199-205 (1996)

Ishihara, K., Nomura, H., Mihara, T., Kurita, K., Iwasaki, Y., and Nakabayashi, N. Why do phospholipid polymers reduce protein adsorption? *Journal of Biomedical Materials Research* **39**, 323-330 (1998)

Isikman, S. O., Bishara, W., Mavandadi, S., Yu, F. W., Feng, S., Lau, R., and Ozcan, A. Lens-free optical tomographic microscope with a large imaging volume on a chip. *Proceedings of the National Academy of Sciences of the United States of America* **108**, 7296-7301 (2011)

Isikman, S. O., Bishara, W., Sikora, U., Yaglidere, O., Yeah, J., and Ozcan, A. Field-portable lensfree tomographic microscope. *Lab on a Chip* **11**, 2222-2230 (2011)

Iwase, E., and Shimoyama, I. A design method for out-of-plane structures by multi-step magnetic self-assembly. *Sensors and Actuators A-Physical* **127**, 310-315 (2006)

Iwase, E., and Shimoyama, I. Multistep sequential batch assembly of three-dimensional ferromagnetic microstructures with elastic hinges. *Journal of Microelectromechanical Systems* **14**, 1265-1271 (2005)

Jager, E. W., Inganas, O., and Lundstrom, I. Microrobots for micrometer-size objects in aqueous media: potential tools for single-cell manipulation. *Science* **288**, 2335-2338 (2000a)

Jager, E. W., Smela, E., and Inganas, O. Microfabricating conjugated polymer actuators. *Science* **290**, 1540-1545 (2000)

Jinno, S., Moeller, H. C., Chen, C. L., Rajalingam, B., Chung, B. G., Dokmeci, M. R., and Khademhosseini, A. Microfabricated multilayer parylene-C stencils for the generation of patterned dynamic co-cultures. *Journal of Biomedical Materials Research Part A* **86**, 278-288 (2008)

Judy, J. W., and Muller, R. S. Magnetic microactuation of torsional polysilicon structures. *Sensors and*

Actuators A-Physical **53**, 392-397 (1996)

Judy, J. W., and Muller, R. S. Magnetically actuated, addressable microstructures. *Journal of Microelectromechanical Systems* **6**, 249-256 (1997)

Kaajakari, V., and Lal, A. Thermokinetic actuation for batch assembly of microscale hinged structures. *Journal of Microelectromechanical Systems* **12**, 425-432 (2003)

Kay, R. R., Langridge, P., Traynor, D., and Hoeller, O. Changing directions in the study of chemotaxis. *Nature Reviews Molecular Cell Biology* **9**, 455-463 (2008)

Kennedy, J. P., McCandless, S. P., Lasher, R. A., and Hitchcock, R. W. The mechanically enhanced phase separation of sprayed polyurethane scaffolds and their effect on the alignment of fibroblasts. *Biomaterials* **31**, 1126-1132 (2010)

Khetan, S., and Burdick, J. A. Patterning hydrogels in three dimensions towards controlling cellular interactions. *Soft Matter* **7**, 830-838 (2011)

Khodagholy, D., Doublet, T., Gurfinkel, M., Quilichini, P., Ismailova, E., Leleux, P., Herve, T., Sanaur, S., Bernard, C., and Malliaras, G. G. Highly conformable conducting polymer electrodes for in vivo recordings. *Advanced Materials* **23**, H268-272 (2011)

Kievit, F. M., and Zhang, M. Cancer nanotheranostics: improving imaging and therapy by targeted delivery across biological barriers. *Advanced Materials* **23**, H217-247 (2011)

Kim, H. S., Lee, C. G., and Lee, E. Y. Alginate Lyase: Structure, Property, and Application. *Biotechnology and Bioprocess Engineering* **16**, 843-851 (2011a)

Kim, J., Choi, S. E., Lee, H., and Kwon, S. Magnetochromatic microactuators for a micropixellated color-changing surface. *Advanced Materials* **25**, 1415-1419 (2013)

Kim, J., Chung, S. E., Choi, S. E., Lee, H., Kim, J., and Kwon, S. Programming magnetic anisotropy in polymeric microactuators. *Nature Materials* **10**, 747-752 (2011)

Kim, L. N., Choi, S. E., Kim, J., Kim, H., and Kwon, S. Single exposure fabrication and manipulation of 3D hydrogel cell microcarriers. *Lab on a Chip* **11**, 48-51 (2011)

Kim, Y. S., Dagalakis, N. G., and Gupta, S. K. Creating large out-of-plane displacement electrothermal motion stage by incorporating beams with step features. *Journal of Micromechanics and Microengineering* **23**, 055008 (2013)

King, N. The unicellular ancestry of animal development. *Dev Cell* **7**, 313-325 (2004)

Kiriya, D., Ikeda, M., Onoe, H., Takinoue, M., Komatsu, H., Shimoyama, Y., Hamachi, I., and Takeuchi, S. Meter-Long and Robust Supramolecular Strands Encapsulated in Hydrogel Jackets. *Angewandte Chemie-International Edition* **51**, 1553-1557 (2012)

Knodler, L. A., Celli, J., and Finlay, B. B. Pathogenic trickery: deception of host cell processes. *Nature Reviews Molecular Cell Biology* **2**, 578-588 (2001)

Kumar, K., Hoshino, K., and Zhang, X. J. Handheld subcellular-resolution single-fiber confocal microscope using high-reflectivity two-axis vertical combdrive silicon microscanner. *Biomedical Microdevices* **10**, 653-660 (2008)

Kuribayashi-Shigetomi, K., Onoe, H., and Takeuchi, S. Cell origami: self-folding of three-dimensional cell-laden microstructures driven by cell traction force. *PLoS One* **7**, e51085 (2012)

Kwon, O. H., and Zewail, A. H. 4D electron tomography. *Science* **328**, 1668-1673 (2010)

Lemmon, C. A., Chen, C. S., and Romer, L. H. Cell Traction Forces Direct Fibronectin Matrix Assembly. *Biophysical Journal* **96**, 729-738 (2009)

Li, N., Hill, K. S., and Elferink, L. A. Analysis of receptor tyrosine kinase internalization using flow cytometry. *Methods in Molecular Biology* **457**, 305-317 (2008)

Liburdy, R. P. Calcium signaling in lymphocytes and ELF fields: evidence for an electric field metric and a site of interaction involving the calcium ion channel (vol 301, pg 53, 1992). *FEBS Letters* **478**, 304-304 (2000)

Liburdy, R. P., Callahan, D. E., Harland, J., Dunham, E., Sloma, T. R., and Yaswen, P. Experimental-Evidence for 60-Hz Magnetic-Fields Operating through the Signal-Transduction Cascade - Effects on Calcium Influx and C-Myc Messenger-Rna Induction. *FEBS Letters* **334**, 301-308 (1993)

Lindstrom, S., and Andersson-Svahn, H. Overview of single-cell analyses: microdevices and applications. *Lab on a Chip* **10**, 3363-3372 (2010)

Liu, J., Sun, Y. D., Drubin, D. G., and Oster, G. F. The Mechanochemistry of Endocytosis. *PLoS Biology* **7**, e1000204 (2009)

Llobet, A., Beaumont, V., and Lagnado, L. Real-time measurement of exocytosis and endocytosis using interference of light. *Neuron* **40**, 1075-1086 (2003)

Ma, X., Wehland, M., Aleshcheva, G., Hauslage, J., Wasser, K., Hemmersbach, R., Infanger, M., Bauer, J., and Grimm, D. Interleukin-6 Expression under Gravitational Stress Due to Vibration and

Hypergravity in Follicular Thyroid Cancer Cells. *PLoS One* **8**, e68140 (2013)

Matsumoto, T., Hoshino, T., Akiyama, Y., and Morishima, K. (2011). A novel application of carbon nano coils for intracellular nano-robots. *Proceedings of IEEE International Conference on Nano/Micro Engineered and Molecular Systems (NEMS)*, 2011.

McMahon, H. T., and Gallop, J. L. Membrane curvature and mechanisms of dynamic cell membrane remodelling. *Nature* **438**, 590-596 (2005)

Meng, E., Li, P. Y., and Tai, Y. C. Plasma removal of parylene c. *Journal of Micromechanics and Microengineering* **18**, 045004 (2008)

Morisaki, J. H., Heuser, J. E., and Sibley, L. D. Invasion of Toxoplasma gondii occurs by active penetration of the host cell. *Journal of Cell Science* **108**, 2457-2464 (1995)

Nagai, M., Asai, H., and Fujita, H. Non-Invasive Detachment of Vorticella from Calcium Alginate Membrane. *e-Journal of Surface Science and Nanotechnology* **11**, 25-28 (2013)

Nikolaev, N. I., Liu, Y., Hussein, H., and Williams, D. J. The sensitivity of human mesenchymal stem cells to vibration and cold storage conditions representative of cold transportation. *Journal of the Royal Society Interface* **9**, 2503-2515 (2012)

Onoe, H., and Takeuchi, S. Microfabricated mobile microplates for handling single adherent cells. *Journal of Micromechanics and Microengineering* **18**, 095003 (2008)

Park, K., Millet, L. J., Kim, N., Li, H., Jin, X., Popescu, G., Aluru, N. R., Hsia, K. J., and Bashir, R. Measurement of adherent cell mass and growth. *Proc Natl Acad Sci U S A* **107**, 20691-20696 (2010)

Petit, T., Zhang, L., Peyer, K. E., Kratochvil, B. E., and Nelson, B. J. Selective Trapping and Manipulation of Microscale Objects Using Mobile Microvortices. *Nano Letters* **12**, 156-160 (2012)

Pister, K. S. J., Judy, M. W., Burgett, S. R., and Fearing, R. S. Microfabricated Hinges. *Sensors and Actuators A-Physical* **33**, 249-256 (1992)

Purich, D. L., and Southwick, F. S. Actin-based motility of the intracellular pathogen Listeria monocytogenes: assessing the inhibitory specificity of ABM-1 peptide analogues. *Molecular Cell Biology Research Communications* **1**, 176-181 (1999)

Qian, A. R., Di, S. M., Gao, X., Zhang, W., Tian, Z. C., Li, J. B., Hu, L. F., Yang, P. F., Yin, D. C., and Shang, P. cDNA microarray reveals the alterations of cytoskeleton-related genes in osteoblast under high magneto-gravitational environment. *Acta Biochimica Et Biophysica Sinica* **41**, 561-577 (2009)

Rao, C. V., Wolf, D. M., and Arkin, A. P. Control, exploitation and tolerance of intracellular noise. *Nature*

420, 231-237 (2002)

Rappoport, J. Z., and Simon, S. M. Real-time analysis of clathrin-mediated endocytosis during cell migration. *Journal of Cell Science* **116**, 847-855 (2003)

Reid, J. R., Bright, V. M., and Comtois, J. H. (1997). Automated assembly of flip-up micromirrors. *Proceedings of International Conference on Solid State Sensors and Actuators TRANSDUCERS '97 Chicago*., (1997)

Riglar, D. T., Richard, D., Wilson, D. W., Boyle, M. J., Dekiwadia, C., Turnbull, L., Angrisano, F., Marapana, D. S., Rogers, K. L., Whitchurch, C. B., *et al.* Super-Resolution Dissection of Coordinated Events during Malaria Parasite Invasion of the Human Erythrocyte. *Cell Host & Microbe* **9**, 9-20 (2011)

Robaina, R. R., Lopez-Martinez, M. J., Esteve, J., Perez-Castillejos, R., and Plaza, J. A. Directed Fracture for the Fabrication of Free-Standing Multilayered Submicrometer Structures. *Small* **7**, 558-562 (2011)

Sakar, M. S., Steager, E. B., Cowley, A., Kumar, V., and Pappas, G. J. (2011). Wireless manipulation of single cells using magnetic microtransporters. *Proceedings of IEEE International Conference on Robotics and Automation (ICRA)*, 2011

Sakar, M. S., Steager, E. B., Kim, D. H., Kim, M. J., Pappas, G. J., and Kumar, V. Single cell manipulation using ferromagnetic composite microtransporters. *Applied Physics Letters* **96**, 043705 (2010)

Sakaue-Sawano, A., Kurokawa, H., Morimura, T., Hanyu, A., Hama, H., Osawa, H., Kashiwagi, S., Fukami, K., Miyata, T., Miyoshi, H., *et al.* Visualizing spatiotemporal dynamics of multicellular cell-cycle progression. *Cell* **132**, 487-498 (2008)

Salazar, G. T., Wang, Y., Young, G., Bachman, M., Sims, C. E., Li, G. P., and Allbritton, N. L. Micropallet arrays for the separation of single, adherent cells. *Analytical Chemistry* **79**, 682-687 (2007)

Santi, P. A. Light sheet fluorescence microscopy: a review. *Journal of Histochemistry & Cytochemistry* **59**, 129-138 (2011)

Schmidt, O. G., Deneke, C., Schmarje, N., Muller, C., and Jin-Phillipp, N. Y. Free-standing semiconductor micro- and nano-objects. *Materials Science & Engineering C-Biomimetic and Supramolecular Systems* **19**, 393-396 (2002)

Sheetz, M. P. Cell control by membrane-cytoskeleton adhesion. *Nature Reviews Molecular Cell Biology* **2**, 392-396 (2001)

Shin, D., Pierce, M. C., Gillenwater, A. M., Williams, M. D., and Richards-Kortum, R. R. A Fiber-Optic Fluorescence Microscope Using a Consumer-Grade Digital Camera for In Vivo Cellular Imaging. *PLoS One* **5**, DOI: 10.1371/journal.pone.0011218 (2010)

Shulman, Z., Cohen, S. J., Roediger, B., Kalchenko, V., Jain, R., Grabovsky, V., Klein, E., Shinder, V., Stoler-Barak, L., Feigelson, S. W., *et al.* Transendothelial migration of lymphocytes mediated by intraendothelial vesicle stores rather than by extracellular chemokine depots. *Nature Immunology* **13**, 67-76 (2012)

Skelley, A. M., Kirak, O., Suh, H., Jaenisch, R., and Voldman, J. Microfluidic control of cell pairing and fusion. *Nature Methods* **6**, 147-152 (2009)

Soldati, T., and Schliwa, M. Powering membrane traffic in endocytosis and recycling. *Nature Reviews Molecular Cell Biology* **7**, 897-908 (2006)

Spiller, D. G., Wood, C. D., Rand, D. A., and White, M. R. Measurement of single-cell dynamics. *Nature* **465**, 736-745 (2010)

Sudhof, T. C., and Rothman, J. E. Membrane fusion: grappling with SNARE and SM proteins. *Science* **323**, 474-477 (2009)

Suzuki, K., Shimoyama, I., and Miura, H. Insect-Model Based Microrobot with Elastic Hinges. *Journal of Microelectromechanical Systems* **3**, 4-9 (1994)

Sweeney, K. R., Morrissette, N. S., LaChapelle, S., and Blader, I. J. Host Cell Invasion by Toxoplasma gondii Is Temporally Regulated by the Host Microtubule Cytoskeleton. *Eukaryotic Cell* **9**, 1680-1689 (2010)

Tabony, J., and Job, D. Gravitational Symmetry-Breaking in Microtubular Dissipative Structures. *Proceedings of the National Academy of Sciences of the United States of America* **89**, 6948-6952 (1992)

Takeuchi, S., and Shimoyama, I. Standing microcoil actuator array. *Japanese Journal of Applied Physics* **42**, 3695-3697 (2003)

Tam, C., Idone, V., Devlin, C., Fernandes, M. C., Flannery, A., He, X., Schuchman, E., Tabas, I., and Andrews, N. W. Exocytosis of acid sphingomyelinase by wounded cells promotes endocytosis and plasma membrane repair. *The Journal of Cell Biology* **189**, 1027-1038 (2010)

Tan, J. L., Tien, J., Pirone, D. M., Gray, D. S., Bhadriraju, K., and Chen, C. S. Cells lying on a bed of microneedles: An approach to isolate mechanical force. *Proceedings of the National Academy of Sciences of the United States of America* **100**, 1484-1489 (2003)

Tan, W. H., and Takeuchi, S. A trap-and-release integrated microfluidic system for dynamic microarray applications. *Proceedings of the National Academy of Sciences of the United States of America* **104**, 1146-1151 (2007)

Tan, W. H., and Takeuchi, S. Dynamic microarray system with gentle retrieval mechanism for cell-encapsulating hydrogel beads. *Lab on a Chip* **8**, 259-266 (2008)

Tan, W. H., and Takeuchi, S. Monodisperse alginate hydrogel microbeads for cell encapsulation. *Advanced Materials* **19**, 2696 (2007)

Teshima, T., Ishihara, H., Iwai, K., Adachi, A., and Takeuchi, S. A dynamic microarray device for paired bead-based analysis. *Lab on a Chip* **10**, 2443-2448 (2010)

Teshima, T., Onoe, H., Kuribayashi-Shigetomi, K., and Takeuchi, S. (2011b). Pairing single adherent cells in the dynamic microarray. *Proceedings of IEEE 24th International Conference on Micro Electro Mechanical Systems (MEMS)*, 2011

Teshima, T., kuribayashi-Shigetomi, K., Onoe, H., Tonooka, T., and Takeuchi, S. A PAIRED MICROFLAP ARRAY FOR SINGLE CELL INTERACTION ANALYSIS. *Proceedings of International Conference, MicroTAS 2013*, 1704-1706 (2011a)

Thery, M. Micropatterning as a tool to decipher cell morphogenesis and functions. *Journal of Cell Science* **123**, 4201-4213 (2010)

Thery, M., Racine, V., Piel, M., Pepin, A., Dimitrov, A., Chen, Y., Sibarita, J. B., and Bornens, M. Anisotropy of cell adhesive microenvironment governs cell internal organization and orientation of polarity. *Proceedings of the National Academy of Sciences of the United States of America* **103**, 19771-19776 (2006b)

Thery, M., and Bornens, M. Cell shape and cell division. *Curr Opin Cell Biol* **18**, 648-657 (2006)

Thomas, J. A., and Rana, F. R. The influence of environmental conditions, lipid composition, and phase behavior on the origin of cell membranes. *Origins of Life and Evolution of Biospheres* **37**, 267-285 (2007)

Tonkin, M. L., Roques, M., Lamarque, M. H., Pugniere, M., Douguet, D., Crawford, J., Lebrun, M., and Boulanger, M. J. Host cell invasion by apicomplexan parasites: insights from the co-structure of AMA1 with a RON2 peptide. *Science* **333**, 463-467 (2011)

Toomre, D., and Bewersdorf, J. A new wave of cellular imaging. *Annual Review of Cell and Developmental Biology* **26**, 285-314 (2010)

Tottori, S., Zhang, L., Qiu, F. M., Krawczyk, K. K., Franco-Obregon, A., and Nelson, B. J. Magnetic Helical Micromachines: Fabrication, Controlled Swimming, and Cargo Transport. *Advanced Materials* **24**, 811-816 (2012)

Tsai, K. L., Ziaei-Moayyed, M., Candler, R. N., Hu, W., Brand, V., Klejwa, N., Wang, S. X., and Howe, R. T. Magnetic, Mechanical, and Optical Characterization of a Magnetic Nanoparticle-Embedded Polymer for Microactuation. *Journal of Microelectromechanical Systems* **20**, 65-72 (2011)

Tseng, P., Judy, J. W., and Di Carlo, D. Magnetic nanoparticle-mediated massively parallel mechanical modulation of single-cell behavior. *Nature Methods* **9**, 1113-1119 (2012)

Ueki, Y., Sakamoto, N., and Sato, M. Direct measurement of shear strain in adherent vascular endothelial cells exposed to fluid shear stress. *Biochemical and Biophysical Research Communications* **394**, 94-99 (2010)

Unsworth, C. P., Delivopoulos, E., Gillespie, T., and Murray, A. F. Isolating single primary rat hippocampal neurons & astrocytes on ultra-thin patterned parylene-C/silicon dioxide substrates. *Biomaterials* **32**, 2566-2574 (2011)

Versaevel, M., Grevesse, T., and Gabriele, S. Spatial coordination between cell and nuclear shape within micropatterned endothelial cells. *Nature Communications* **3**, 671 (2012)

Vogel, V., and Sheetz, M. Local force and geometry sensing regulate cell functions. *Nature Reviews Molecular Cell Biology* **7**, 265-275 (2006)

Wan, L. Q., Ronaldson, K., Park, M., Taylor, G., Zhang, Y., Gimble, J. M., and Vunjak-Novakovic, G. Micropatterned mammalian cells exhibit phenotype-specific left-right asymmetry. *Proceedings of the National Academy of Sciences of the United States of America* **108**, 12295-12300 (2011)

Wang, Y. L., Salazar, G. T., Pai, J. H., Shadpour, H., Sims, C. E., and Allbritton, N. L. Micropallet arrays with poly(ethylene glycol) walls. *Lab on a Chip* **8**, 734-740 (2008)

Wang, Y., Phillips, C., Xu, W., Pai, J. H., Dhopeshwarkar, R., Sims, C. E., and Allbritton, N. Micromolded arrays for separation of adherent cells. *Lab on a Chip* **10**, 2917-2924 (2010)

Wang, Y., Young, G., Aoto, P. C., Pai, J. H., Bachman, M., Li, G. P., Sims, C. E., and Allbritton, N. L. Broadening cell selection criteria with micropallet arrays of adherent cells. *Cytometry A* **71**, 866-874 (2007)

Weninger, W. J., Geyer, S. H., Mohun, T. J., Rasskin-Gutman, D., Matsui, T., Ribeiro, I., Costa Lda, F., Izpisua-Belmonte, J. C., and Muller, G. B. High-resolution episcopic microscopy: a rapid technique for high detailed 3D analysis of gene activity in the context of tissue architecture and morphology.

Anatomy and Embryology **211**, 213-221 (2006)

W ilson, T., and Carlini A. R., Size of the detector in confocal imaging systems. *OPTICS LETTERS* **12**, 227-229 (1987)

Wodarz, A. Establishing cell polarity in development. *Nature Cell Biology* **4**, E39-44 (2002)

Wong, T. Y., Preston, L. A., and Schiller, N. L. ALGINATE LYASE: review of major sources and enzyme characteristics, structure-function analysis, biological roles, and applications. *Annual Review of Microbiology* **54**, 289-340 (2000)

Wright, D., Rajalingam, B., Selvarasah, S., Dokmeci, M. R., and Khademhosseini, A. Generation of static and dynamic patterned co-cultures using microfabricated parylene-C stencils. *Lab on a Chip* **7**, 1272-1279 (2007)

Wu, M. C. Micromachining for optical and optoelectronic systems. *Proceedings of the IEEE* **85**, 1833-1856 (1997)

Wu, Y., Ghitani, A., Christensen, R., Santella, A., Du, Z., Rondeau, G., Bao, Z., Colon-Ramos, D., and Shroff, H. Inverted selective plane illumination microscopy (iSPIM) enables coupled cell identity lineaging and neurodevelopmental imaging in Caenorhabditis elegans. *Proceedings of the National Academy of Sciences of the United States of America* **108**, 17708-17713 (2011)

Wymann, M. P., and Schneiter, R. Lipid signalling in disease. *Nature Reviews Molecular Cell Biology* **9**, 162-176 (2008)

Yi, Y. W., and Liu, C. Magnetic actuation of hinged microstructures. *Journal of Microelectromechanical Systems* **8**, 10-17 (1999)

Yoshida, S., Teshima, T., Kuribayashi-Shigetomi, K., and Takeuchi, S. Mobile Microplates for Handling Morphologically Controlled Single Neural Cells. *Proceedings of International Conference, MicroTAS 2013*, 452-454 (2013)

Zhou, X. Z., Boey, F., Huo, F. W., Huang, L., and Zhang, H. Chemically Functionalized Surface Patterning. *Small* **7**, 2273-2289 (2011)

Zou, J., Chen, J., Liu, C., and Schutt-Aine, J. E. Plastic deformation magnetic assembly (PDMA) of out-of-plane microstructures: Technology and application. *Journal of Microelectromechanical Systems* **10**, 302-309 (2001)

du Roure, O., Saez, A., Buguin, A., Austin, R. H., Chavrier, P., Silberzan, P., and Ladoux, B. Force mapping in epithelial cell migration. *Proceedings of the National Academy of Sciences of the United*

States of America **102**, 2390-2395 (2005)

van Meer, G., Voelker, D. R., and Feigenson, G. W. Membrane lipids: where they are and how they behave. *Nature Reviews Molecular Cell Biology* **9**, 112-124 (2008)

APPENDIX

Appendix A. Reagents

Reagents	Manufacturer
Ethanol (99.5%)	Wako Pure Chemical Industries, Ltd
SU-8	MicroChem Corp.
S1818	Shipley
NMD-3	Tokyo Ohka Kogyo Co., Ltd.
Acetone	Kanto Chemical Co., Inc.
2-propanol (IPA)	Kanto Chemical Co., Inc.
SU-8 developer	Kayaku MicroChem
PDMS Sylgard184	Dow Corning Toray
1mol/L Hydrochloric Acid	Wako Pure Chemical Industries, Ltd
Nitric acid 1.38	Kanto Chemical Co., Inc.
Al etchant	Wako Pure Chemical Industries, Ltd
CellTracker™ Green CMFDA	Invitrogen
CellTracker™ Red CMTPX	Invitrogen
RPMI 1640 MEDIUM	Sigma-Aldrich, Inc.
D-MEM (Dulbecco's Modified Eagle Medium)	Sigma-Aldrich, Inc.
D-MEM (DMEM, Low glucose)	Sigma-Aldrich, Inc.
Trypsin-EDTA	Sigma-Aldrich, Inc.
PBS (Phosphate Buffered Saline) w/o Ca^{2+}, Mg^{2+}	Sigma-Aldrich, Inc.
PBS (Phosphate Buffered Saline) w/ Ca^{2+}, Mg^{2+}	Sigma-Aldrich, Inc.
Sodium Alginate	Wako, Ltd / Sigma-Aldrich, Inc.
Potassium Chloride	Wako Pure Chemical Industries, Ltd
Fetal Bovine Serum (Lot: 10D217)	Nichirei Bioscience Corp.
Calcium chloride	Wako Pure Chemical Industries, Ltd
LIVE/DEAD Cell Viability Assays	Sigma-Aldrich, Inc.
HY solution	Wako Pure Chemical Industries, Ltd
Fibronectin	Biomedical Technologies
Collagen (Type IV)	Sigma-Aldrich, Inc.
Ferric chloride ($FeCl_3$)	Wako Pure Chemical Industries, Ltd
Tween20	Kanto Chemical Co., Inc.

Reagents	Manufacturer
Aluminium (Al)	Nilaco Corp.
Copper (Cu)	
Glass substrate (SiO_2)	Matsunami, 0.12–0.17 mm thick
Chromium (Cr)	New Metals and Chemicals
Permalloy (78 permalloy)	Nilaco Corp.
L−glutamine	Invitrogen
10 μg/ml gentamicin	Invitrogen
10 mM HEPES	Invitrogen
4 wt% paraformaldehyde	Wako Pure Chemical Industries, Ltd
Triton X-100	Alfa Aesar
Hoechst 33528	Sigma-Aldrich, Inc.
TRITC-conjugated phalloidin	Molecular Probes
4.5 μm, Fluoresbrite BB	Polysciences, Inc.
Alginate lyase	Sigma-Aldrich, Inc.
Parylene-C (DPX-C)	Speedline Technology
tert-butyl alcohol	Wako Pure Chemical Industries, Ltd
2 wt% glutaraldehyde	Wako Pure Chemical Industries, Ltd
Monoclonal mouse anti-α-Tubulin antibody	Sigma-Aldrich, Inc.
Poly-L-Lysine	Wako Pure Chemical Industries, Ltd
Alexa Fluor 488 Goat anti-mouse IgG antibody	Life Technologies
Alexa Fluor 555 Goat anti-Mouse IgG antibody	Life Technologies
Alexa Fluor 594 Goat anti-Mouse IgG antibody	Life Technologies
Glycerol	Wako Pure Chemical Industries, Ltd
YG Carboxylate Microspheres 0.20 μm	Fluoresbrite, Polysciences, Inc.
polycarbonate membrane filters	pore size, 3 μm, Millipore
Neodymium (NdFeB) magnet	NeoMag
Calcein-AM	Life Technologies
CellLight Fluorescent Protein (RFP) Tubulin	Life Technologies
CellLight Fluorescent Protein (RFP) Actin	Life Technologies
DiI / DiO	TAKARA BIO Inc.
Bovine Serum Albumins (BSA)	Sigma-Aldrich, Inc.
SIGMA C6219 RABBIT ANTI-CONNEXIN 43	Sigma-Aldrich, Inc.
PKH26/67 Red Fluorescent Cell Linker	Sigma-Aldrich, Inc.
RIPA buffer	NACALAI

Appendix B. Apparatus

Apparatus	Manufacturer	Stock number
Parylene coater	Japan Parylene Godo	LABCOTER PDS2010
Vacuum vapor depositing equipment	Sanyu Electron Co., Ltd	SVC-700
Sputtering equipment	Canon ANELVA Corp.	E-200S
Plasma etching system	SAMCO, Inc.	FA-1
Reactive Ion Etching system	SAMCO, Inc.	RIE-10NR
Mask Aligner	UNION optical co., ltd.	PEM-6M
Maskless Lithography System	NanoSystem Solutions, inc.	DL1000
Rapid prototyping machine	Envision Tec.	Perfactory
Scanning electron microscope	KEYENCE	VE-7800
Time-lapse Microscope	KEYENCE	BIOREVO BZ-9000
Film step height measurement tool	ULVAC	Dektak 6M
Spin-coater	MIKASA Co., Ltd	1H-07-TS
Conditioning mixer	THINKY	AR-100
Vacuum drying oven	Advantec	DRV220DA
CO_2 incubater	SANYO Research	MCO-19AIC
Inverted optical microscope	Olympus	IX70
Inverted optical microscope	Nikon	TE300
Inverted optical microscope	Leica	DM IL LED
Stage top incubator	TOKAI HIT	Thermo Plate
Stereomicroscope	Olympus	MVX10
Confocal fluorescence microscope	Olympus	IX71 (no.1,2,3)
Confocal fluorescence microscope	Carl Zeiss	LSM780
Confocal fluorescence microscope	Leica	Leica TCS SP5
Epioptical digital microscopy	KEYENCE	VHX-900
Laser scanning microscopy	KEYENCE	VK-X200
Optical microscope with CO_2 incubator	Carl Zeiss	Axio Observer
Optical microscope	Mitutoyo Corp.	MF-U
UV/Visible spectrophotometry	JASCO	V-550 ST
Scanning electron microscope	Hitachi	S-4800 FE-SEM
Osmium Coater	VACUUM DEVICE INC.	HPC-30W
Syringe	Hamilton Gastight syringes	1700 series, TLL